CARDIOMYOPATHY IN THE GOLDEN RETRIEVER MODEL OF DUCHENNE MUSCULAR DYSTROPHY: PHENOTYPE, GENE EXPRESSION AND METABOLIC STUDIES

A Dissertation

by

SARAH MORAR SCHNEIDER

Submitted to the Office of Graduate and Professional Studies of
Texas A&M University
in partial fulfillment of the requirements for the degree of

DOCTOR OF PHILOSOPHY

Chair of Committee,	Joe N Kornegay
Committee Members,	Brad Weeks
	Candice Brinkmeyer-Langford
	Peter Nghiem
	Ivan Rusyn
Head of Department,	Ramesh Vemullipalli

May 2019

Major Subject: Veterinary Pathobiology

ABSTRACT

Through three distinct papers, this dissertation aims to increase understanding of cardiomyopathy in golden retriever muscular dystrophy (GRMD), an important model for Duchenne muscular dystrophy (DMD). Unlike the mdx mouse, GRMD dogs develop progressive cardiomyopathy homologous in onset and severity to DMD. In both, cardiomyopathy develops around adolescence, progressing to dilation and eventual heart failure. Clinical cardiomyopathy occurs later than skeletal muscle involvement and is now the major cause of death in DMD. Skeletal and cardiac disease severity do not necessarily track together, suggesting possible different pathogenetic mechanisms. A comprehensive understanding of GRMD cardiomyopathy will be key to using this preclinical model.

First, we report cardiac lesions in a large group of GRMD and carrier dogs. We found semi-quantitative scoring and fibrosis quantification correlate with disease progression and semi-quantitative scores correlated with vascular hypertrophy and late gadolinium enhancement on cardiac MRI. The nature of some lesions suggested functional hypoxia may contribute to disease progression.

Next, we evaluated expression of potential genetic biomarkers in GRMD hearts. Left and right ventricles from 41 dogs (7 normal, 6 carrier, 28 GRMD) were analyzed by qRT-PCR for five genes previously associated with disease in DMD or GRMD: brain-derived neurotropic factor (BDNF), utrophin, matrix-metalloproteinase-9, a-disintegrin-and-metallopeptidase-domain-12, and osteopontin (SPP1). BDNF and SPP1 protein

levels were assessed by western blot. There was differential expression of BDNF and SPP1 in GRMD hearts, extending work suggesting BDNF is preferentially increased in GRMD LV and showing that SPP1 expression tracks with cardiomyopathy evolution.

Finally, we evaluated glucose metabolism as a potential biomarker in GRMD. Skeletal muscle from normal, carrier, and GRMD pelvic limbs and LV were analyzed by mRNA profiling, qPCR, western blotting, and immunofluorescence microscopy for the glucose transporter (GLUT4). Physiologic glucose handling was measured by fasting glucose tolerance test, insulin levels, and PET-CT using the glucose analog 2-deoxy-2-[18F]fluoro-D-glucose. We found that altered glucose metabolism in GRMD skeletal and cardiac muscle can be monitored with molecular, biochemical, and in vivo imaging and potentially utilized as a biomarker for disease progression and therapeutic response.

Together, these studies deepen the understanding of the histologic, physiologic and metabolic changes in GRMD cardiomyopathy.

DEDICATION

This dissertation is dedicated to my family, especially my husband Drew, my daughter Lillian, and my oldest child, my dog Janis sadly lost before this work was finished. They stuck with me through all the B.S, and continually remind me what is important.

.

ACKNOWLEDGEMENTS

As always with acknowledgements, I fear I will miss many important people. I expect most of the people who assisted in this effort will never read it, so I will endeavor to thank them in person, and keep this section brief.

I'd like to acknowledge: my committee members, Drs. Kornegay, Weeks, Brinkmeyer-Langford, Nghiem, and Rusyn for their time and commitment to these projects; Drs. Clubb and O'Brien for their help with heart anatomy and sectioning; the GI lab at Texas A&M for the generous use of their digital slide scanner, especially Kim Green for her assistance; Dr. Furuya for technical help and equipment use for the trichrome analysis; Drs. Glowcwski, Sridhar, and Guo for all their help in teaching me about imaging studies; Cindy Balog-Alvarez for all her invaluable assistance in learning and completing the lab work; and Margaret Foster the Texas A&M librarian who helped compile the systemic review resources.

Beyond that I'd like to acknowledge: Drs. Porter, Rodrigues, Weeks, Edwards, Mansell, Corapi, Pool and Stoica for an excellent residency and training me to do a job I love; my resident mates, Dr. Nikki Jackson and Dr. Kristin Eden for helping through that training and being good friends; the POWER writing program at Texas A&M for teaching me skills I didn't even realize I could learn, and ultimately easing the anxiety around the writing process; and my writing groups for helping me keep at it and stay relatively intact.

CONTRIBUTORS AND FUNDING SOURCES

This work was supported by a dissertation committee consisting of Professor Joe N. Kornegay [advisor] and Professor Brad Weeks of the Department of Veterinary Pathobiology and Professor(s) Peter P. Nghiem, Candice Brinkmeyer-Langford and Ivan Rusyn of the Department of Veterinary Integrative Biosciences.

Some of the statistics in Chapters 2 and 3 were completed by Dr. Garett Sansom in the Texas A&M School of Public Health. The cMRI and left ventricular ejection fraction data in Chapters 2 and 3 were provided by Dr. Lee Jae Guo, collected as a part of his Ph.D. research (not yet published). A portion of the western blot data in Chapter 3 was collected by Cindy Balog (lab manager), Katherine Hulbert, and Taylor R. Gourley (two veterinary students). The mRNA, qPCR, western blot and confocal data in Chapter 4 were provided by Dr. Peter Nghiem. Assistance with formatting and proof-reading this document were provided by Drew Schneider, MS.

All other work conducted for the dissertation was completed by the student independently.

Graduate study was supported by a Zoetis-Morris Animal Foundation fellowship [grant number D14CA-903] and the Department of Pathobiology. Studies in Chapter 2 and initial mRNA studies in Chapter 3 were supported by a startup fund to Dr. Kornegay. Some of the later protein work in Chapter 3 was funded through a gift from Solid Biosciences. Studies in Chapter 4 were supported by a start-up fund to Dr. Nghiem.

TABLE OF CONTENTS

Page

ABSTRACT ii

DEDICATION iv

ACKNOWLEDGEMENTS v

CONTRIBUTORS AND FUNDING SOURCES vi

TABLE OF CONTENTS vii

LIST OF FIGURES ix

LIST OF TABLES xii

INTRODUCTION 1

- Duchenne Muscular Dystrophy 1
- Golden Retriever Muscular Dystrophy Model 3
- Cardiomyopathy in DMD and GRMD 3
- Previous studies of GRMD and CXMD cardiomyopathy 5
- Genetic Modifiers of Skeletal and Cardiac Phenotype 8
- Cardiac metabolism and PET-CT 11
- Summary 12

NATURAL HISTORY OF PATHOLOGIC CHANGES IN THE CARDIOMYOPATHY OF GOLDEN RETRIEVER MUSCULAR DYSTROPHY 13

- Introduction 13
- Methods 15
- Results 25
- Discussion 37
- Conclusions 43

BRAIN-DERIVED NEUROTROPIC FACTOR (BDNF) AND OSTEOPONTIN (SPP1) ARE ASSOCIATED WITH CARDIOMYOPATHY IN GOLDEN RETREIVER MUSCULAR DYSTROPHY 44

- Introduction 44
- Materials and Methods 46

Results 53
Discussion 61
Conclusions 66

GLUCOSE METABOLISM AS A PRE-CLINICAL BIOMARKER FOR THE GOLDEN RETRIEVER MODEL OF DUCHENNE MUSCULAR DYSTROPHY 67

Introduction 67
Materials and Methods 69
Results: 76
Discussion 84

CONCLUSION 93

REFERENCES 97

APPENDIX 122

LIST OF FIGURES

Page

Figure 1. Representative gross images of a GRMD heart showing the whole heart (A), the basal cross section with LV and RV dilation (B), and all ventricular cross sections (C). 17

Figure 2. Fibrotic lesions were not always evenly distributed within the wall. In both GRMD dogs and DMD boys, the sub-epicardial myocardium is sometimes preferentially affected (A). However, other locations within the wall may predominate (B and C) Subendocardial changes are rare and were only seen in the RV when observed (C). 22

Figure 3. Fatty infiltration was a prominent feature in some older GRMD dogs. (A) A section of LVFW with large bands of fat replacing normal myocardial muscle, and predominating over fibrosis. In some cases, fatty infiltration was more diffuse (B). In several dogs, the RV showed striking mid-myocardial replacement by bands of fat with minimal fibrotic tissue (C). Trichrome staining, 10x magnification. 29

Figure 4. Coagulative myocardial necrosis was a feature in some dogs. (A) Areas of infarct-like coagulative necrosis characterized by loss of cytoplasmic detail and maintenance of tissue architecture (stars) are surrounded by proliferating macrophages and pericytes (arrows); H&E, 5x magnification. (B) Acute coagulative necrosis with loss of nuclei and hypereosinophilic cytoplasm (representative cells with stars); cells on the margins of lesions have granular basophilic mineralization (arrows). H&E, 20x magnification... 30

Figure 5. Purkinje fiber vacuolation in the heart of a GRMD dog. Paler staining Purkinje fibers (outlined) with large vacuolation (arrows). H&E, 20x magnification. 33

Figure 6. (A) Increased fibrous tissue (blue) in an arteriole of a normal dog. Trichrome, 5x magnification. (B) Marked medial and intimal hypertrophy and vascular proliferation in arterioles in the heart of a GRMD dog. H&E, 5x magnification. 34

Figure 7. Boxplots of gene expression by disease status. Box plots compare the normalized mRNA expression levels in the LV and RV of WT, Carrier, and GRMD dogs. One-way ANOVA demonstrated significant differences in BDNF expression in the LV (A) of GRMD dogs (n=25; 23.44 +/- 21.05) compared to carrier (n=6; 3.33 +/- 2.71) and WT (n=7; 2.64 +/-2.01) animals. SPP1 expression in the LV appears upregulated, but low numbers

and a high standard deviation precluded detection of significance. Values were similar between disease groups in the RV (A), with individual dogs having markedly increased BDNF, SPP1 and MMP9. 55

Figure 8. Two way scatterplots of age and normalized gene expression in GRMD LV for SPP1 (A), BDNF (B), UTRN (C), and ADAM12 (D). The mRNA expression in LV of 25 GRMD dogs was plotted against age with corresponding Pearson's r coefficients and p-values. (MMP9 was also plotted and was not significantly different). SPP1 (A) is positively correlated with age (r=0.413; p<0.001), while BDNF (B) (r=0.045; p=0.309), UTRN (C) (r=0.068; p=0.189), and ADAM12 (D) (r=0.010; p=0.632) were not significantly different across ages in the LV. MMP9 was also assessed, and not significantly correlated with age (graph not included). 56

Figure 9. Two-way scatterplots of age and gene expression in normal dog hearts for SPP1 (A), BDNF (B), UTRN (C), and ADAM12 (D). The mRNA expression in LV of 15 WT dogs was plotted against age corresponding Pearson's r coefficients and p-values. (MMP9 was not detected in enough normal samples for analysis). SPP1 (A) (r=0.169; p=0.022) was modestly, positively correlated with age and BDNF (B) (r=0.122; p=0.064) trended upward with age. UTRN (C) (r=-0.035; p=0.865) and ADAM12 (D) (r=-0.034; p=0.945) were not significantly correlated with age. 58

Figure 10. BDNF and SPP1 protein expression in GRMD LV and RV. BDNF protein expression was measured in the LV and RV of 14 GRMD dogs by western blots and normalized total protein. Dogs ranged in age from 3 to 42 months. BDNF was positively correlated with age in the LV (r = 0.56) [A] and negatively correlated with age in the RV (r = -0.59) [B]; p < 0.05 for both. ... 60

Figure 11. GLUT4 mRNA expression was reduced in GRMD versus normal muscle. (a) GLUT4 mRNA expression was compared in the CS, LDE, and VL of GRMD (black bars) and normal (open bars) dogs at 4-9 weeks and 6 months. Levels were significantly lower in GRMD dogs; differences were most pronounced in the LDE (50% decrease). (b) QPCR for GLUT4 on GRMD LDE microarrayed muscle at 6 months confirmed downregulation by a fold change of -1.894, while hexokinase 1 was upregulated by a fold change of +2.13. *=p<.05, **=p<.01. Reprinted.[138] 77

Figure 12. GLUT4 protein in GRMD vs normal muscles. GLUT4 expression was similar in CS (a) and VL (b) between GRMD (black bars) and normal (white) dogs, but increased in GRMD LDE (c) at 6 months. GLUT4 expression was normalized to total protein per lane on the PVDF membrane. * = p<.05. Reprinted.[138] 77

Figure 13. Peri-membranous localization of GLUT4 in GRMD skeletal muscle. Confocal microscopy showed increased localization of GLUT4 (green) at the myofiber membrane (white asterisk and arrows) in GRMD skeletal muscle (CS, LDE, VL, cranial tibial, diaphragm; b, d) compared to normal (a, c). Mainly cytoplasmic GLUT4 localization was observed in normal muscle (asterisk; a, c). Note that GRMD also demonstrated cytoplasmic GLUT4 aggregates. In cardiomyocytes, there was no statistical difference in GLUT-4 expression at the membrane between normal and GRMD (e, f). Quantification (g) showed a nearly 4 fold increase of GLUT4 at the membrane in GRMD skeletal muscle (p=.047). a and b = 20X objective (oil immersion); c-f = 100X objective (oil immersion). Nuclei = blue. Spectrin = red. N = 5-6 per group for skeletal muscle; N = 3 per group for cardiac muscle. Reprinted.[138] 79

Figure 14. Rapid dextrose uptake in GRMD with an intravenous glucose tolerance test. At early time points, glucose (a) and insulin (b) curves were significantly different between GRMD and carrier/normal dogs. Resting (basal, time = 0) blood glucose was significantly higher in GRMD (104.5 mg/dl +/- 7.3) compared to normal/carrier dogs (92.0 mg/dl +/- 8.9). Dextrose uptake was rapid in GRMD dogs compared to normal 5 min post injection. Glucose levels were similar between genotypes at later time points. Resting (basal) insulin levels were significantly higher in GRMD dogs (31.26 uIU/ml +/- 6.1; 35% increase) vs. normal and carrier dogs (21.61 uIU/ml +/- 7.27) and GRMD insulin peaked at the 5-min time point compared to 15 min in carrier and normal dogs. Insulin levels were similar between genotypes at later time points. **=p<.01. Reprinted.[138] 80

Figure 15. Differential [^{18}F]DG uptake with PET-CT in GRMD versus normal/carrier dogs in skeletal and cardiac muscle. (a) GRMD VL, rectus femoris, and CS (top, white oval) had higher SUV than a normal littermates (bottom; white oval). (b)The skeletal muscle had significantly increased mean SUV at 5 min post [^{18}F]DG/insulin in GRMD compared to normal. (c)GRMD skeletal muscle had significantly higher CoV at 1 hour. In cardiac muscle, max (d) and mean (g) SUV were lower in the GRMD left ventricle (f, top) compared to normal (f, bottom) and carrier at 5 minutes post ^{18}FDG/insulin (white circle outlining the heart). At 1 hour, max SUV (e) trended and mean SUV (h) were significantly lower compared to normal left ventricle. *=p<.05. Reprinted.[138] 83

LIST OF TABLES

Page

Table 1. Averages of gross heart measurements for GRMD, Carrier and Normal dogs..18

Table 2. Averages of histologic changes for groups. 19

Table 3. Semiquantitative scores for individual dogs. 21

Table 4. Population characteristics for PCR of GRMD, carrier, and normal dogs. 47

Table 5. Gene expression fold change between ventricles in GRMD and normal dogs..54

Table 6. ANOVA Gene fold expression between age categories for GRMD status samples. 57

INTRODUCTION

Duchenne Muscular Dystrophy

Duchenne muscular dystrophy (DMD) is an X-linked inherited disorder, occurring in 1 out of every ~5000 boys at birth.[1] A mutation in the *DMD* gene leads to loss of the structural protein dystrophin at the muscle cell membrane and dissolution of its associated glycoprotein complex. This deficiency leads to progressive degenerative muscle disease characterized by myofiber necrosis, mineralization, and fibrosis,[2] with eventual atrophy of most muscles. Boys with DMD become non-ambulant in the first or second decade of life and succumb to complications, including respiratory and cardiac failure, usually in the third decade of life.[3]

Although the genetic cause of DMD has been known for over 30 years[2] treatment is still largely symptomatic; standard of care remains glucocorticoid treatment, with the addition of nocturnal ventilation as the disease progresses.[4] Only recently have targeted therapies to repair the missing/defective protein been approved for use in human trials.[5] Dystrophin is the largest known human gene and over 276 mutations that lead to dystrophinopathy have been identified.[6] This large size hinders complete gene replacement, leading to development of truncated AAV microdystrophin therapies, while targeted exon-skipping therapies only benefit a subset of patients.

In recent years, following the implementation of improved respiratory therapy including assisted ventilation at night,[3] cardiac complications have become the leading cause of death in DMD boys. Cardiac disease severity has also been linked with long-term survival prognosis.[7] Despite the recognition of cardiac involvement in the earliest

descriptions of DMD[8,9] and recommendations for regular cardiac monitoring and assessment, the study, diagnosis, and treatment of cardiac issues in boys has lagged behind skeletal and respiratory therapy.[10] As supportive therapeutics continue to increase survival time in DMD boys and young men, progressive cardiomyopathy, which manifests later in life, will require greater attention.

A recent special report recognized the increased need for improved diagnostics and early detection of DMD cardiomyopathy, as well as an expanded role for large animal models in understanding the pathogenesis of cardiomyopathy and the different responses of skeletal and cardiac muscle in dystrophinopathies.[3,10] Indeed, although 90% of DMD boys over the age of 18 will have detectable signs of cardiac involvement,[8] best practices for diagnosis, monitoring and initiation of treatment for heart disease are still not established and patients are often underdiagnosed and under-treated for this disease.[11] This lag may be driven in part by the relative lack of cardiac associated clinical signs even when electrocardiogram (ECG) and echocardiography show evidence of heart involvement.[8]

The progression of cardiac disease cannot be extrapolated from skeletal or pulmonary measures.[3,7,12] Although both the heart and skeletal muscle are striated and express dystrophin at the sarcolemma, the loss of dystrophin, while causing electrophysiological abnormalities, does not manifest as cardiomyopathy in most boys until adolescence.[8] Underlying differences in regenerative capacity, calcium homeostasis[13–15] overall metabolism,[16] and the localization of the dystrophin-glycoprotein complex[17–19] between the two muscle types likely contribute to the

differences in disease expression. Importantly, therapy aimed at improving skeletal muscle function may not cure or improve cardiac function.[20,21] In fact, in some instances, improvement of skeletal muscle phenotype without addressing cardiac disease can lead to worsening of cardiac phenotype.[3,20]

Golden Retriever Muscular Dystrophy Model

Well-characterized animal models that replicate the phenotypic and genotypic features of DMD boys are critical in the effort to improve diagnostics, early detection, and treatment modalities aimed at cardiomyopathy in DMD.[10,22] The two main animal models of DMD are the golden retriever muscular dystrophy (GRMD) dog and the X-linked muscular dystrophy (mdx) mouse.[23–25] Both are genetic homologs caused by mutations in the *DMD* gene.[23,25]

The GRMD dog more closely resembles DMD[24,26]. Unlike mdx mice, which have a mild disease with minimal cardiomyopathy,[27–29] GRMD dogs have similar disease severity to DMD boys, including progressive muscle loss and weakness, worsening clinical disease around adolescence (10-12 in boys,[8] ~6 months in dogs[26]), severe cardiomyopathy, and a shortened lifespan.[24] Dogs also have the advantage of having a similar size and immune and inflammatory response to boys[30] and serve as an important large animal model for DMD, particularly for preclinical trials to assess treatment and diagnostic modalities.[10,23]

Cardiomyopathy in DMD and GRMD

DMD and GRMD have similar severity and disease expression in the heart. Initially, the DMD heart appears grossly and histologically normal. Typically, around

adolescence, the heart develops lesions including fibrosis and mineralization, beginning in the basal left ventricle (LV) and progressing to the septum, LV free wall and remainder of the heart.[12,31] Eventually, dilated cardiomyopathy develops with decreased ejection fraction, reduced contractility and myocardial thinning in areas of fibrosis.[12,31] Analogous cardiomyopathy development occurs in the GRMD dog, where lesions are first detectable around 6 months of age, progressing in time to severe dilated cardiomyopathy and heart failure.[24,26,32]

Although structural changes are rarely evident until adolescence, studies have found evidence of altered cellular function much earlier. A stereotypical ECG change—a tall precordial R wave and deep Q wave—can be detected in both DMD and GRMD individuals,[33–35] demonstrating altered electroconduction in the heart prior to the development of fibrosis. Similarly, PET-CT and scintigraphy studies[36–39] have shown early alterations in cardiac metabolism. Studies to further clarify these early differences will help find ways to better intervene and monitor cardiac disease in these patients.

In addition to the similarities between affected boys and dogs, women and bitches heterozygous for the *DMD* mutation (carriers) also have cardiac lesions. Due to random X-inactivation, carrier hearts have mosaic dystrophin expression.[28,40] While changes are usually subclinical, carrier hearts are not completely normal. Women can have detectable ECG abnormalities like those seen in affected boys.[41,42] Moreover, carrier women and dogs have cardiomyocyte loss and fibrosis, similar in appearance, if not severity, to those in affected individuals[40,43–45] and symptomatic cardiomyopathy can

develop.[44,46] As such, studies in GRMD cardiomyopathy should include carrier females to produce the fullest understanding.

The relative sparing of the cardia (myocardium) from histologic and functional disease signs until later in life suggests there are genetic or metabolic factors that initially protect the cardiac muscle or enhance the dramatic necrosis, inflammation and fibrosis seen in the skeletal muscle from birth. The lack of lesions early in life also complicates decisions on treatment, intervention, and monitoring. As such, many questions remain on when to institute treatments and how best to monitor the disease progression in DMD cardiomyopathy.

Previous studies of GRMD and CXMD cardiomyopathy

The clinical characteristics of GRMD cardiomyopathy were first described by Valentine et al in 1989. Out of the 24 dogs in the study, 19 were less than 12 weeks old and had no detectable abnormalities. The bulk of the characterization focused on 5 dogs ranging from 6.5 months to 6 years (6.5 m, 1y, 1y, 1.5 y, and 6 y). These initial descriptions had some of the most comprehensive sampling, including 13 to 17 sections from each dog. All the older dogs had varying degrees of fibrosis, myofiber degeneration and size variation with vacuolation and lipid deposition; mineralization/mineral deposition appeared more prominent in the 6.5 to 18m old dogs. This study also described electron microscopy (EM) changes, including increased collagen, mitochondrial abnormalities and attenuation of myofilaments.

Later studies demonstrated mosaic distribution of dystrophin in the hearts of carrier dogs,[28] and nearly all the 11 carrier dogs examined for one study[43] showed

similar lesions to affected dogs including variable degrees of myocardial fibrosis, necrosis, mineralization and fatty infiltration concentrated in the LV free wall, with fewer dogs having changes in the right ventricle (RV) and interventricular septum (IVS). No correlation was found between age and severity of lesions in these dogs. Interestingly, resting ECG and systolic function were not different between carriers and normal dogs, and although 24-hour Holter monitoring showed an increased risk of cardiac arrhythmia, no correlation was found between age or lesion severity and the number of VPC's in carrier dogs.

Additional descriptive studies of cardiomyopathy in dogs carrying the GRMD mutation include two papers out of Japan, assessing crossbred beagles carrying the GRMD gene ($CXMD_J$). The first paper included only 8 dogs, half of which were under 12 months. Similar to the Valentine study, young dogs (up to 12 months in this group), had no abnormalities, suggesting a smaller body size or outbreeding may delay cardiac disease.[32] The 4 dogs >12 months showed fibrosis in the posterior LV. Samples were taken at the levels of the apical and basal papillary muscle, with LV and IVS examined at each level. Right ventricular lesions were not noted. A follow-up study of the conduction system in dogs from this colony under 13 months noted "irregular vacuolation of Purkinje fibers" starting at 4 months, which EM demonstrated as degenerate myofibrils surrounding vacuoles.[47]

Two studies describe GRMD dogs in Brazil. The first included 16 dogs, 10 between 7 and 12 months and 6 between 12 and 21 months, and provided an overall assessment of the GRMD phenotype in their colony.[48] In the heart, they noted concentric

hypertrophy, RV dilation and histologically "moderate to pronounced connective tissue, mononuclear inflammation, degeneration, necrosis and calcification." The number of cardiac sites that were sampled was not described. The later study[49] assessed 18 dogs from 6 to 51 months that died spontaneously of cardiac or respiratory arrest. Samples included LV, RV and IVS with H&E, picrosirius red, and Von Kossa stains. Their descriptions suggested that lesions progress through the age groups, "The sequence of cardiac lesions including: mineralization [6-8m], necrosis [8-11m], granulation tissue formation [13-18m], fibrosis [11-21m], and fatty infiltration [20-51m]." This is the only study to suggest that particular lesions became apparent as dogs age. However, the authors were unclear as to whether the lesions listed at each stage were the primary or only lesion present. Since individual lesions would be expected to progress from mineralization through to fibrosis in a manner of weeks, the study is somewhat confusing. Changes typical of necrosis, including mineralization, would be expected early followed by more chronic lesions of fibrosis and fatty deposition, generally in keeping with the sequence of changes reported. However, given the inherent phenotypic variation (see further below) of GRMD, and the progression of disease in individuals, the age at which individual lesions occur undoubtedly varies among dogs, and lesion development is an ongoing or recurring event. Dogs in these studies were assessed only at necropsy. It would be difficult to establish the longitudinal nature of lesions without sampling individual dogs at multiple ages.

Other studies mention cardiac lesions, but often in passing without much detail[33,50–56] or to confirm presence or absence of changes in the face of experimental

manipulation.[57–65] Overall these studies did not provide much systematic or overly descriptive information, although Habeler et al. (2011)[60] did note fibrosis and calcification in the heart as early as 4 months, which is younger than previously described.

The most complete description, in terms of the amount of sampling and description, remains the initial study by Valentine et al. in 1989, though it is essentially based on only 5 dogs. Yugeta et al.[32] had similarly low numbers. The most recent descriptive study out of Brazil included the highest number of dogs at 18, and made the most concerted effort to differentiate lesions among age groups. However, there were fewer samples from each heart than in previous studies, and despite listing a grading scheme based on the percentage of lesions, they did not provide overall graded numbers for their age groups and their lesion interpretation was confusing. Additionally, all the dogs in this study purportedly died of heart failure, likely indicating more severe cardiac changes.

Genetic Modifiers of Skeletal and Cardiac Phenotype

In both DMD and GRMD, there can be tremendous phenotypic variation. Much of the variation in DMD can be explained by different mutations, with out-of-frame mutations producing more severe skeletal muscle disease.[66] For instance, Becker's muscular dystrophy (BMD) and X-linked dilated cardiomyopathy are produced by in-frame mutations in the DMD gene resulting in truncated dystrophin. Interestingly, while these boys have a mild skeletal phenotype, there is typically more severe cardiomyopathy,[67] perhaps because the heart is strained by the greater skeletal muscle

activity. However, even in siblings with identical mutations, cardiac and pulmonary function are not correlated, and severity can differ widely.[68] Likewise, within the GRMD model, where all dogs carry the same mutation in exon 6 resulting in skipping of intron 7 and an early stop codon,[69] phenotypic variability is quite marked, even amongst littermates.[70] This remarkable variability with a single gene mutation strongly suggests genetic modifiers outside of the *DMD* gene impact disease expression.

Although both skeletal and cardiac muscle contain striated fibers with similar cytoplasmic organization, function, and dystrophin localization, the disease process develops differently between the two muscle types. The lack of proportionality between skeletal muscle and cardiomyopathy severity[71,72] is further evidence that pathogenesis differs in these two tissues. This discrepancy supports our hypothesis that genetic modifiers are likely different between the two systems. As a result, findings from skeletal muscle research cannot be merely extrapolated to understand the cardiac disease. Put another way, studies with specific cardiac endpoints are important for understanding the cardiomyopathy separate from skeletal muscle. A few studies have specifically assessed potential modifiers of cardiomyopathy in DMD and animal models.[18,50,73–76]

One of the first modifiers recognized was utrophin, an autosomal homolog of dystrophin. Utrophin is upregulated in mdx mice skeletal muscle, likely contributing to its relatively mild phenotype and, significant to our study, is particularly upregulated in their hearts.[77] Utrophin is likewise upregulated, to a lesser degree, in the muscle of DMD and BMD boys, and is correlated with phenotypic severity.[78–80] Utrophin expression is

also increased at the sarcolemma in GRMD (referred to in this paper as canine X-linked muscular dystrophy [CXMD]) dogs as they age, regardless of phenotype.[81] The presence and significance of utrophin in the heart has been less studied. Utrophin appears to complex with proteins other than dystrophin in the heart.[82] One study in GRMD dogs did not find a difference in utrophin expression in the myocardium of GRMD and normal dogs.[57] Two others demonstrated diffuse utrophin expression with immunofluorescence at the cardiac sarcolemma in GRMD/CXMD dogs,[51,53] although, RNA and protein levels were not assessed. Urasawa et al. (2008)[47] found increased sarcolemmal utrophin expression in Purkinje fibers at 4m of age with corresponding upregulation in these cells; it is unclear if the rest of the myocardium was assessed.

Genes involved in inflammatory modulation have also been shown to be important modifiers of phenotypic severity in DMD boys and mdx mice. In particular, the inflammatory mediators osteopontin (SPP1),[67,73,74,83–86] matrix-metalloproteinase-9 (MMP9)[87–90] and a disintegrin and metallopeptidase-12 (ADAM12)[91–94] have been shown to modify phenotypic variability in DMD and mdx cardiomyopathy.

Conversely, a recent GWAS study in dogs and humans found that while osteopontin expression was specifically associated with skeletal muscle disease, the BDNF gene was specifically upregulated in the hearts of GRMD dogs and serum of DMD boys,[50] Importantly, serum levels correlated with ejection fraction in DMD patients.[16,50,95] BDNF is a contraction inducible protein[96] that enhances lipid oxidation and increases angiogenesis. In keeping with its apparent beneficial effect in DMD, it has been associated with improved outcomes and prognosis in a variety of human

cardiomyopathies[97,98] and other heart diseases,[97–100] including models of cardiac ischemia.[101,102] BDNF is an intriguing genetic modifier, as it has potential to serve as a biomarker for disease.

Cardiac metabolism and PET-CT

In addition to structural changes, loss of dystrophin leads to metabolic derangements. Key among these are an increased metabolic stress due to decreased glycolytic and oxidative enzyme expression, lower mitochondrial numbers, and mitochondrial abnormalities in the face of increased metabolic demands due to stresses induced by membrane fragility.[103–108] These differences may precede the stage when dystrophin would normally be expressed.[106] Eventually, these changes lead to the development of a 'metabolic crisis,' with a reduced capacity to respond to the metabolic demands of contraction.

Cardiac metabolism differs slightly from that of skeletal muscle. Although both rely on GLUT4 as the primary transporter of glucose and have insulin and contraction stimulated pathways,[109] glucose uptake requires slightly different protein sets.[110,111] Additionally, GLUT1 may play a role in basal glucose uptake in cardiac muscle.[112] Finally, cardiac muscle has a higher capacity and reliance on fatty oxidation for its energy.[113]

PET-CT is a sensitive detector of metabolic changes and markers can be manufactured for any small molecule. The glucose analog 2-deoxy-2-[^{18}F]fluoro-D-glucose ([^{18}F]DG) is frequently used as a marker for glucose metabolism in tissues and is also primarily transported by GLUT4. There is evidence that the subcellular location

of GLUT4 is altered in dystrophin deficiency.[114,115] PET-CT and scintigraphy studies have shown a shift toward increased glucose metabolism and decreased fatty acid metabolism in the absence of detectable blood flow alterations,[36–39] suggesting that oxygenation or metabolic changes are altered in early disease development. These cardiac studies also showed regional differences in both GRMD dogs[36] and DMD and BMD boys.[37] ECG alterations and PET-CT changes are both regional, affecting the LV basal wall—the initial site for lesion development—suggesting the changes are a precursor to necrosis, fibrosis and mineralization. Studies to further clarify these early differences will help find ways to better intervene and monitor cardiac disease in these patients.

Summary

The cardiomyopathy in GRMD, like that in DMD, is characterized by lesion progression, genetic expression, and metabolic differences distinct from those in skeletal muscle. Through a detailed and standardized descriptive study of GRMD hearts, gene and protein expression in GRMD hearts, and PET imaging, we aimed to better characterize the distinct features of dystrophin deficient cardiomyopathy and define potential clinical biomarkers of disease progression in the heart to help in future treatment evaluation.

NATURAL HISTORY OF PATHOLOGIC CHANGES IN THE CARDIOMYOPATHY OF GOLDEN RETRIEVER MUSCULAR DYSTROPHY

Introduction

Duchenne muscular dystrophy (DMD) and golden retriever muscular dystrophy (GRMD) are genetically homologous and phenotypically analogous degenerative muscle diseases caused by mutations in the *DMD* gene coding for the dystrophin protein.[23,24] Loss of dystrophin at the sarcolemma leads to membrane fragility and both skeletal[2] and cardiac muscle lesions.[12,31] Cardiac complications are the leading cause of death in young men with DMD.[3]

Although heart and skeletal muscle share the same underlying loss of dystrophin, differences in Ca2+ homeostasis,[13–15] metabolism[16] and localization of the dystrophin-glycoprotein complex[17–19] contribute to variable pathologic changes in the two tissues. While some studies have shown that cardiac and skeletal muscle functional loss track together, others have shown variable progression.[3,12,68,116,117] The potential for discordance has clinical significance. Clinical features typically used to identify cardiac disease may not be present in DMD boys who use wheelchairs.[118,119] More importantly, improvement in skeletal muscle function alone could, in principle, increase strain on the heart and accelerate progression of cardiac disease.[3,20,21,118,119] Features of cardiac disease should be monitored carefully, with recommended management moving towards early intervention.

The GRMD dog is an important large animal model of DMD.[23,24] Progression of cardiac disease in affected dogs closely parallels that in boys, including ECG

abnormalities,[33–35] initial onset of lesions around adolescence,[12,26,31] predominance of changes in the basolateral left ventricle (LV),[12,26,31,32] and ultimate progression to clinical dilated cardiomyopathy with reduced ejection fraction and heart failure.[12,23,24,31] Previous descriptive studies, including the first paper by Valentine et al. in 1989,[26] established the basic features of GRMD cardiomyopathy.[24,26,32,47–49] Out of the 24 dogs in the Valentine study, 19 were less than 12 weeks old and had no detectable abnormalities. Accordingly, that paper focused on only 5 dogs ranging from 6.5 months (m) to 6 years (y) and included comprehensive sampling of 13 to 17 sections from each dog. Lesions were seen in each dog, establishing 6.5m as the age of onset for pathologic changes. Yugeta et al.[32] had similarly low numbers, with only 4 dogs having lesions. These cross-bred beagles appeared to have a later onset of disease at 12m. The most recent descriptive study out of Brazil[49] included the highest number of dogs at 18, and also made the most concerted effort to differentiate lesions among age groups. However, only single sites from the LV and right ventricle (RV) were examined for each animal. Additionally, all the dogs in that study purportedly died of heart failure, probably reflecting a more severe cardiac phenotype.

Women carriers heterozygous for *DMD* gene mutations are also at increased risk for clinical heart disease[40,42,44,45] due to mosaic cardiac dystrophin expression.[40] Canine GRMD carriers have an analogous mosaic pattern of dystrophin expression in the heart[120] and have similar lesions to affected dogs, including variable degrees of myocardial fibrosis, necrosis, mineralization and fatty infiltration concentrated in the LV free wall.[43]

Given the similarities between the DMD and GRMD cardiomyopathies, preclinical studies in affected dogs should inform management of DMD patients. Pathologic studies typically serve as the gold standard for establishing disease progression and aid selection of appropriate diagnostic and prognostic biomarkers. We report here a semi quantitative natural history study of histopathologic changes of cardiomyopathy in a large cohort of GRMD dogs across a wide age range.

Methods

Hearts

Animal care was governed by principles outlined in the National Research Council's Guide for the Care and Use of Laboratory Animals and Texas A&M animal use protocols 2015-0110 (Standard Operating Procedures-Canine X-Linked Muscular Dystrophy) and 2015-0164 (Emergency Medicine Didactive Elective VTPP 948). In our colony, affected males are usually bred to carrier females, producing 25% each normal males, carrier females, and both dystrophic hemizygous males and homozygous females. GRMD affected and carrier hearts were collected at necropsy from dogs that died or were euthanized due to declining quality of life (defined as an inability to maintain sternal recumbence or progression to intractable heart failure) or at terminal end-points of unrelated studies. Unaffected control hearts were collected from an unrelated colony of working hound dogs that died from non-cardiac events.

In all hearts, samples from the LV and RV free walls were snap frozen at necropsy and banked for potential gene expression and immunohistochemistry studies; the remainder of the whole heart was placed in formalin. Hearts from a total of 38 dogs,

including 7 normal hounds (controls; 2-10 y; 5F, 2M), 5 GRMD carriers (3 m-4.5y), and 26 with GRMD divided among four age groups (< 6m [5], 6-12m [7], 12-24m [5], and >24m up to 76m [9]). GRMD dogs were evenly split between hemizygous males and homozygous females.

Gross pathology and sectioning

Fixed hearts were weighed and photographed in 6 views (cranial, caudal, lateral from each side, base, and apex). Each heart was cross-sectioned through the short axis of the ventricles at 1cm intervals to the level of the atrioventricular valves and sections were photographed (Figure 1). Hearts were weighed and the thickness of the fixed LV, RV and intraventricular septum (IVS) was measured (Table 1 and Supplement 2).

Each heart was systematically sectioned for histology. Seventeen sections of the LV (including septum) were taken to correspond with standard segmentation for advanced imaging.[121] Additionally, four sections of the RV (anterior and inferior as available at the basal and mid-level) and the left and right atria were collected. The atrioventricular node was isolated by sectioning the septal junction of the right atrium below the foramen ovale and the septal aortic valve leaflet and the sinoatrial node was sectioned at the junction of the vena cava and the right atrium.[122] Tissue cassettes containing the sections were photographed for reference, paraffin embedded, and routinely processed. Slides were cut at 5μm thickness and stained with hematoxylin and eosin (H&E) and Masson's trichrome. All slides were digitally scanned at 20x on a Hamamatsu NanoZoomer 2.0-HT whole slide imager (Hamamatsu Corporation; Bridgewater, NJ).

Figure 1. Representative gross images of a GRMD heart showing the whole heart (A), the basal cross section with LV and RV dilation (B), and all ventricular cross sections (C).

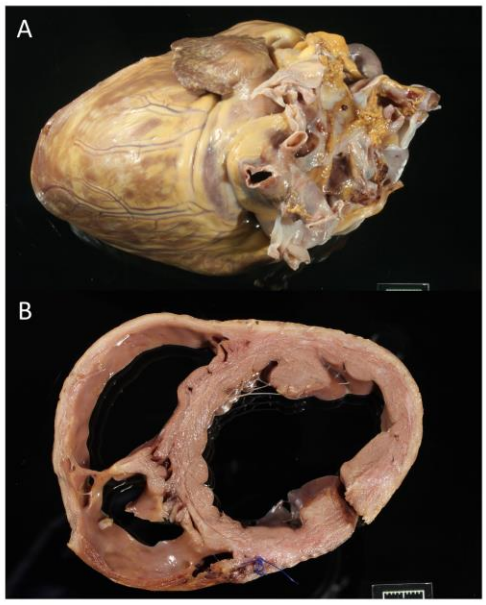

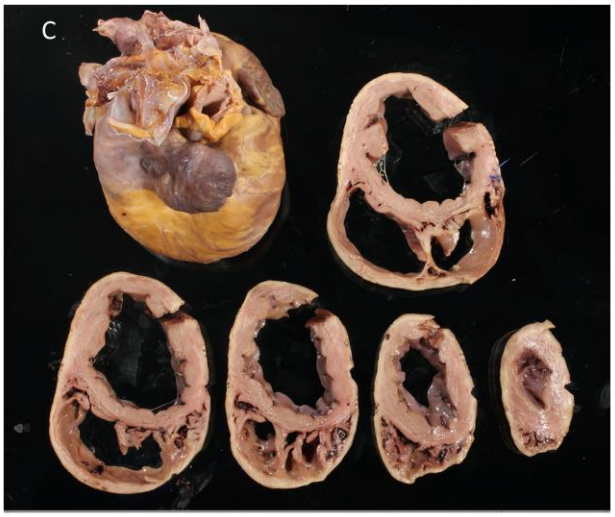

Table 1. Averages of gross heart measurements for GRMD, Carrier and Normal dogs.

	Averages (±SD)								
Group (N)	HW [g]	BW [kg]	LV [cm]	RV [cm]	Septum [m]	HW/BW [g/kg]	RV/LV	LV/Sept	LV/HW [mm/g]
GRMD (26)	118.04 (±50.92)	15.43 (±7.47)	1.09 (±0.27)	0.46 (±0.14)	0.98 (±0.25)	8.74 (±5.33)	0.43 (±0.11)	1.15 (±0.33)	0.11 (±0.04)
Carrier (5)	175.6 (±68.09)	15.32 (±3.22)	1.38 (±0.16)	0.66 (±0.05)	1.22 (±0.17)	12.32 (±6.44)	0.48 (±0.06)	1.14 (±0.12)	0.09 (±0.05)
Normal (7)	210.83 (±30)	25.09 (±0.9)	1.86 (±0.05)	0.9 (±0)	1.91 (±0.05)	8.48 (±0.10)	0.49 (±0.04)	0.99 (±0.09)	0.09 (±0)
GRMD subdivided by age group (N)									
<6m (5)	46.2 (±3.87)	7.16 (±1)	0.8 (±0.14)	0.3 (±0)	0.78 (±0.17)	6.52 (±0.62)	0.39 (±0.07)	1.05 (±0.21)	0.11 (±0.04)
6m to 1y (7)	109.86 (±17.14)	17.67 (±7.12)	1.19 (±0.2)	0.57 (±0.12)	1.17 (±0.22)	6.90 (±1.88)	0.48 (±0.07)	1.02 (±0.11)	0.1 (±0.01)
1y to 2y (4)	94.75 (±8.1)	16.78 (±6.1)	0.95 (±0.21)	0.39 (±0.05)	0.98 (±0.04)	6.36 (±1.96)	0.42(±0.06)	0.97 (±0.19)	0.1 (±0.02)
All <2y (16)	86.19 (±30.21)	14.16 (±7.36)	1.01 (±0.25)	0.44 (±0.14)	1 (±0.24)	6.65 (±1.64)	0.44 (±0.08)	1.02 (±0.17)	0.09 (±0.04)
> 2y (10)	169 (±32.57)	17.46 (±7.2)	1.23 (±0.25)	0.5 (0±.12)	0.95 (±0.25)	12.09 (±7.16)	0.43(±0.15)	1.37 (±0.39)	0.09 (±0.02)

Table 2. Averages of histologic changes for groups.

Group (N)	Semi-Quantitative Average Lesion Score	Frequency for Individual Lesions Listed					
		Fatty Infiltration	Inflammation	Acute necrosis	Mineral	Vascular changes	Purkinje fiber vacuolation
GRMD age groups (N)							
<6m (5)	0.33	-	-	-	-	-/+	+
6m to 1y (7)	0.85	+	+++	+	+++	++	++
1y to 2y (4)	0.73	+	++	+	+	+	+++
> 2y (10)	1.63	++++	++	-/+	+++	++	++
Carrier (5)	0.55	++++	+	-/+	+	+	+
Normal (7)	0.30	+	+	-/+	-	+	+

The second column from the left depicts semi-quantitative average score severity of all lesions taken together across LV and RV. Right six columns depict the percentage of all examined sections with the individual lesions listed: - = 0, -/+ < 0.5, + = 0.5-20, ++ = 20-30, +++ =30-40, ++++ > 40.

Microscopic pathology

The digital slide images were evaluated by a single pathologist (Schneider) using two methods to assess disease severity. Each section was given an overall semi quantitative grade for approximate percent of cross-sectional area affected by histopathologic lesions, generally following the system described by Kane et al. 2013[43] (0 = none, 1 = 1 to 10%, 2 = 11-20%, 3 = 21 to 30%, and 4 > 30%). These scores were averaged across sections and groups for statistical comparisons (Supplement 3). In a second method, individual histopathologic lesions were scored as absent/present and notations were made for the nature of some changes. Lesions assessed included: fatty infiltration absent/present); acute necrosis (absent/present); inflammatory infiltrates (none, primarily histiocytic inflammation, or primarily lymphoplasmacytic inflammation); mineralization (absent/present); Purkinje fiber vacuolation (positive if >50 of fiber cytoplasm was affected by vacuolation) and the nature of vascular changes

(none, fibrosis, wall hypertrophy, and intimal hypertrophy). For quantifying these changes, a modified "+" approach was used, whereby - = 0, -/+ < 0.5, + = 0.5-20, ++ = 20-30, +++ =30-40, ++++ > 40 percent of the examined sections with lesions (Tables 2 and 3).

Trichrome slides were quantitatively analyzed for percentage fibrosis. The NDPI files for each slide were exported as a JPEG at 5x magnification using the NDPI to OME-TIFF Converter v1.5 (https://matthias-baldauf.at/software/ndpi-converter/). These JPEGs were cropped in Graphic Converter (http://www.graphic-converter.net/) to remove duplicate tissue sections and large blood clots. The final JPEGS were analyzed in ImageJ using batch macros (Supplement 1).

Additionally, the primary localization of lesions within each segment was classified as being either subepicardial (outer 1/3), midmyocardial (middle 1/3), subendocardial (inner 1/3), or panmyocardial (evenly distributed across the wall) (Figure 2).

Table 3. Semiquantitative scores for individual dogs.

Age (m) and sex	Semi-Quantitative Overall Lesion Score	Frequency for Individual Lesions Listed					
		Fatty Infiltration	Inflammation	Acute necrosis	Mineral	Vascular changes	Purkinje fiber vacuolation
GRMD							
3 F	0.2	-	-	-	-	-	+
3 F	0.4	-	-	-	-	-	+++
3 F	0.58	-	-	-	-	-/+	-
3 M	0.16	-	-	-	-	-	-/+
3 M	0.22	-	-	-	-	-/+	+++
10 M	0.19	-/+	-/+	-	-	+	++++
11 F	1.05	++	++++	-/+	++++	+	-
11 M	0.3	-/+	+	-	-	+	++
12 F	1.47	++++	++++	-/+	++++	+++	+++
12 F	0.76	-	++++	++++	++++	++	-/+
12 F	1.39	-	++++	++	+++	+	+
12 M	0.81	-	++	+	+	++	++++
15 M	0.67	-	+	-	-/+	+	++
17 M	0	-	-	-	-	+	++++
21 F	1.29	++	++++	+	+	+	++
21 F	0.95	-/+	++	-/+	+	+	+++
28 F	1.93	+++	++	-/+	+++	+	-
36 M	0.95	++++	+++	-/+	++++	-/+	++++
38 M	1.19	++++	+	+	-	+++	++++
40 F	1.74	++++	+	+	++++	+	+
40 F	1.95	++++	-	-	+++	++++	-
40 M	1.86	++++	+	-	+	++	++
45 F	2.26	++++	+	-	++++	++++	+
51 M	2.38	++++	++++	-	+	+	++++
76 M	1.07	++++	++++	-	++++	++++	-
76 M	1	++++	+	-	+	+	++
Carrier							
3 F	0.13	-	-	-	-	-	-
12 F	0.05	+	-/+	-	++	+	+
46 F	1.4	++++	++++	+	+	++	-
56 F	0.37	++++	-	-	-	+	-
65 F	0.80	++++	+	-/+	-	++	+
Normal							
22 F	0.38	+	-	-/+	-	-	+
36 F	0	-	+	-	-	+	-/+
46 F	0.68	-/+	++++	-	-	-/+	-
61 M	0.14	-	-	-	-	+	+
75 F	0.35	+++	-/+	+	-	+	++
102 F	0.09	+	-	-	-	-/+	-
124 M	0.45	++	+	+	-	-	-

The second column from the left depicts semi-quantitative average score severity of all lesions together across LV and RV. Right six columns depict the percentage of all examined sections with the individual lesions listed: - = 0, -/+ < 0.5, + = 0.5-20, ++ = 20-30, +++ =30-40, ++++ > 40.

Figure 2. Fibrotic lesions were not always evenly distributed within the wall. In both GRMD dogs and DMD boys, the sub-epicardial myocardium is sometimes preferentially affected (A). However, other locations within the wall may predominate (B and C) Subendocardial changes are rare and were only seen in the RV when observed (C).

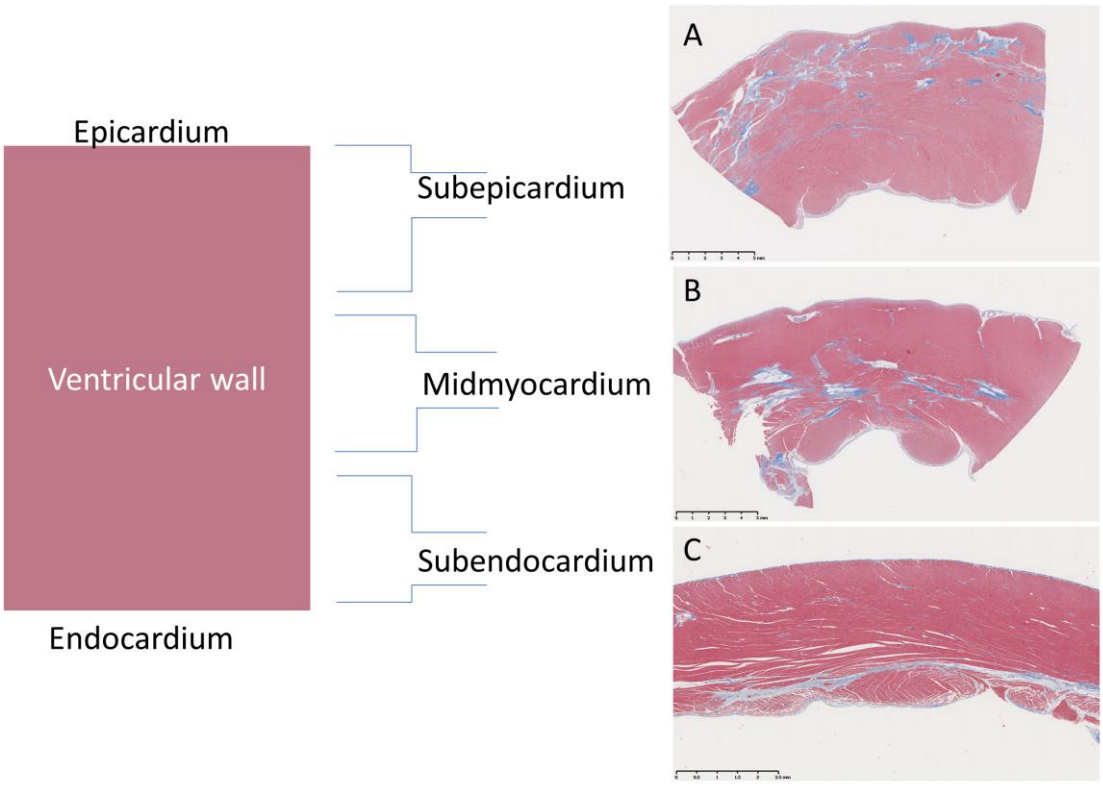

Cardiac magnetic resonance imaging (CMR)

Dogs were premedicated intramuscularly with atropine sulfate (0.04 mg/kg) followed by acepromazine maleate (0.02 mg/kg) and butorphanol tartrate (0.4 mg/kg), masked with Sevoflurane (4–5%) to allow intubation, and then maintained under anesthesia with Sevoflurane (2–3%) during the scanning period. Premedications were avoided during induction in dogs with signs of congestive heart failure. All CMR scans were performed on a 3 Tesla MRI machine (Siemens 3T Magnetom Verio, Siemens Medical Solutions, Erlangen, Germany) with dogs in a dorsal recumbent position. A

cardiac dedicated surface coil was used with ECG or pulse-oximetry gating systems. Breath hold or free breathing sequence was selected based on the dog's anesthetic status. Three long-axis (two, four, and three chamber) views and a series of short-axis views, from the LV base to apex, were scanned using fast low angle shot imaging (FLASH) or true fast imaging with steady-state free precession (TrueFISP) sequences to generate the cine images. Late gadolinium enhancement (LGE) imaging was performed 10 minutes after injecting 0.2 mmol/kg gadolinium intravenously. The two and four chamber long-axis and LV short-axis views were collected using a phase sensitive inversion recovery (PSIR) sequence for LGE imaging.

A semi-quantitative method was developed to assess LGE lesions in CMR. We identified 16 myocardial segments from the short-axis LGE images by modifying American Heart Association (AHA) standards for myocardial segmentation.[121] The apex was excluded because of imaging overlap between the apex and sternum. The degree of LGE in the 16 myocardial segments was scored from 0 to 2 to indicate enhancement levels ranging from none (dark and black, 0) to either intermediate (grey, 1) or marked (bright and white, 2). The higher score indicated the segment was more enhanced by gadolinium, suggesting extracellular matrix expansion secondary to myocardial fibrosis. The LGE scores and myocardial segments were used for further analysis.

Statistics

Descriptive statistics were calculated for each variable, including gender and age. Gross measurements were averaged for groups and means were compared with t-tests. F-test two-sample for variance between groups was performed to compare variability in

HW/BW ratios. Sections of the heart were categorized into 25 regions for comparisons (as described above, 17 LV segments, 4 RV segments, the left and right atria, the atrioventricular node, and the sinoatrial node). One-way analysis of variance (ANOVA) was conducted comparing the mean and standard deviation of fibrosis percentage and semi-quantitative lesion scores across all regions of the heart. ANOVA was also used to compare fibrosis percentage among GRMD, carrier, and normal specimens. Ordinal logistics regression was used to determine if the ordered independence variable, age, was associated with an increase in semi-quantitative cross-sectional lesion score. The average number of sections with changes was calculated for each of fatty infiltration, acute necrosis, inflammation, mineralization, and Purkinje fiber vacuolation. An ANOVA was then used to compare frequency of these changes among GRMD, carrier, and normal as well as between GRMD age groups for each feature. An independent-sample t-test comparing fibrosis percent was calculated stratified by gender. An ordered logistic regression was performed comparing a rise in semi-quantitative lesion and vascular scores. To evaluate the correlation between the two assessments a Spearman's test was used to compare average LGE and average pathological scores of the LV sections of the heart. Finally, a Chi-squared test was used to compare the semi-quantitative scores between LGE and pathological assessments for each section. Statistics were calculated using STATA 15 (College Station, TX) and Microsoft Excel (Redmond, WA). Spearman's test and Chi-squared analyses were run on JMP Pro 12 (SAS Institute Inc., Cary, NC).

Results

Gross findings

No gross lesions were noted in dogs less than 6m of age. Most older dogs had multiple lesions that varied in severity and distribution. Of the dogs from 10-12m of age, 5/7 had gross changes including LV (3/7) or RV pallor and streaking (1/7) and foci of fibrosis or mineralization in the papillary muscle (3/7). Only 1/7 had clear concomitant LV and RV dilation on gross exam. In the four 12-24m dogs, one each had RV or LV dilation (1/4). All 10 dogs > 24m had gross changes, including LV dilation (7/10); RV dilation (4/10); atrial dilation (2/10); thinning of the ventricular walls (2/10); and pallor and streaking in the LV (6/10), RV (3/10), septum (3/10), or pallor with mineralization in the papillary muscle (3/10). For carrier dogs, 4/5 (all >12 m) had gross changes, including thickening of the LV and septum (3/5), right auricle enlargement (1/5), and LV and septal pallor and streaking (1/5).

T-tests were used to compare means of gross measurements among groups (Table 1). For comparison of body weights (BW), heart weights (HW), and ventricular wall measurements, the immature (<6m) dogs were excluded unless otherwise noted. This was done because these dogs (and their hearts) were smaller due to immaturity and HW/BW are naturally increased in immature dogs compared to adult dogs even when normal.[123] The normal hounds were significantly heavier (25.09±0.09kg) than either the carrier (15.32±3.22kg) or adult GRMD dogs (17.4±6.98 kg; $p<0.001$ for both); carrier and adult GRMD BW was not significantly different. Similarly, average HW differed among groups, with adult GRMD (135.14±41.05 g) < carrier (175.6±68.9 g) < normal

(210.83±0.05g), but only normal and GRMD were significantly different ($p<0.001$) (Table 1). To better account for the effect of body size on heart weight, HW/BW ratios were calculated and did not differ among GRMD (8.74 ±5.33), carrier (12.32 ±6.44), and normal dogs (8.48 ±0.10) when comparing all ages or when comparing only dogs >6m (9.27 ±5.80) (Table 1). Results for individual dogs are included in Supplement 2.

F-test two-sample for variance was done to compare variability in HW/BW ratios in the dogs. Interestingly, GRMD dogs >2 y and carriers >1y had significantly greater variance in the HW/BW ratios than either normal dogs or GRMD dogs <2yr, reflecting the wide phenotypic variation and disease progression in older dogs. In the GRMD dogs >2y, HW/BW ratio ranged from 6.6 to 31.4g/kg (Table 1), with 4 dogs falling well above the previously reported range of 4.53 to 10.04g/kg in large adult dogs.[123] Similarly, the 3 carrier dogs >1 y (3.5 to 5.5y) had higher HW/BW ratios of 13.5 to 23.1g/kg. BW did not differ significantly between GRMD >2y and adult GRMD <2y, while HW was significantly higher in the older group (169±32.6g vs 104.4±16.2g; $p < 0.001$). This suggests that increased HW/BW ratio is driven by a relative increase in HW in the older dogs.

Average LV thickness varied significantly among groups with GRMD (1.09±0.27 cm) < carrier (1.38±0.16cm) < normal (1.86±0.05cm) ($p<0.05$) (Table 1). However, the ratio of LV to RV thickness did not differ among groups. Of the 5 carriers, 4 had relative thickening of the walls and papillary muscles on gross exam. However, when correcting LV thickness for overall HW, the groups were not significantly different (Table 1), which suggests hearts with thicker walls were proportionally heavier.

Semi-quantitative scoring of lesions in GRMD dogs

Using both H&E and trichrome images, sections were scored semi-quantitatively based on the total cross-sectional area percentage, as generally described by Kane et al. Sections of the heart were categorized into 25 regions for comparisons (as described above, 17 LV segments, 4 RV segments, the left and right atria, the atrioventricular node, and the sinoatrial node). Scores for individual sections for GRMD dogs varied from 0.7 (several sites) to 1.4 (basal anterolateral) (note, from the Methods above, a score of 1 = 1 to 10% and 2 = 11-20% affected cross sectional area). Those for carriers were lower, varying from 0.3 to 1.2, and sites of greater/lesser involvement did not correspond to GRMD. Normal dogs had lower values, ranging from 0.1 to 0.7. Overall average cross-sectional lesion area was higher in the GRMD vs normal dogs (1.02 vs 0.3; $p<0.001$). While the average score for carriers (0.6) was intermediate, it was not significantly different from either GRMD or normal dogs. On evaluation of one-way ANOVA comparing the average cross-sectional area score among sections, no section had a significantly higher or lower cross-sectional area score. Values for individual dogs and section averages are shown in Supplement 3.

Ordinal logistics regression was used to determine if the ordered independence variable, age, was associated with an increase in semi-quantitative lesion score. Scores for each section showed a highly statistically significant (<0.001) correlation with age, consistent with disease progression over time. Due to low numbers in the age groups, lesion scores across the LV and RV sections within GRMD age groups could not be evaluated.

Fatty infiltration

Fatty infiltration (Figure 3 A and B) was a prominent feature in older GRMD and carrier dogs (Table 2). While percentage of affected sections in each normal heart ranged from 0 to 30%, GRMD and carrier dog >24m of age all had >50% of sections showing fatty infiltration and degeneration. In GRMD dogs >24 m, 195/232 (84%) of examined sections had fatty change. A similar percentage of sections (56/76 [74%]) in carriers also showed fatty degeneration, while only 18/149 (12%) of normal sections had this lesion. However, only the differences between GRMD and normal dogs were significant ($p < 0.01$), probably because of the GRMD dogs > 24 mrelatively low number of carriers.

Fatty infiltration and degeneration increased with age, but was not observed in any dog <6m. Within the GRMD group, dogs > 24m had a significantly higher proportion of sections with fatty infiltration (84.05%) than any of the younger groups (0% 6m, 14.75% 6-12m, 16.95% 12-24m; $p<0.001$) (Table 2). The same was likely true for carriers, in which only 2 sections in one dog <12m had fatty infiltration, although numbers were too small to determine significance. No normal dogs were less than 22 m; the oldest 3 normal dogs had the highest number of affected sections in this group (Table 3).

Figure 3. Fatty infiltration was a prominent feature in some older GRMD dogs. (A) A section of LVFW with large bands of fat replacing normal myocardial muscle, and predominating over fibrosis. In some cases, fatty infiltration was more diffuse (B). In several dogs, the RV showed striking mid-myocardial replacement by bands of fat with minimal fibrotic tissue (C). Trichrome staining, 10x magnification.

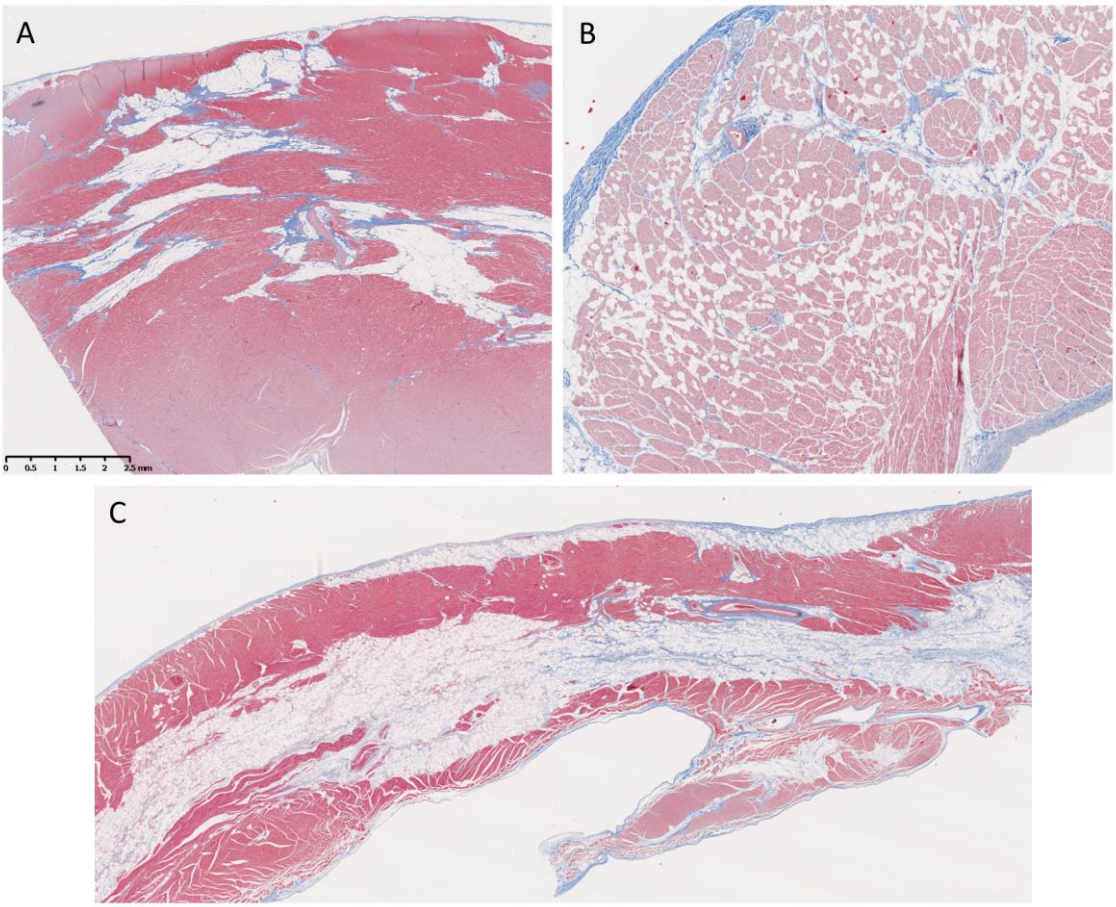

Fatty replacement of the mid-myocardium was a prominent feature of the RV in some GRMD dogs (Figure 3C), with only small bands of muscle remaining on either side of a central section of adipose tissue. This pattern of replacement was not observed in the left ventricle, where patchy areas of fat tended to surround vessels and be mixed with areas of fibrosis (Figure 3A).

Acute necrosis

Of the 26 GRMD dogs, 0/5 dogs (0%) <6m, 5/7 dogs (71%) 6-12m, 2/4 dogs (50%) 12-24m, and 4/10 dogs (40%) >24m of age had at least one section with acute coagulative necrosis (Figure 4). Nearly half the GRMD dogs with this change (5/11) had three or more sections with acute necrosis. The majority of dogs with acute necrosis (7/11) were 6-24 m, pointing to the relatively early onset of this lesion. Acute necrosis was found at least once in the various examined sections (17 LV and 4 RV), with no one section of the heart having a higher likelihood of lesions. Acute necrosis was not found in the atria. Incidentally, 3/7 normal dogs and 2/5 carrier dogs, each greater than >24m, also had at least 1, but no more than 3 sections, with acute necrosis (Table 3).

Figure 4. Coagulative myocardial necrosis was a feature in some dogs. (A) Areas of infarct-like coagulative necrosis characterized by loss of cytoplasmic detail and maintenance of tissue architecture (stars) are surrounded by proliferating macrophages and pericytes (arrows); H&E, 5x magnification. (B) Acute coagulative necrosis with loss of nuclei and hypereosinophilic cytoplasm (representative cells with stars); cells on the margins of lesions have granular basophilic mineralization (arrows). H&E, 20x magnification.

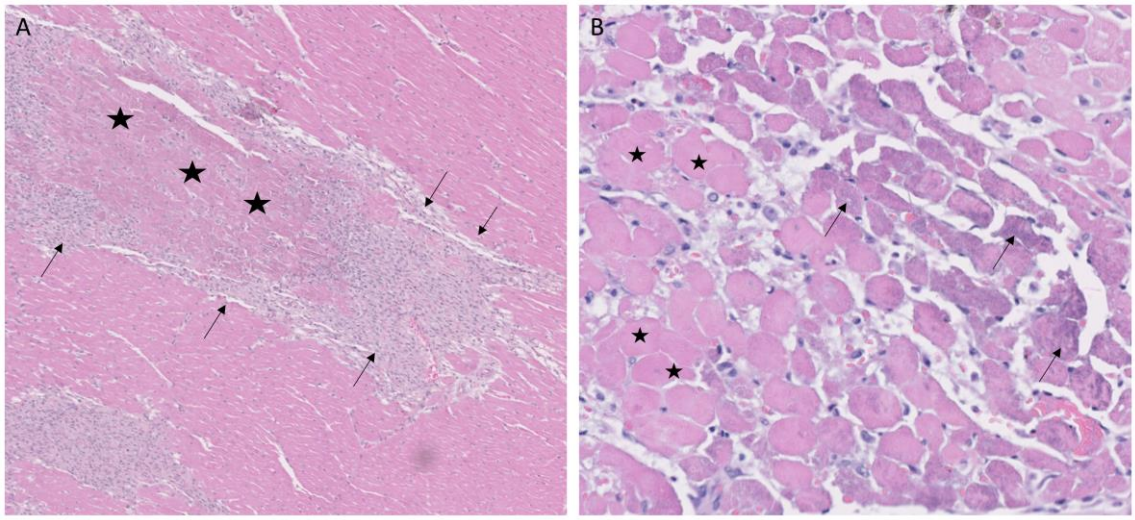

One 12m F GRMD dog had markedly more affected sections, with 14/27 heart segments having foci of acute myocardial necrosis. This dog had an incident of marked abdominal breathing and dark urine following an episode of anesthesia for wound treatment at ~6 m of age. She was euthanized at 1y of age while under anesthesia as part of a non-cardiac study.

Inflammation

Inflammatory cells were seen in all disease groups and did not differ among ages, even if the youngest dogs were excluded (Table 2). While the overall scores for inflammation among normal, GRMD, and carrier dogs did not differ, there were differences in the types of cells. Normal dogs had lymphoplasmacytic infiltrates, with one 46m old dog having infiltrates in almost every examined section. Although normal dogs were euthanized for non-cardiac lesions, two dogs initially examined for the study were excluded due to chronic Chagas disease detected histologically and by PCR. *Trypanosoma* was not detected in the remaining dogs, but exposure with associated lesions cannot be ruled out, and may explain the unexpected inflammation. Conversely, carriers and GRMD dogs had few sections with lymphoplasmacytic infiltration (4 in all the examined dogs), with a predominance of histiocytic inflammation. Histiocytic inflammation is typical secondary to degeneration and acute necrosis, initially occurring within 48 hours, and peaking around 6 to 10 days, with slow resolution as the tissue remodels.[124]

Interestingly, when comparing age groups, dogs <6m had significantly fewer sections with inflammation (no inflammation) than 10-12 m and >24m dogs ($p < 0.05$

and $p < 0.01$), but were not significantly different from the small group of 12-24m dogs. Dogs 10-12m trended toward more inflamed sections than 12-24m dogs ($p=0.054$), while dogs > 24m had significantly more affected sections than 12-24m dogs ($p <0.05$). However, the 10-12m dogs and >24m were not different from each other. This is likely due to the small numbers and relatively mild disease seen in the 12-24m age group in our study.

Mineralization

No mineral was noted in the hearts of normal dogs. All GRMD dogs >10m had mineral in at least 1 section with the exception of a 17m male that had few lesions of any type (Table 3). The average number of sections containing mineral differed significantly ($p < 0.05$) among the age groups of GRMD dogs (<6m, [0 sections, no detectable mineral], 6-12 m [8.4 sections]; 12- 24m [2 sections], >24m [8.8 sections]). Low numbers in the 12-24m group likely reflect the relatively mild lesions in this age group in our study, as the degree of mineralization has previously been shown to decline with age.[26] Two of five carriers also had mineral in at least one section.

Purkinje fibers

Previous studies described but did not score the severity of Purkinje fiber vacuolation starting at under 6m in the GRMD (CXMDJ) heart.[47] Degenerative changes have also been described in Purkinje fibers of DMD boys.[125] We scored Purkinje fiber vacuolation as present if vacuoles affected 50% or more of overall fiber cytoplasm (Figure 5). Of the 26 GRMD dogs, 4/5 dogs (80%) <6m, 6/7 dogs (86%) 6-12m, 4/4 dogs (100%) 12-24m, and 7/10 dogs (70%) >24m had at least one segment with

vacuolation. GRMD dogs had significantly increased fiber vacuolation (avg. 6.9 affected sections; range 0-19) compared to both carriers (1.4 sections; $p<0.01$) and normal dogs (1.6 sections; $p<0.01$) (Tables 2 and 3). Purkinje fiber vacuolation did not differ between carrier and normal dogs nor among age groups in the GRMD cohort. Unlike the previous $CXMD_J$ study, some GRMD dogs had no Purkinje fiber vacuolation detected. Moreover, vacuolation was not correlated with age or either semi-quantitative or quantitative lesion scores in the heart. Indeed, vacuolation was marked in some of the youngest dogs, which otherwise had no lesions. Comparison of H&E slides among groups did not show an appreciable visual difference in the vacuoles when present. The sinoatrial and atrioventricular nodes did not have observable abnormalities with H&E and trichrome staining.

Figure 5. Purkinje fiber vacuolation in the heart of a GRMD dog. Paler staining Purkinje fibers (outlined) with large vacuolation (arrows). H&E, 20x magnification.

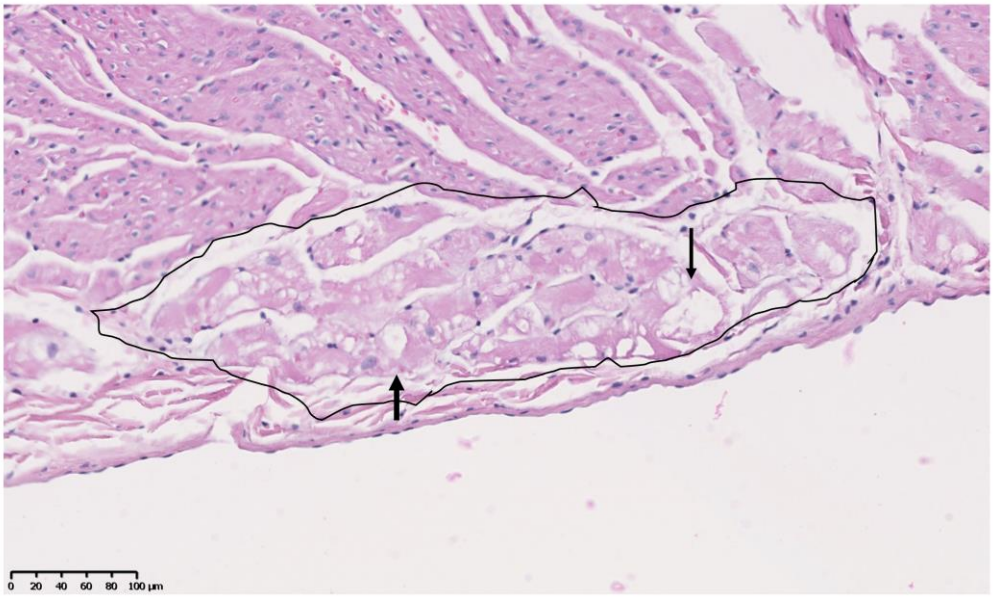

Vascular changes

Vascular changes of fibrosis and medial hypertrophy (Figure 6) were evaluated. Hearts from GRMD dogs <6 m had only rare changes. Those from adult (>6m) GRMD dogs had significantly greater vascular wall hypertrophy than normal dogs (5.2 vs 1.7 sections; $p<0.01$). Although low numbers prevented detection of difference between normal and carrier dogs, two of the carriers had hypertrophy in twice as many sections as the highest normal dogs. Inclusion of more carriers would likely have shown significant differences.

Figure 6. (A) Increased fibrous tissue (blue) in an arteriole of a normal dog. Trichrome, 5x magnification. (B) Marked medial and intimal hypertrophy and vascular proliferation in arterioles in the heart of a GRMD dog. H&E, 5x magnification.

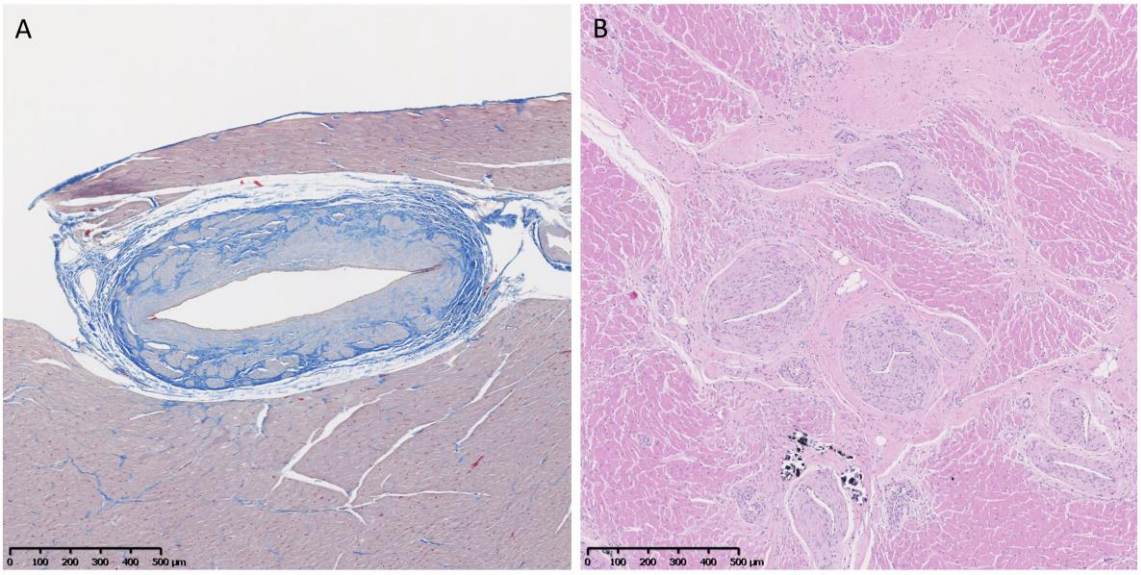

Ordered logistic regression comparing a rise in the semi-quantitative cross-sectional score (which does not include vascular changes) and vascular scores in GRMD

dogs showed a highly significant association between arteriolar hypertrophy and a rise in semi-quantitative severity score. For every 1-point increase in the vascular score, there was a 0.32 rise in the semi-quantitative severity score (z score = 3.91, p <0.001). Although correlated, it is not clear if either is causative, or if both represent a cumulative increase in degenerative changes with age.

Additionally, aortic mineralization was a prominent feature in GRMD dogs, with 11/26 having prominent mineralization in the aorta: 0/5 <6m, 4/7 6-12m, 1/4 12-24m, and 6/10 >24m of age. Aortic mineralization was not noted in the carriers, while 2/7 of the oldest normal hounds had much smaller mineral deposits in the aortic wall.

Although endothelial hypertrophy was described in one dog by Valentine et al., it was not detected in this study.

Quantitative fibrosis

An analysis of variance was performed to assess the relationship between disease status and percentage of cross-sectional area fibrosis as measured by trichrome staining. Data from all age groups, including more mildly affected dogs <6 m, were included. All three groups were significantly different (p <0.001); carriers had greater fibrosis (mean 9.82±1.01% blue staining) compared to GRMD at (7.84±0/25%), while normal dogs (4.35±0.26%) had the lowest percentage. An independent t-test indicated no difference between the sexes in fibrosis.

Additionally, the degree of fibrosis staining differed significantly among GRMD age groups as determined by one-way ANOVA (f score = 15.01, p <0.001). A Tukey post-hoc test revealed that the mean value at 6-12m (5.38±3.54%) was significantly

lower than all other groups ($p<0.05$), and that the 12-24m group had the highest degree of fibrosis (9.80±8.31%), being higher than even the >24m group (8.28±5.23%; $p<0.05$). Lower values in the oldest dogs could reflect greater fat, which is not detected in a trichrome stain, with proportionally lower fibrosis.

A one-way ANOVA was conducted to determine if fibrosis staining differed among ventricular sections (17 LV and 4 RV) for GRMD dogs. There was a statistically significant difference between groups (f score = 7.64, $p <0.001$). A Tukey post-hoc test revealed that the RV sections had the highest levels of fibrosis compared to the other sections, but were similar among themselves ($p<0.001$). Mid anterolateral LV had significantly lower fibrosis than other sections.

Localization of lesions within the wall.

Previous studies of GRMD[26] and DMD[31] describe a diffuse cardiomyopathy with sometimes prominent sub-epicardial localization of fibrosis and other lesions. We scored the predominant localization in each section as primarily sub-epicardial, mid-myocardial, sub-endocardial, or transmural (even distribution across the myocardial wall) (Figure 2). Consistent with the previous observations, degenerative lesions were initially concentrated in the outer half of the myocardium (the sub-epicardium and mid-myocardium or the RV portion of the septum wall). In older dogs, more sections had transmural lesions, as might be expected in a progressive disease. In general, the basal and septal sections had a greater degree of outer (or sub-epicardial) lesions, while the RV and more apical portions had a more diffuse/transmural distribution overall or, as

described above, a prominent mid-myocardial distribution, particularly in the more apical RV.

Correlation with cardiac MRI and LGE

Correlating specific histologic findings with diagnostic imaging and functional measures is the ultimate goal in better tracking cardiomyopathy progression. CMR with late gadolinium enhancement (LGE) is a promising modality for clinical assessment of cardiomyopathy in GRMD and DMD.[126] Eight GRMD dogs in this study had been evaluated with CMR and LGE within one month prior to heart collection, allowing retrospective comparison of the results. The Spearman's test was used to compare average LGE score and average semi-quantitative score of the LV (excluding the apex), to evaluate the correlation between two assessments. Chi-squared test was used to compare the semi-quantitative scores between LGE and pathological assessments for each segment.

Comparing the average LGE score of the entire LV with the average semi-quantitative score, Spearman's test showed a positive correlation between LGE and pathological assessments ($r = 0.7748$; $p < 0.05$). By further using the chi-square test to evaluate the correlation between the two semi-quantitative methods (LGE and pathology) in each section, the correlation was identified (likelihood ratio: 42.701; $p = <0.0001$). A higher LGE score was highly correlated with a higher (worse) semi-quantitative pathology score for each section.

Discussion

The DMD cardiomyopathy is classically defined as a dilated cardiomyopathy,

with lesions and functional changes being more pronounced in the LV versus RV.[3,12,31] Prior studies of the GRMD cardiomyopathy have been limited by either the number of dogs studied or the number of anatomical sections assessed.[26,32] The current study describes the gross and histologic lesions across the heart in a large cohort of GRMD dogs ranging from 3 to 76m in age. Like the previous studies, we did not see an overall increase in HW/BW ratio typically associated with hypertrophic cardiomyopathy. However, the HW/BW ratios of some GRMD and carrier dogs were 3 to 4 times higher than the normal range.[123,127] While decreased BW due to muscle atrophy in GRMD dogs could contribute to increased HW/BW ratio, there was little difference in BW among the groups. On the other hand, HW increased in the oldest GRMD and carrier dogs. HW was not directly correlated with age in the adult dogs. Taken together, these findings suggest that elevated HW/BW ratios in affected and carrier hearts occurred due to eccentric cardiac hypertrophy seen in canine dilated cardiomyopathy.[128] Additional measurements, including average fibers size diameter and cardiomyocytes number would be necessary to confirm this.

Similar to other studies,[26,32,49] in assessing specific histopathologic changes, lesion severity tended to increase with age. But, despite this general trend, some older dogs had few if any lesions (Table 3), in keeping with the marked phenotypic variation seen in the DMD cardiomyopathy. Previous histologic and pre-mortem imaging studies have suggested that lesions of cardiomyopathy in DMD boys and GRMD dogs first appear in the basoinferior portion of the left ventricle.[31,126] Lesion scores generally showed 10-20% cross sectional involvement of all areas of the heart assessed in GRMD

dogs, reflecting uniform disease. Carrier hearts had lower levels of involvement, with normal dogs having even lower scores. The lack of regional involvement may have occurred because multiple dogs were assessed at a single time point rather than longitudinally. The fact that many of our dogs were older and had lesions in all examined sections, and that there were relatively few dogs in the potentially critical 12 to 24m age range group, may also have prevented detection of regional differences in lesion development.

We quantified fibrosis using the trichrome stain. When assessing adult dogs, those at 6-12m had significantly less fibrosis than either of the two older groups, as expected. However, unexpectedly, the >24m dogs had less pronounced collagen staining than those at 12-24m, even though half of these younger dogs had relatively mild lesions. Lesions such as fat, non-compact fibrosis, and mineralization, do not stain blue with trichrome. Fat, in particular, increased in the older dogs, which likely accounted for the proportionally lower level of collagen staining. Importantly, this demonstrates that methods aimed solely at fibrosis detection may underestimate phenotypic severity in older GRMD dogs. Semi-quantitative scoring of total cross-sectional lesion area as well as the percent of sections showing various lesions more clearly demonstrated a strong correlation with age and disease progression. This scoring also highlighted the large phenotypic variation of cardiac lesions in GRMD dogs, similar to the variation in skeletal muscle disease.[23] In particular, one 17m GRMD male had no lesions.

Even more than fibrosis, fatty infiltration was a feature of cardiomyopathy progression in older GRMD dogs. While some degree of fatty infiltration may be seen

with normal aging, this change was particularly pronounced in the GRMD dogs and is seen with other chronic canine cardiomyopathies.[128–132] Lipomatous (fatty) metaplasia is also seen with chronic degenerative conditions in the hearts of dogs and humans, most frequently with chronic ischemic cardiomyopathy and ischemic scar replacement[133,134] and is associated with an increased propensity for ventricular tachycardia and arrhythmias.[129,135] Although we cannot rule out a specific response to dystrophin deficiency, the occurrence of similar fatty change in a variety of diseases suggests this change is a general reaction to chronic myocardial degeneration and remodeling.

Notably, we have seen a syndrome of acute myocardial infarction in GRMD dogs and a similar condition has been described in DMD.[118,136] This has led to speculation that dystrophin deficient cardiomyocytes are operating in a state of functional hypoxia,[107,136,137] and that dystrophin deficient muscle has a reduced capacity to compensate for increased metabolic demands.[103,138] Coagulative necrosis is associated with anoxia/hypoxia, and often seen subsequent to ischemia, infarction, or toxicosis, rather than ongoing degeneration. Lesions are detected histologically at ~12-24 hours post-event, become infiltrated by sheets of macrophages within 48-72 hours, and contain foci of interstitial cell and vascular proliferation by 10 days to 6 weeks.[139] We found each of these lesions in all GRMD age groups older than 6m, in keeping with the full range of cardiac necrosis and healing described by Malvestio et al.[49] Considering that vascular thrombosis is not a feature of DMD/GRMD, these changes more likely occur secondary to non-occlusive hypoxia. Extending the potential significance of vascular/hypoxic disease in GRMD cardiomyopathy, we also found a positive

correlation between arteriolar hypertrophy and worse semi-quantitative lesion scores that did not include vascular changes. Dystrophin-deficient mdx mice also have enhanced neointimal formation, with wall thickening and narrow lumens due to vascular smooth muscle proliferation.[140] In principle, these changes could occur due to chronic degenerative lesions in dystrophin-deficient smooth muscle and might be a factor in the acute myocardial syndrome seen in DMD/GRMD. While increased wall thickness and connective tissue are a reported aging change in cardiac arterioles of senescent dogs,[141] the normal dogs in this study had significantly less smooth muscle hypertrophy than GRMD dogs, indicating this change is part of disease progression.

Dystrophin deficiency in vascular smooth muscle in both mdx mice and GRMD dogs has been shown to have functional consequences, including altered sympathetic vasoregulation and reduced attenuation of vasoconstriction during contraction.[140,142–145] This change is partly due to loss of sarcolemmal nNOS in skeletal and cardiac muscle, leading to decreased nitric oxide induced vasodilation. However, selective expression of dystrophin in vascular smooth muscle partially rectified vasoregulatory responses[145] in mdx mice, suggesting smooth muscle dystrophin may have a primary functional role in vasoregulation. In combination with the types of degeneration seen in the hearts of GRMD dogs of our study, these vascular changes could support the "two hit" hypothesis for lesions in dystrophin deficiency,[146] with functional ischemia related to altered vasoregulation combined with increased susceptibility to metabolic stress leading to impaired myocyte survival.

Stereotypical ECG abnormalities are a feature of a large percentage of DMD and

GRMD patients. Purkinje fibers are modified cardiomyocytes that function as part of the cardiac conduction system. Like other cardiomyocytes, dystrophin is normally expressed in Purkinje fibers, and is lost in dystrophinopathies. Degenerative changes in the Purkinje fibers of affected boys[125] and dogs[47] have been proposed as a possible contributing factor to ECG abnormalities. Urasawa et al.[47] described marked abnormal vacuolation in Purkinje fibers associated with ultrastructural degenerative changes in young crossbred beagles with the GRMD mutation ($CXMD_J$). We also detected increased Purkinje fiber vacuolation, starting with the youngest GRMD dogs, though this lesion was not present in all GRMD dogs and normal dogs also had Purkinje fiber vacuolation. Interestingly, carrier dogs of this study did not have Purkinje fiber vacuolation, even though they also have conduction abnormalities[43]. Additionally, vacuolation did not correlate with cross-sectional lesion severity in our dogs. Given the retrospective nature of this study, ECG was not available for correlation with conduction differences or increased arrhythmia.

The pattern of LGE changes in DMD patients tends to parallel the distribution of histopathologic changes, beginning in the LV posterior basal and subepicardial wall.[126] Because we were still optimizing our technique, our LGE imaging quality was insufficient to localize lesions to the subepicardial region, pathological results were consistent with the LGE findings. Moreover, semi-quantitative assessments for histopathologic lesion score and LGE severity also correlated, further validating the association between our pathologic and cardiac MRI findings. As with the Purkinje fiber changes, we didn't have an opportunity to determine whether there was an association

between ECG findings such as the occurrence of deep Q waves with septal fibrosis. This would require a detailed longitudinal prospective study.

While data reported here substantially extended prior pathologic studies of the GRMD cardiomyopathy, there were limitations, mainly relating to its retrospective nature. Weaknesses included our inability to perfectly match the ages of dogs across disease groups, the low number of carrier dogs, and the necessity for using control normal hearts from dogs outside the colony. Although there may be minimal differences between hearts of normal dogs from within or outside, variable housing and management could have altered the cardiac phenotype. For instance, we were surprised by the finding of inflammation in normal hearts.

Conclusions

This study provides the largest comprehensive gross pathologic and histopathologic review of GRMD cardiomyopathy to date. Our findings highlight differences in disease severity and suggest, at least in our hands, semi-quantitative scoring is preferable to fibrosis quantification for assessing overall lesion severity. The severity of the semi-quantitative histopathologic changes correlated positively with LGE and the degree of vascular hypertrophy. Fatty infiltration was particularly pronounced in older dogs. Finally, the nature of some lesions suggested functional hypoxia or non-thrombotic ischemia may contribute to disease progression.

BRAIN-DERIVED NEUROTROPIC FACTOR (BDNF) AND OSTEOPONTIN (SPP1) ARE ASSOCIATED WITH CARDIOMYOPATHY IN GOLDEN RETRIEVER MUSCULAR DYSTROPHY

Introduction

Duchenne muscular dystrophy (DMD) is an X-linked disease in which loss of the structural protein dystrophin leads to progressive skeletal and cardiac muscle degeneration. Death most frequently occurs from cardiopulmonary complications in the third decade of life.[3] While skeletal muscle involvement delays the age at which early functional ambulatory milestones are reached, cardiomyopathy does not manifest clinically until adolescence.[8,12] The later onset of cardiac disease suggests that protective pathways may spare the heart,[16] at least initially, or, alternatively, other genes may predispose to greater skeletal muscle involvement. Importantly, conflicting results have been found on whether skeletal and cardiac muscle disease track together. A 1978 paper by Heymsfield et al.[12] showed no association between cardiac indices and manual muscle testing, concluding that "DMD may progress at different rates in heart and skeletal muscle."[12] More recently, skeletal muscle parameters were shown to track with cardiac indices,[117,147] including serum N-terminal pro-brain natriuretic peptide (NT-proBNP.)[147]

Studies in animal models provide a platform to both define biomarkers that track with disease and also better understand disease mechanisms contributing to differential skeletal and cardiac muscle involvement.[10] Golden retriever muscular dystrophy (GRMD) is a phenotypic and genotypic homologue of DMD.[23,26] While the mdx mouse

has minimal cardiac involvement,[27] cardiac changes in GRMD dogs develop detectable pathologic lesions beginning around 6-12 months,[23,26] mirroring those seen at adolescence in DMD. These changes are associated with electrocardiographic and echocardiographic abnormalities in affected dogs.[33] Ultimately, both DMD patients and GRMD dogs develop progressive dilated cardiomyopathy characterized by predominantly subepicardial fibrosis, more severe left ventricle (LV) involvement, and eventual reduced ejection fraction and heart failure.[26,33]

In an effort to screen potential genetic modifiers involved in the distinctive phenotypes seen in skeletal and cardiac muscle of DMD and GRMD patients, we assessed expression of a group of five genes, utrophin (UTRN),[148,77–79,81] osteopontin (SPP1),[67,73,74,83–86] matrix metalloproteinase 9 (MMP9),[74,87–90] a disintegrin and metallopeptidase domain 12 (ADAM12),[91–94] and brain-derived neurotropic factor (BDNF)[16,50,149,150] in the hearts of a large cohort of GRMD, carrier, and normal dogs. These five genes have all been shown to modify phenotypic severity in either dystrophin-deficient mice, humans, and/or dogs. In particular, BDNF was recently found to be preferentially up-regulated in a small group of GRMD dogs [6 dogs with age matched controls and 3 older dogs] and DMD boys and serum levels correlated with ejection fraction in DMD patients.[16,50] In addition to a larger group of normal controls, we also assessed expression of these genes in carrier hearts, which have a chimeric expression of dystrophin and variable cardiac lesions in both dogs and women.[40,41,43,120]

Large animal studies often suffer from small cohorts, due to the limited availability of animals. We aimed to confirm that BDNF was upregulated in GRMD

versus normal dog hearts in a much wider group of animals than the earlier study,[16,50] including more normal and carrier dogs that have chimeric expression of dystrophin plus a broader age range. We hypothesized that carriers would have intermediate gene expression and that gene levels would differ across age groups. Additionally, since disease occurs later in the heart and the LV is preferentially affected, at least initially,[26] we also hypothesized that expression of BDNF and the other genes would differ in the LV compared to the right (RV) ventricle, a hypothesis which has not been previously tested. Based on differences noted via qRT-PCR, western blots were performed for SPP1 and BDNF in a subset of normal and affected dogs and previously collected ejection fraction data were compared to mRNA expression.

Materials and Methods

Animals

Dogs were housed and cared for according to principles outlined in the National Research Council Guide for the Care and Use of Laboratory Animals. Studies were performed at both the University of North Carolina-Chapel Hill (UNC-CH) and Texas A&M University (TAMU) with defined institutional SOP's approved by the respective IACUC committees. In our standard necropsy procedure, samples of the left (LV) and right (RV) ventricular free walls were harvested immediately and snap frozen at -80^{o}C. The remaining largely grossly intact heart was then immersion fixed in formalin for later pathologic assessment.

There were two sets of real-time quantitative reverse transcription polymerase chain reaction (qRT-PCR) experiments and one western blot study. In an initial study, a

total of 41 dogs were examined by qRT-PCR: 7 normal, 6 carrier, and 28 GRMD dogs, ranging in age from 3 to 76 months (Table 4). A near even split existed between hemizygous GRMD males (n = 20; 48.75%) and homozygous females (n = 21; 51.25%), with a mean overall age of 23.8 months. Hearts became available when dogs were euthanized at the end point of separate studies, or due to disease progression (defined as an inability to maintain sternal recumbence or progression to intractable heart failure).

Table 4. Population characteristics for PCR of GRMD, carrier, and normal dogs.

Characteristics	**N (%)**
Disease Status	
Normal	7 (17.1)
Carrier	6 (14.6)
GRMD	28 (68.3)
Gender (GRMD)	
Male	13 (46.4)
Female	15 (53.5)
Age (range in months)	**Mean±SD**
All dogs (3-76)	23.8±21.07
Normal (6-12)	9.4±3.0
Carrier (3-65)	35.8±25.4
GRMD (3-76)	24.3±20.5
GRMD age groups	**N (%)**
0-3	5 (17.8)
11-24	13 (46.4)
Over 24	10 (35.7)

In a second qRT-PCR study, both LV and RV samples were obtained from a larger group of 16 normal control dogs euthanized for non-cardiac reasons, including an

additional 9 made available through a tissue sharing program at the TAMU College of Veterinary Medicine. These dogs ranged from 6 months to 10 years of age, with a mean±SD of 42.5±38.00 months (Supplement 4). For sake of analysis, these normal dogs were further divided among three age groups: 0-10, (n = 3; 19.35%), 11-24 (n = 5; 29.03%), and > 25 months (n = 8; 51.61 %).

Based on the differences seen in gene expression, BDNF and SPP1 protein levels were examined by western blot in 7 normal and 14 GRMD dogs. Samples from each ventricle were assessed in all but one dog in which only LV was available. Normal dogs were all male, with 3 at 6 months and 4 at 12 months of age. For GRMD dogs, genders were approximately even (6 hemizygous males and 8 homozygous females) and age groups were balanced with 5 dogs ~ 3 months, 5 dogs ~ 12 months, and 4 dogs > 40 months of age.

RNA isolation

LV and RV free wall sections were harvested immediately after euthanasia, snap frozen in liquid nitrogen, and stored at -80ºC to preserve RNA**.** Two hundred mg of frozen myocardium was homogenized in 3ml of Tripure using an IKA T10 basic Ultra turrax homogenizer. Total RNA was extracted using the Tripure method following the manufacturer's protocol (Roche Diagnostics GmbH, Mannheim, Germany). After extraction, concentration was measured on a NanoDrop 200c UV-Vis Spectrophotometer (Thermo Fischer Scientific, Wilmington, DE). Next, a 10ug aliquot of RNA from each sample was DNase treated using Ambion's "DNA-Free kit" (Life Technologies, Carlsbad, CA), and concentration was again measured on the NanoDrop.

Separate 100ng aliquots were prepared for reverse transcription and 3ul of each sample were sent to the Texas A&M Center for Translational Environmental Health Research (CTEHR) Genomics & Bioinformatics Facility Core for quality testing (RNA Integrity Number [RIN] ≥ 7) on an Agilent 2100 Bioanalyzer (Agilent technologies, Waldbronn, Germany).

Reverse Transcription

Samples were reverse transcribed using Invitrogen's SuperscriptII reverse transcriptase kit (Life Technologies, Carlsbad, CA). Briefly, 100ng of DNase treated total RNA was reverse transcribed with random octamer primers and oligo dt. This mixture was incubated at 65°C for 5 min and then cooled to room temp. Next, 10ul 5 times first strand buffer, 5ul 0.1M DTT, 1.0ul RNase block (Superasin), 2.5ul 10mM dNTPs, and 2.0ul SuperscriptII Reverse Transcriptase were added; the sample was mixed; and then centrifuged briefly and incubated at 37°C for 1 hr. The reaction was terminated by heating at 90°C for 5 min. The reverse transcribed samples were stored at -20°C.

Real Time PCR

We designed forward and reverse primers (Supplement 5) for the genes of interest (UTRN, SPP1, BDNF, ADAM12, and MMP9) using Primer Express 3.0 software from Applied Biosystems. Samples for qRT-PCR were run in triplicate on 384 well plates using the Power SYBR green protocol (Applied Biosystems, Foster City, CA) on a 7900HT Fast Real-time PCR system by Applied Biosystems. A cross-platform of

SYBR Green PCR arrays found that this modality delivers results highly comparable with other methods including TaqMan PCR and high-density microarrays.[151]

Two housekeeping genes (hypoxanthine phosphoribosyl transferase [HPRT][152] and glyceraldehyde-3-phosphate dehydrogenase [GAPDH]) were tested using previously designed primers. Bartlett's test for equal variances was used to assess HPRT and GAPDH across the different strata of disease status, muscle location (LV or RV), and age categories. HPRT produced non-significant results when compared across normal, carrier, or GRMD samples ($Chi^2 = 2.79$, $p = 0.249$), LV and RV ($Chi^2 = 1.58$, $p = 0.209$), and different age categories ($Chi^2 = 1.64$, $p = 0.44$). GAPDH had comparable variances across disease status ($Chi^2 = 2.11$, $p = 0.349$) and muscle location ($Chi^2 = 0.06$, $p = 0.806$), but not for different age categories ($Chi^2 = 14.21$, $p < 0.001$). Accordingly, HPRT was used as the housekeeping gene to normalize Ct gene expression for each dependent variable.

Protein Extraction

Archived tissue stored at -80ºC was used for protein studies. Protein was extracted from approximately 0.5 to 0.25 g of frozen LV and RV (one dog < 6 months had only LV to evaluate) using the Santa Cruz protein tissue prep protocol (Santa Cruz Biotechnologies, Dallas, TX). Briefly, ~0.5 g of frozen tissue was thawed in RIPA buffer containing 10ul/ml of protease and phosphatase inhibitor cocktail (Peirce biotechnology, Rockford, IL) homogenized at 4ºC, incubated in the buffer for 30 minutes and then centrifuged at 10,000 x g for 10 min at 4ºC. Protein concentration of this total cell lysate was evaluated using the BioRad RC DC protein concentration assay (Bio-Rad

Laboratories, Hercules, CA) and measured on the NanoDrop using the Lowry setting and a 2nd order polynomial standard curve.

Western Blots

Western blots were run on 12% StainFree gels (Bio-Rad laboratories, Hercules, CA) with 50µg protein per lane. Gels were blotted to Amersham's Hybond P 0.45 PVDF membrane. Running buffer and transfer buffer were prepared from recipes provided by BioRad. Blots for SPP1were blocked over night at 4ºC in 5% BSA 0.1%TBST, and hybridized with primary antibody SPP1 (Rockland Inc. Limerick, PA; catalog # 100-401-404S, rabbit polyclonal osteopontin antibody), diluted 1:100 in 5% BSA 0.1% TBST overnight at 4ºC. Blots were washed in 0.1% TBST per protocol. Blots for BDNF were blocked over night at 4ºC in 5% milk 0.1% PBST and primary antibody (Aviva Systems Biology, San Diego, CA; ARP4169_P050, Rabbit polyclonal BDNF N-terminal Region antibody), diluted 1:1000 in 5% milk 0.1% PBST overnight at 4ºC. Blots were washed in 0.1% PBST per protocol (3 times for 5 minutes). Both SSP1 and BDNF were hybridized with secondary antibody goat ANTI-rabbit (Abcam) diluted 1:5000 on a rocker at room temp for 1 hour. Developing was done with Supersignal West Pico PLUS Chemiluminescent substrate (Thermo Scientific), using 0.1ml working solution per cm^2 of membrane, per manufacturer's suggestion. The blots were exposed to film and run through the developing machine clearly showing the expected size of 27kDa (for BDNF) or ~35kDa and ~60kDa (for SPP1). Lanes and bands on the film were quantified using a Bio Rad Gel Doc EZ Imager.[153]

Ejection Fraction

This was a retrospective study intended primarily to assess cardiac gene expression. So to assess the potential clinical significance of cardiac BDNF and SPP1 gene expression, mRNA levels were correlated with LV ejection fraction (LVEF) from 9 GRMD dogs ranging from 9 to 77m. LVEF was calculated using Siemens Argus software (Siemens Medical Solutions USA, Inc., Malvern, PA) from 3 Tesla cardiac magnetic resonance imaging (MRI) scans (Siemens 3T Magnetom Verio, Siemens Medical Solutions, Erlangen, Germany) obtained within 1 month of tissue sample collection during an unrelated natural history study (data in preparation for publication).

Statistical Analysis

Two endogenous genes, HPRT and GAPDH, were separately analyzed for sake of normalizing the raw threshold cycle (Ct) expression data (see above). Variance was analyzed across strata of disease status, LV or RV, and age categories using Bartlett's test for equal variances. Chi-square and p-values were reported. HPRT was selected and used for final normalization.

Descriptive statistics were calculated for each variable, including sample characteristics of the cohort. The Ct value was transformed for each of the five genes of interest (BDNF, SPP1, MMP9, ADAM12, and UTRN) using HPRT gene to normalize the data. The transformation $2^{-\Delta\Delta Ct}$ was utilized, according to the approach outlined by Schmittgen et al.[154] Statistical analysis used the normalized transformed data.

The mean values of the transformed Ct expressions and standard deviations were calculated for each gene of interest. One-way analyses of variance (ANOVA) were

performed to assess for significant differences between gene expression among diseases status (normal, carrier, or GRMD), location (LV or RV), and sex (male or female). A two-way scatterplot was created, with corresponding Pearson R^2 coefficients and p-values, to determine correlation between fold change in gene expression and age (in months) for all five genes of interest. Regression analyses were performed to compare gene expression across EF values. Statistics were calculated using STATA 14 (StataCorp, College Station, TX) and Microsoft Excel.

For the normal dog qRT-PCR data set, standardized gene fold expressions failed to provide normally distributed data; therefore, the nonparametric test for equality of populations Kruskal-Wallis rank test was utilized. Distribution of dependent variables, while not normal, were consistent between groups, meeting the required assumptions for this method.

Results

Expression of mRNA across disease status, LV vs. RV, and age groups.

For the initial qRT-PCR, samples from both the LV and RV were assessed for all dogs, with the exception of one female and one male in which only one ventricular sample was available, giving a total of 39 dogs and 78 ventricular samples. GRMD hemizygous male and homozygous female mRNA expression did not differ so all dogs were considered as a group.

Disease groups. For BDNF in both ventricles, mean expression in GRMD was upregulated compared to carriers and normal dogs, and carriers were upregulated compared to normal samples (Figure 7). However, due partially to small sample

numbers and large confidence intervals, significance was only reached for BDNF in the LV for which GRMD levels (23.44±21.1) were over 8 times those of normal samples (2.64±2.0) and 7 times those in carriers (3.33±2.7) ($p < 0.01$ for both). Similarly, RV GRMD mean BDNF expression (7.40±14.5) was upregulated compared to normal (0.52±0.28) and carriers (2.07±2.77), although marked variance in GRMD expression levels and values precluded significance. SPP1, ADAM12, MMP9, and UTRN did not show significant differences across groups in either ventricle.

Table 5. Gene expression fold change between ventricles in GRMD and normal dogs.

	BDNF	**SPP1**	**MMP9**	**ADAM12**	**UTRN**
GRMD	**Mean±SD (N)**				
Left ventricle	23.44±21.1 (25)	8.66±9.7 (24)	2.23±3.99 (21)	1.52±1.3 (26)	2.23±1.7 (26)
Right Ventricle	7.40±14.5** (27)	7.58±10.7 2 (24)	2.82±4.57 (20)	1.57±1.38 (27)	2.14±1.76 (27)
Normal	**Mean±SE[a] (N)**				
Left ventricle	1.27±0.59 (12)	3.88±2.19 (13)	2.82±2.06 (8)	1.72±0.73 (13)	2.11±1.03 (13)
Right Ventricle	5.21±2.43 (13)	2.80±1.51 (14)	2.27±1.15 (8)	1.35±0.30 (14)	1.32±0.29 (14)

**$p < 0.01$;[a]Krukal-Wallis test used to compare gene-fold expression in normal dogs.

Figure 7. Boxplots of gene expression by disease status. Box plots compare the normalized mRNA expression levels in the LV and RV of WT, Carrier, and GRMD dogs. One-way ANOVA demonstrated significant differences in BDNF expression in the LV (A) of GRMD dogs (n=25; 23.44 +/- 21.05) compared to carrier (n=6; 3.33 +/- 2.71) and WT (n=7; 2.64 +/-2.01) animals. SPP1 expression in the LV appears upregulated, but low numbers and a high standard deviation precluded detection of significance. Values were similar between disease groups in the RV (A), with individual dogs having markedly increased BDNF, SPP1 and MMP9.

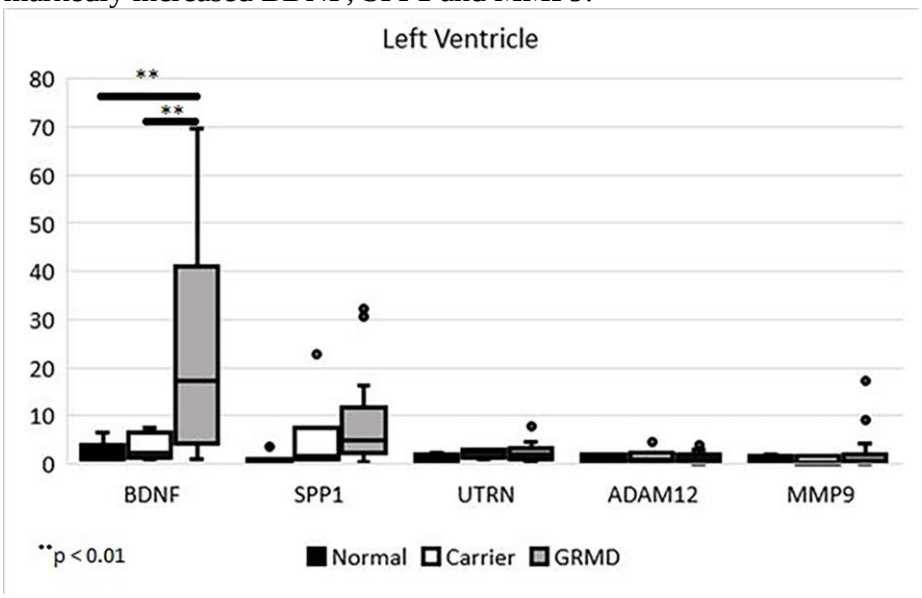

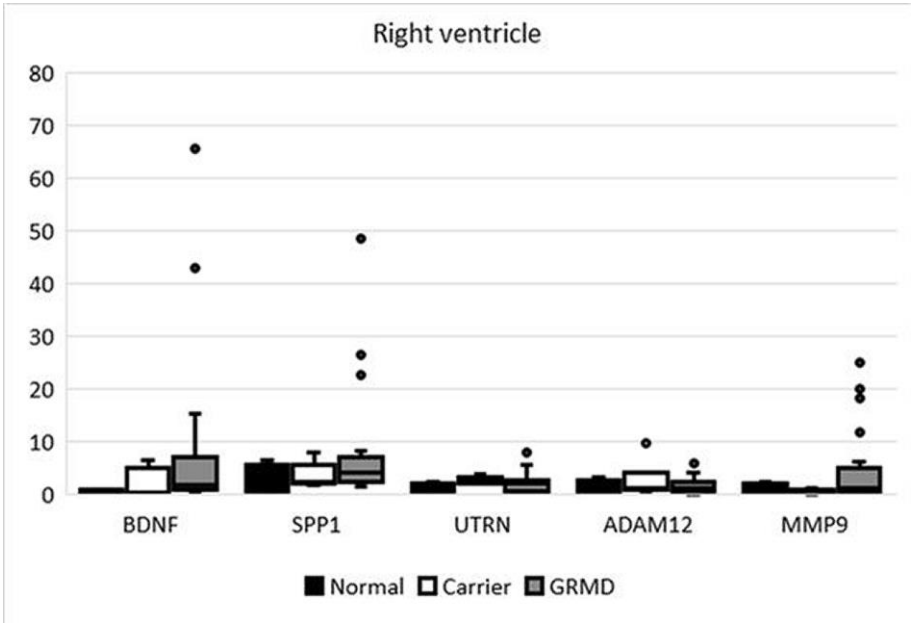

LV vs. RV. Gene expression levels were mostly similar in the LV and RV samples of GRMD and normal dogs, with the exception of BDNF, which was increased in GRMD LV (23.44±21.1) compared to RV (7.40±14.5; $p < 0.01$) (Table 5). A reverse pattern was seen for normal dogs, with values in the RV (5.21±2.43) being nearly 5 times those in the LV (1.27±0.59), but significance was not reached.

Figure 8. Two way scatterplots of age and normalized gene expression in GRMD LV for SPP1 (A), BDNF (B), UTRN (C), and ADAM12 (D). The mRNA expression in LV of 25 GRMD dogs was plotted against age with corresponding Pearson's r coefficients and p-values. (MMP9 was also plotted and was not significantly different). SPP1 (A) is positively correlated with age (r=0.413; p<0.001), while BDNF (B) (r=0.045; p=0.309), UTRN (C) (r=0.068; p=0.189), and ADAM12 (D) (r=0.010; p=0.632) were not significantly different across ages in the LV. MMP9 was also assessed, and not significantly correlated with age (graph not included).

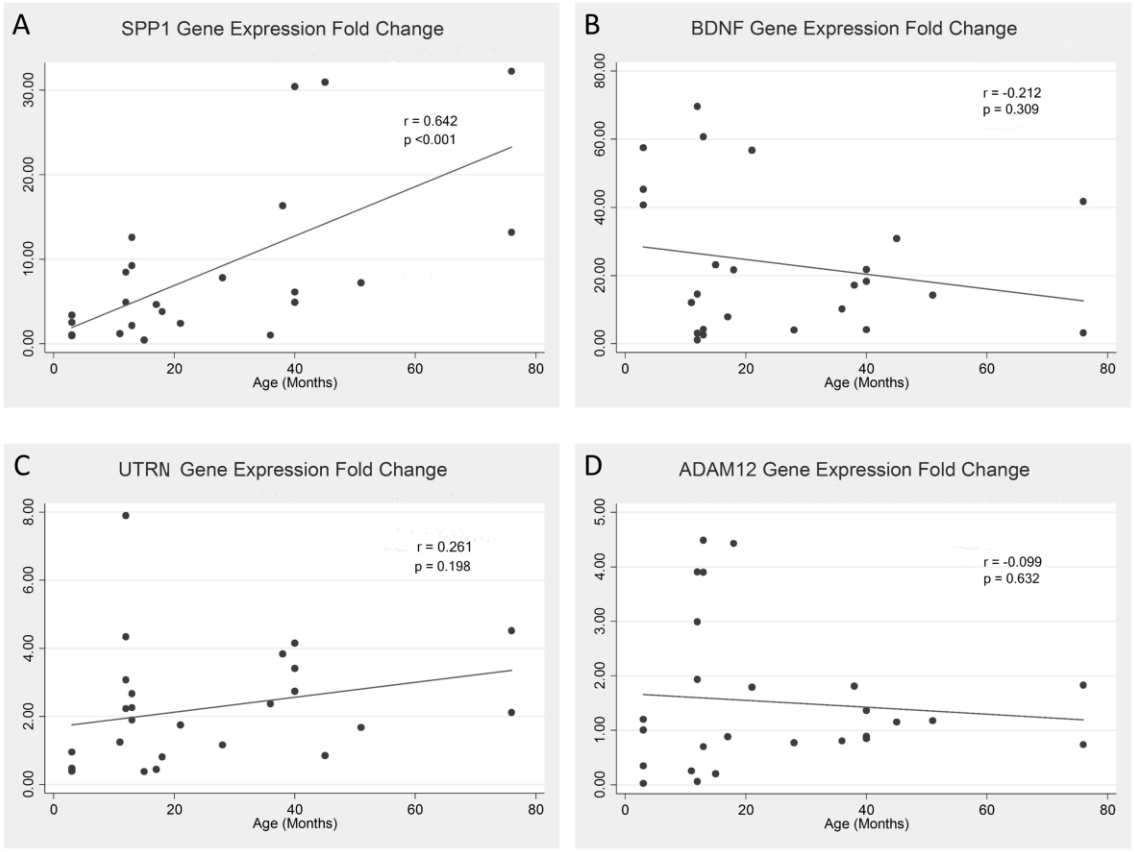

Age. Only SPP1 and UTRN differed significantly among the three age groups (< 12, 12-24, and >24 months) in GRMD dogs (Table 6), with LV levels for both being ~ 3 times higher in dogs > 24m versus < 12 m ($p < 0.05$ and 0.01, respectively). The relationship between age and gene expression was further illustrated by scatterplots for GRMD (Figure 8) and normal (Figure 9) samples. SPP1 expression in the LV also correlated positively with age for GRMD ($r = 0.642$, $p < 0.001$) and, to a lesser extent, normal ($r = 0.169$, $p < 0.05$) dogs. Notably, LV BDNF expression levels trended down with age for GRMD and up for normal dogs, although significance was not reached in either group.

Table 6. ANOVA Gene fold expression between age categories for GRMD status samples.

Age in months	BDNF Mean±SD (N)	SPP1	MMP9	ADAM12	UTRN
<12	21.94±21.89 (10)	4.16±6.21 (11)	3.34±4.04 (8)	1.16±1.70 (11)	0.76±0.65 ** (11)
12-24	17.38±23.21 (22)	5.01±3.25 (18)	3.52±5.67 (16)	1.98±1.54 (22)	2.45±2.12 (22)
>24	9.21±11.56 (20)	13.36±13.68* (19)	1.19±2.08 (17)	1.27±0.66 (20)	2.67±1.24 (20)

* $p < 0.05$ >24 vs 12-24 and <12; ** $p < 0.01$ <12 vs 12-24 and >24

Figure 9. Two-way scatterplots of age and gene expression in normal dog hearts for SPP1 (A), BDNF (B), UTRN (C), and ADAM12 (D). The mRNA expression in LV of 15 WT dogs was plotted against age corresponding Pearson's r coefficients and p-values. (MMP9 was not detected in enough normal samples for analysis). SPP1 (A) (r=0.169; p=0.022) was modestly, positively correlated with age and BDNF (B) (r=0.122; p=0.064) trended upward with age. UTRN (C) (r=-0.035; p=0.865) and ADAM12 (D) (r=-0.034; p=0.945) were not significantly correlated with age.

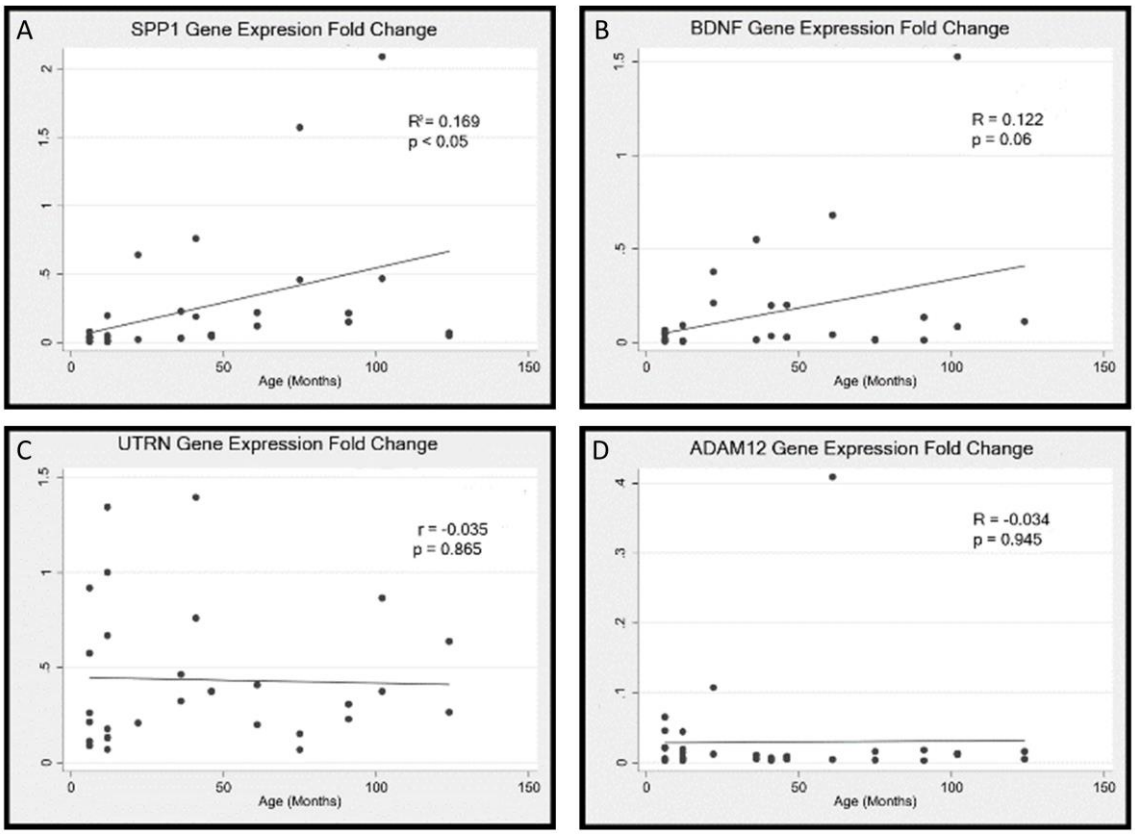

BDNF and SPP1 protein expression.

Two forms of SPP1, unconjugated (~35kDa) and conjugated (~60kDa), were identified. Levels were equally expressed and correlated with each other. Expression levels did not differ between males and females. Western blot images are in Supplement 6-8.

Disease groups. BDNF normalized densitometry values (NDV) (0.891±0.064) were significantly lower in GRMD RV than normal (1.424±3.14) ($p < 0.05$). While LV values were also lower in GRMD than in normal (0.386±0.088 vs. 0.638±0.492), the difference was not significant ($p = 0.242$). Similarly, NDV for SPP1 were lower in GRMD than normal in both the RV (0.908±0.341 vs. 1.379±0.142; $p < 0.05$) and LV (0.701±0.149 vs. 1.658±1.042; $p < 0.001$).

LV vs RV. GRMD BDNF was nearly 2.5 times higher in the RV (0.819±0.064) versus the LV (0.385±0.088) ($p < 0.01$). A similar but insignificant difference was seen in normal dogs (2.210±3.142 vs. 0.638±0.495; $p = 0.071$). SPP1 levels did not differ between ventricles for either group.

Age. GRMD BDNF protein expression positively correlated with age in the LV ($r = 0.56$) and negatively in the RV ($r = -0.59$) ($p < 0.05$ for both) (Figure 10). However, in an ANOVA comparison of the age groups (<6m, 12m, >40m), BDNF did not differ significantly in either ventricle. On the other hand, SPP1 did differ between all age groups in the RV, with levels in GRMD dogs at 12 months (0.422±0.16) being less than half those at either 3 months (1.48±0.037) or >40 months (1.09±0.046) ($p < 0.001$ for both); levels were also significantly higher in dogs at 3 versus >40 months ($p=0.001$). SPP1 only differed in the LV between dogs at 12 and >40 months, being higher in the older dogs (0.557±0.077 versus 0.857±0.031; $p<0.05$). Neither BDNF nor SPP1 differed in normal dogs between 6 and 12 months of age.

Figure 10. BDNF and SPP1 protein expression in GRMD LV and RV. BDNF protein expression was measured in the LV and RV of 14 GRMD dogs by western blots and normalized total protein. Dogs ranged in age from 3 to 42 months. BDNF was positively correlated with age in the LV (r = 0.56) [A] and negatively correlated with age in the RV (r = -0.59) [B]; $p < 0.05$ for both.

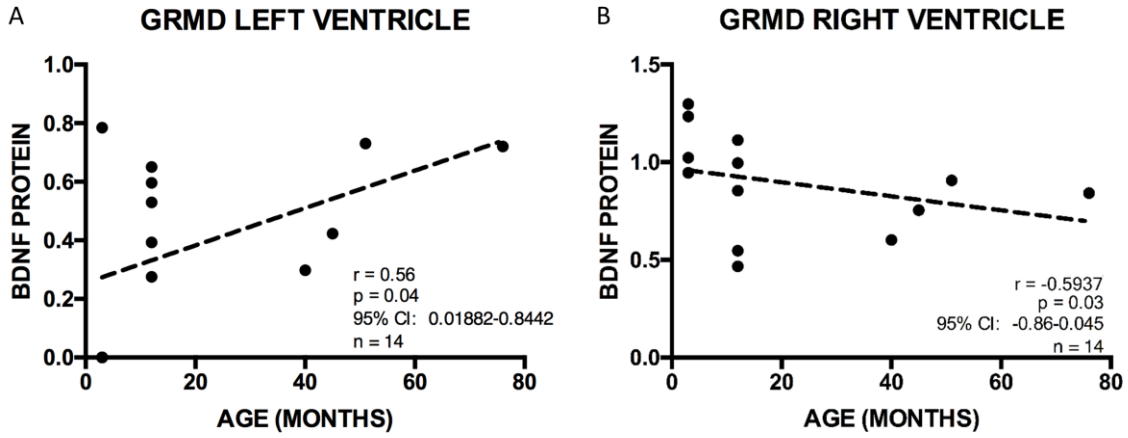

Comparison of mRNA expression with ejection fraction

This was a retrospective study and serum samples were not available. To gain insight on whether BDNF and SPP1 influenced cardiac function, we compared mRNA expression in both LV and RV in a cohort of 9 GRMD dogs aged 9-77 months to LVEF assessed by cardiac MRI within 1 month of tissue collection. Cardiac disease severity varied, with LVEF ranging from 9.8 to 65.4%. Protein expression was not compared as LVEF was only available for 3 dogs with accompanying protein lysates. While BDNF mRNA levels did not correlate with LVEF in GRMD dogs (LV r^2 =0.04; p =0.6; RV r^2 =0.09; p =0.44), LV expression of SPP1 correlated negatively (LV r^2 =0.65; p <0.01; RV r^2 =0.21; p =0.22). That is, as LVEF decreased with disease progression over time, SPP1 mRNA increased in keeping with findings in 3.1.3.

Discussion

This paper extends our previously published GRMD microarray study that identified BDNF and SPP1 as potential biomarkers for cardiac and skeletal muscle involvement, respectively.[50] The previous paper assessed BDNF and SPP1 in the LV of 9 GRMD dogs spread across three age groups (6, 12, and 47+ m; n = 3 for each) and an additional 6 normal dogs matched to the 6 and 12 month age groups. These relatively low numbers and the limited age range are consistent with many large animal studies, wherein low numbers and repeatability are perennial concerns. Findings reported in this current study substantially expand upon the earlier paper. Expression of three additional genes was assessed, providing context for the importance of BDNF and SPP1 as potential GRMD and DMD genetic biomarkers/modifiers. We also examined more GRMD (28 vs. 9) and normal (16 vs. 6) dogs from a broader age group and included carriers, providing insight on whether mosaic dystrophin expression influences the dystrophic cardiac genotype. Moreover, whereas the earlier paper only assessed the LV, we ran parallel tests in the RV, which is relatively protected in DMD. Finally, to better understand the impact of BDNF and SPP1 on cardiac function, mRNA levels from LV and RV were correlated with LVEF in a group of 9 GRMD dogs.

Consistent with the previous microarray paper,[50] BDNF mRNA was increased whereas protein was decreased in the LV of GRMD versus normal dogs. Similarly, SPP1 protein levels were lower than normal in both GRMD ventricles. This may be due to depressed metabolism and protein production overall in GRMD cells. BDNF and SPP1 serum levels were also assessed in GRMD dogs and DMD patients in the previous

microarray study. When compared to normal, BDNF was markedly higher in DMD patients overall and in 12-month-old but not younger or older GRMD dogs. We speculated that the lower LV protein and higher serum levels could be due to rapid BDNF release from the myocardium. Alternatively, this differential pattern might reflect a feedback mechanism, to include BDNF receptor density in the heart. As an example, while BDNF cardiac tissue levels did not differ between young and aged wild type mice, receptors were increased.[100] Future work should address blood levels as well the density and location of BDNF receptors in the dystrophic heart.

In our earlier microarray study, serum BDNF values in DMD tracked with higher LVEF and less fibrosis on cardiac MRI, suggesting a protective effect.[50] Serum SPP1 levels also trended higher in DMD and 12-month-old GRMD dogs compared to normal controls and there was an analogous but insignificant association between SPP1 and cardiac function in DMD patients. Serum was not available from dogs in the current study. Instead, we correlated mRNA levels with LVEF. While BDNF did not associate with cardiac function, LV SPP1 mRNA levels inversely correlated with LVEF consistent with its tracking with worsening cardiac disease and further substantiating its potential role as a cardiac biomarker.

Previous cardiac gene expression studies have focused mostly on the LV or have not specified the location. The predominant earlier and more severe involvement of the LV in DMD cardiomyopathy likely occurs due to its larger proportional size and attendant greater stress during cardiac contraction. Given this predominant involvement of the LV in both DMD and GRMD, differential LV versus RV gene expression might

be expected. Here, we evaluated mRNA expression of BDNF, SPP1, UTRN, MMP9, and ADAM12 and protein expression of BDNF and SPP1 in both the LV and RV in the same expanded group of GRMD dogs subdivided into three age groups. Consistent with its projected role in the pathogenesis of cardiomyopathy, BDNF mRNA expression was nearly three times higher in the LV than the RV in GRMD dogs. A reverse relationship was seen in normal dogs, with expression being almost twice as high in the RV, although low numbers precluded detection of significance. As with the comparative mRNA data for normal versus GRMD dogs, there was an opposite pattern for BDNF protein expression, with levels being nearly 2.5 times higher in the RV versus the LV for GRMD dogs. A similar but insignificant differential was seen in normal dogs.

We also hypothesized that BDNF and SPP1 expression would vary with age as cardiac lesions progressed. While neither BDNF mRNA nor protein levels differed across the three GRMD age groups, mRNA trended higher in older GRMD dogs and lower in normal dogs. Protein expression positively correlated with age in the LV and negatively in the RV. SPP1 mRNA expression in the LV also correlated positively with age for GRMD and, to a lesser extent, normal dogs. Protein levels of SPP1 in the RV at 12 months were less than half those at either 3 months or > 40 months and higher in the LV in dogs > 40 versus 12 months. Selective increases of BDNF and SPP1 in the LV and in older dogs would be consistent with attempts to delay or repair cardiac lesions.

Taken together, the distinctive pattern of BDNF expression between normal and GRMD dogs, the LV and RV, and across different age groups supports its role as a biomarker and also infers potential involvement in disease pathogenesis. BDNF has been

shown to have positive effects in many other human cardiac conditions, with roles in angiogenesis,[101] metabolic efficiency and inflammatory modulation,[155] as well as better outcomes in patients hospitalized for cardiomyopathy,[97,99] and is also associated with improved survival in some ischemic cardiac models.[102] We speculated that further insight on potential benefits of BDNF or other genes could be gained through studies of female carriers. Carriers of both GRMD[43,120] and DMD[156,157] have mosaic loss of dystrophin and associated lesions and functional defects in the heart. Gene and protein expression, beyond dystrophin, has not been studied in carriers, so it is unclear whether their expression is intermediate, as might be expected. In our study, BDNF mRNA levels were intermediate between normal and GRMD dogs but differences were not significant. Other genes did not differ in carriers and protein expression was not examined. As concerns about cardiomyopathy in carriers become more recognized, future studies should better characterize their cardiac gene and protein expression.

SPP1 was assessed, in part, to extend the earlier GRMD microarray study[16,50] that showed a selective increase of both mRNA and protein in skeletal muscle, but not cardiac muscle in age matched controls, and that serum levels correlated with manual muscle testing but not ejection fraction in DMD patients.[50] We had previously shown that SPP1 levels are increased in the cranial sartorius muscle of GRMD dogs, correlate with muscle size, and increase with age, seemingly tracking with disease progression.[158] The microarray paper had some trends to suggest SPP1 might track with cardiac disease progression, such as increased mRNA levels in the oldest affected dogs and a trend toward higher serum levels in GRMD versus normal dogs. However, that study did not

detect changes in protein levels in the LV, and mRNA levels were not correlated with LVEF. Thus, findings reported here more strongly suggest that SPP1 could be involved in the temporal evolution of the GRMD cardiomyopathy. Given the deleterious role that SPP1 generally plays in skeletal muscle, via its proinflammatory and fibrotic properties,[83,84,86] adverse effects might be expected in the heart. But, with skeletal muscle, SPP1 can also promote muscle regeneration through defined molecular mechanisms[83,159] and could play an analogous protective role in the heart. For instance, transplantation of an osteopontin peptide to the ventricular wall in a hamster model of cardiomyopathy was shown to improve cardiac function, in part through enhanced angiogenesis.[160] Our findings linking SPP1 to the pathogenesis of the GRMD cardiomyopathy complement this work and a recent mdx study[74] in which higher SPP1 was associated with increased MMP9. This led the authors to hypothesize that SPP1 induces expression of MMP9, leading to cardiac fibrosis. While our GRMD study was not intended to test this hypothesis, we found no increases in MMP9 in dystrophic canine hearts. And, rather than a deleterious effect, SPP1 LV mRNA tracked with increased LVEF in line with the earlier microarray study in which serum SPP1 protein seemed to associate with improved cardiac function, similar to BDNF.[50]

Proving further context for the importance of BDNF and SPP1 in cardiac gene expression and their roles as potential biomarkers of disease progression, we found few differences in expression of three additional genes, UTRN, MMP-9, and ADAM12, known to be associated with skeletal or cardiac muscle disease in GRMD and DMD. Among the five genes studied, only BDNF was differentially expressed between GRMD

and normal dogs and the LV and RV. Interestingly, UTRN was more highly expressed in older GRMD dogs, which could suggest it is upregulated with age. This would differ from an earlier study in which UTRN did not increase with age or treatment of GRMD dogs.[57] On the other hand, UTRN is increased in the skeletal muscle of dystrophic dogs, potentially as a surrogate for dystrophin.[81,148,161] Further testing, beyond the scope of this study, would be necessary to better understand utrophin's role in the heart.

Conclusions

Our findings support earlier microarray work suggesting that BDNF may be useful as a cardiac disease marker in GRMD dogs. While most of the genes had similar LV and RV expression, BDNF expression was driven by increases in the LV over the RV. Although low numbers precluded significance, BDNF values were also higher in carriers versus normal dogs. For the first time, we also showed a differential pattern of SPP1 expression that appeared to track with GRMD cardiomyopathy progression. Supporting the relative specificity of BDNF and SPP1 as DMD/GRMD cardiac biomarkers, UTRN, MMP-9, and ADAM12 were not differentially expressed in GRMD versus normal hearts.

GLUCOSE METABOLISM AS A PRE-CLINICAL BIOMARKER FOR THE GOLDEN RETRIEVER MODEL OF DUCHENNE MUSCULAR DYSTROPHY*[1]

Introduction

Duchenne muscular dystrophy (DMD) is an x-linked, progressive muscle wasting disease affecting ~ 1 in every 5,000 boys.[1] Mutations in the *DMD* gene lead to loss of the membrane protein dystrophin.[2] Membrane fragility causes myofiber degeneration and fibrofatty replacement, which leads to loss of ambulation in adolescence and eventual death, most often from cardiorespiratory complications.[162] In addition to, or as a consequence of, membrane fragility, dystrophin deficient muscle is under increased metabolic stress due to decreased glycolytic and oxidative enzyme expression.[103–108] There are also lower mitochondrial numbers, including some with abnormal structure, decreased intracellular ATP, and increased reactive oxygen species production. Studies in myoblasts suggest this metabolic derangement in dystrophic muscle may precede the stage when dystrophin would normally be expressed.[106] Nevertheless, these alterations in dystrophic muscle lead to a "metabolic crisis" and a reduced capacity to respond to metabolic demands such as muscle contraction.

Recent work has shown that the main glucose transporter in cardiac and skeletal muscle,[109] glucose transporter- 4 (GLUT4), is abnormally located in subcellular aggregates in DMD.[114] On the other hand, in the mdx mouse model for DMD, GLUT4

---

*Reprinted with permission from "Glucose metabolism as a pre-clinical biomarker for the golden retriever model of Duchenne muscular dystrophy" by S Schneider, V Sridhar, A Bettis, H Heath-Barnett, C Balog-Alvarez, L-J Gou, R Johnson, S Jaques, S Vitha, A Glowcwski, J Kornegay, P Nghiem; 2018, *Molecular Imaging and Biology*, vol 20, pp780-788, Copyright 2018 Springer Publishing

was found in membrane preps of a sub-cellular fractionation study, suggesting a compensatory mechanism.[114,115] GLUT4 translocation is controlled by both insulin and muscle contraction, which act through independent molecular pathways to increase cytoplasmic vesicle translocation to the cell membrane. GLUT4 transports back to the cytoplasm after insulin stimulation or contraction are withdrawn.[110] Since different vesicle pools of GLUT4 respond to insulin and contraction,[163–165] these two pathways may be cumulative. The membrane localization of GLUT4 in mdx mice may have functional significance, because dystrophic myofibers have an altered response to insulin.[114,163,164]

Dogs with golden retriever muscular dystrophy (GRMD) have a frameshifting *DMD* gene mutation, resulting in absent dystrophin.[69,166] The GRMD phenotype is more severe compared to mdx mice, suggesting that preclinical studies in affected dogs may better mirror anticipated outcomes in DMD. Specifically, GRMD dogs show a similar metabolic crisis in dystrophic muscle, with reduced glycolytic enzymes, decreased and abnormal mitochondria, and dysregulated AMPK expression.[103,167] We hypothesized that GRMD myofibers would have altered GLUT4 localization (similar to DMD muscle) and subsequent altered (reduced) glucose metabolism. Based on our initial findings, GLUT4 was surprisingly localized to the sarcolemmal membrane, which led to rapid clearance of blood glucose and increased muscle uptake of a glucose analogue. Our results suggest that glucose metabolism can be monitored and potentially utilized as a pre-clinical biomarker in GRMD dogs.

Materials and Methods

Animals

The dogs used in this study were part of a colony carrying the GRMD mutation. Animal care was governed by Texas A&M animal use protocol 2015-0110 (Standard Operating Procedures-Canine X-Linked Muscular Dystrophy) and principles outlined in the National Research Council's Guide for the Care and Use of Laboratory Animals. For the glucose tolerance testing (GTT) and PET-CT scans, we used 6 GRMD dogs (heterozygous male-4, homozygous female-2; 8 months [mo.] to 6 years [y] of age); 6 GRMD carriers (dystrophin +/-; 8mo to 6y) and 6 normal dogs (M-4, F-2, 6mo to 2y). Dogs were fed LabDiet Advanced Protocol High Density Canine dry or wet food (PMI Nutrition, St. Louis, MO).

MRNA Profiling

Quantification and analysis methods have been described previously.[152,168] We queried GLUT4 mRNA expression from previously performed genome-wide mRNA profiles from normal and GRMD dogs at 4-9 weeks and 6 mo. of age in the cranial sartorius (CS), long digital extensor (LDE), and vastus lateralis (VL) muscles. One probe set—Cfa.3539.1.S1_s_at— was identified for GLUT4.

RNA isolation and quantification

Total cellular RNA was isolated with Tripure reagent (Roche, Indianapolis, IN) from frozen skeletal muscle (LDE) and DNase treated with DNA-free kit (Applied Biosystems, Foster City, CA). The RNA concentrations in the individual samples were quantified using a NanoDrop 2000 spectrophotometer and assessed for quality on a 2100

Bioanalyzer (Agilent Technologies, Santa Clara, CA). The 16 RIN values ranged from 8.0-9.0.

Quantitative PCR analyses

Quantitative RT-PCR (qPCR) primers were designed for genes of interest (GLUT4, hexokimase-1 [HK1]) using Primer Express 3.0 software (Applied Biosystems, Foster City, CA). RNA samples from the microarrayed skeletal muscle (LDE)[152,168] were DNase treated and reverse transcribed with oligo-dT, random primers, and Superscript II (Invitrogen, Carlsbad, CA). The reverse transcription reactions consisted of 100ng of DNase treated RNA in a 50ul reaction, ultra pure H20, oligo dt (2.5ul of 500ng/ul) and random hexamer (0.48ul of 1mM stock) heated to 65 degrees for 5 minutes (min) and cooled to room temperature. The remaining reagents: Superscript II (2ul), 5X 1st Strand buffer (10ul), 0.1M DTT (5ul), 10mM dNTPs (2.5ul) and an RNase block Ambion's Superasin (1ul). All were heated to 37 degrees C for one hour and terminated by heating at 90 degrees C. for 5 min. QRT-PCR was performed in triplicate reactions with Power Sybr Green Master Mix. All assays performed on a 7900HT FastStart Real-Time PCR System (Applied Biosystems). Reactions were loaded on a MicroAmp Fast Optical 384 well plate (Applied Biosystems) and consisted of Power Sybr Green, 300nM of each forward and reverse primer, PCR grade water, and 0.5ul of each reverse transcription reaction (cDNA). The cycling parameters on the 7900HT machine were; 50 degrees C for 2 min, 95 degrees C for 10 min, and 40 cycling repeats of 95 degrees for 15 seconds and 60 degrees for 1 min with a dissociation curve added to validate primers.

Western blotting

Protein extraction, quantification, and analysis methods were described previously.[103] GLUT4 antibody (ab65267; Abcam; Cambridge, UK) was incubated with the PVDF membrane at 1:1,000 dilution in 5% BSA overnight at 4°C. Total protein on the pre-blotted PVDF membrane were used as the loading control to normalize GLUT-4 protein values.[169,170] Secondary rabbit anti-mouse IgG horseradish peroxidase antibody from Abcam (ab6728) was diluted to 1:5,000 in 5% BSA.

Confocal (immunofluorescence) microscopy

Sample preparation was described previously.[152] Muscle samples were taken by surgical biopsy or at necropsy from the LDE, CS, VL, cranial tibial, diaphragm, and left ventricle of the heart; muscles from a combination of seven normal and nine GRMD samples were analyzed. Samples were imaged with an Olympus (Waltham, MA) FV1000 laser scanning confocal microscope using 20x/0.85 and 100x/1.4 oil immersion objectives. Images were examined with Olympus Fluoview FV1000 software. GLUT4 antibody (ab65267), Anti-SPTBN1 (ab72239), and goat anti-mouse IgG H&L (Alexa Fluor 488; ab 150113) were from Abcam.

ImageJ (NIH; Bethesda, MD) 1.47v software was used for quantification of GLUT4 expression at the myofiber membrane in GRMD and normal muscle samples. Bitmap images taken at 20X objective were uploaded. For skeletal muscle analysis, a software-enabled standard default threshold was set for each image in color red with a dark background. The unit of length was set to "micron". Fluorescent particles were analyzed with measurements ranging from 50 microns^2 to infinity. The area and mean

fluorescence of all particles were summed and the normalized fluorescence was calculated per image (summed area/summed fluorescence). Normalized values for all GRMD and normal muscle images were compared. Since cardiac muscle fibers differs in morphology, we could not use the same methodology as for skeletal muscle. As such, we measured the mean and peak intensity of GLUT-4 signal across the cardiomyocyte membrane. An average of 10 cells per image for the mean and peak intensities were used per sample. GRMD was then compared to normal.

Intravenous (IV) glucose tolerance test (GTT)

Dogs were fasted for 15 hours (hr) prior to testing. Weights were taken the day of the procedure and catheters placed in both cephalic veins. After baseline glucose and insulin testing (0 min), each dog received a bolus of 50% dextrose solution intravenously (IV) at 1 g/kg body weight over 30 seconds. The opposite catheter was used for blood sampling. Three milliliters of blood were collected at 0 (pre-dextrose administration), 5, 15, 30, 45, 60, and 120 min post-dextrose administration. The samples were centrifuged within 30 min and the serum frozen at -80 degrees C for later analysis. Blood glucose (BG) was measured with a Gluco-quant Glucose/HK kit (Roche Diagnostics, Mannheim, Germany) on an AU480 analyzer (Beckman-Coulter, Brea, California). Blood insulin was measured by a radioimmunoassay kit (EMD Millipore Corp., St Charles, Missouri) on an ISO Data 20/20. Area under curve was calculated for glucose and insulin, as described previously.[171]

Positron emission tomography-computed tomography (PET-CT) acquisition

PET-CT and GTT testing were completed on separate days. Dogs were fasted

overnight and kept in a quiet transport cage prior to their scan to minimize excitement, which could influence glucose analogue uptake. Dogs were premedicated (intramuscular acepromazine 0.02 mg/kg, butorphanol 0.4 mg/kg, and atropine 0.04mg/kg) and catheters were placed in both cephalic veins. Affected and carrier dogs were induced with Sevoflurane administered via inhalation; normal dogs were induced with IV Propofol (5.5mg/kg, slowly to effect). All dogs were intubated and maintained on Sevoflurane with mechanical ventilation. Intraoperative SpO2, heart rate, and blood pressure were monitored with an Advisor vital signs monitor (SurgiVet, Norwell, MA) and a cuff on the rear limb continuously, with values recorded at 10 min intervals. Blood glucose was measured after anesthetic induction, just prior to IV administration of the radionuclide 2-deoxy-2-[18F]fluoro-D-glucose ([18F]DG; 0.05 to 0.1 mCi/kg of body weight), a glucose analogue shown to behave similarly to endogenous glucose. Insulin (0.05u/kg) was administered IV concurrently with [18F]DG to encourage intracellular uptake of the radionuclide.[172] Blood glucose was checked every 30 min. We took precautions to keep BG in the normal range (80-210 mg/dl) to prevent hypoglycemia, but also to prevent hyperglycemia, as the latter has been shown to interfere with radionuclide uptake. As such, BG levels were maintained between 70-100 mg/dl. A 10ml bolus of 50% dextrose was given IV if BG dropped below 80 mg/dl.

The PET-CT procedure was performed on a 128-slice Siemens Biograph PET/CT scanner (Siemens Medical Solutions USA, Inc., Malvern, Pennsylvania). Dogs were placed in sternal recumbence with the pelvic limbs extended behind them. They were scanned caudal to cranial beginning two-thirds down the tibia (closer to the hock

than the stifle) and progressing to the head with ~20cm steps, 5min/step, for seven steps total. A gated cardiac scan of the chest followed each full-body scan. The topogram prescription scout for the initial scan and the initial pair of PET scans began 5 min after [18F]DG and insulin administration, with a second set of scans at 1 hr. post administration.

Segmentation and analysis

PET-CT images were analyzed using the Inveon Research Workspace (Siemens Medical Solutions USA, Inc., Malvern, Pennsylvania). For the skeletal muscle analysis, the full body scans were reoriented so that the transverse view was perpendicular to the long axis of the femur and the sagittal and dorsal views were parallel to the sagittal and frontal long axes of the femur. Using the CT scout scan, the muscles were manually segmented at every 5th slice, and the whole muscle region of interest (ROI) was interpolated from these slices.[173] As our functional studies suggest that GRMD disease severity was similar between the left and right limbs, one limb from each dog was examined. The mean standard uptake value (SUV) of [18F]DG, maximum (max) SUV and standard deviation (SD) of SUV were measured for each of the CS, VL, and rectus femoris muscles at both 5 min and 1 hr post insulin/[18F]DG administration.

For the cardiac studies, all measurements were obtained using the 4th bin of the gated cardiac scans. Scans were first reoriented such that the transverse, sagittal, and dorsal planes corresponded to the short axis, horizontal long axis (4 chamber), and the vertical long axis (2 chamber) views, respectively. The hearts were analyzed with three methods: (1) a single spherical ROI was placed over the whole left ventricle (LV) to

record the max SUV; (2) the LV wall ROI was drawn: the window for PET was adjusted until the view showed an even uptake in the LV, then the slices in the LV were counted on the vertical long axis view; hearts ranged from 59 to 65 slices. Segmentation excluded the apical 5 slices and the first 10 basal slices to avoid overlapping structures that might otherwise alter results. Mean SUV, max SUV, and SD of SUV were recorded for each dog. To obtain a heterogeneity index, coefficient of variance (CoV) was calculated by dividing SD SUV by mean SUV[174]; and (3) to examine regional wall segments within the LV, 16 individual ROI's within each heart were examined.[121,174] The 16 ROIs were obtained by segmenting representative basal, mid-cavity, and apical slices for each heart as described in the American Heart Association scientific statement on standardized myocardial segmentation[121]; the true apex could not be reliably identified so was not evaluated.

Statistics

Statistics were performed in both Excel for Mac (Microsoft Corporation, Redmond, WA) and confirmed in Prism software version 6 (GraphPad Software, La Jolla, CA). The Prism software was also used for schematic graph generation. Two-way ANOVAs were employed to test significance for mean and max SUV between genotypes (GRMD, carrier, and normal) and muscle (CS, VL, LDE). ANOVAs were also used to look at differences in SUV for the regional segments in the heart. Non-parametric t-tests (Wilcoxon rank sum tests) were used to test significance of GLUT4 expression and CoV between GRMD, carrier and normal dogs. Significance was defined as $p < .05$.

Results

MRNA Profiling and qPCR

Genome-wide, mRNA expression profiles[152,168] of GLUT4 mRNA in the CS, LDE, and VL muscles were compared in GRMD and normal dogs at 4-9 weeks and 6 mo. (Figure 11A). GLUT4 expression was decreased in GRMD at all ages, but patterns of expression varied among the muscles, with differences being most pronounced in the LDE. In GRMD dogs, GLUT4 mRNA expression was approximately 50% less in the LDE compared to normal, while the decrease in the CS and VL was only ~10-25%. The LDE in normal dogs had higher basal GLUT4 expression compared to the CS and VL. We completed qPCR for GLUT4 on the GRMD LDE microarray dogs at 6 months, which confirmed its downregulation by a fold change of -1.894 (standard error of +/- 0.20028; p = .0245) (Figure 11B). Interestingly, in the same set of GRMD microarray dogs, HK1 was upregulated by a fold change of +2.13 (standard error +/- 0.88863; p = .046) (Figure 11B).

Western Blots

GLUT4 protein expression did not significantly differ between normal and GRMD CS, VL, or left ventricle muscles (Figure 12). On the other hand, GLUT4 protein expression at 6 mo. was significantly increased ($p<.05$) in the LDE muscle of GRMD dogs, being nearly twice that of normal dogs.

Figure 11. GLUT4 mRNA expression was reduced in GRMD versus normal muscle. (a) GLUT4 mRNA expression was compared in the CS, LDE, and VL of GRMD (black bars) and normal (open bars) dogs at 4-9 weeks and 6 months. Levels were significantly lower in GRMD dogs; differences were most pronounced in the LDE (50% decrease). (b) QPCR for GLUT4 on GRMD LDE microarrayed muscle at 6 months confirmed downregulation by a fold change of -1.894, while hexokinase 1 was upregulated by a fold change of +2.13. *=p<.05, **=p<.01. Reprinted.[138]

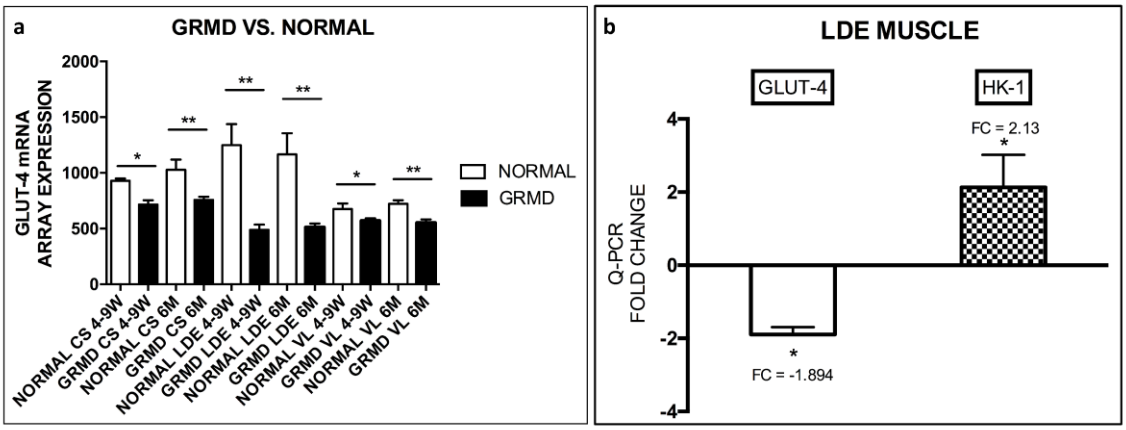

Figure 12. GLUT4 protein in GRMD vs normal muscles. GLUT4 expression was similar in CS (a) and VL (b) between GRMD (black bars) and normal (white) dogs, but increased in GRMD LDE (c) at 6 months. GLUT4 expression was normalized to total protein per lane on the PVDF membrane. * = p<.05. Reprinted.[138]

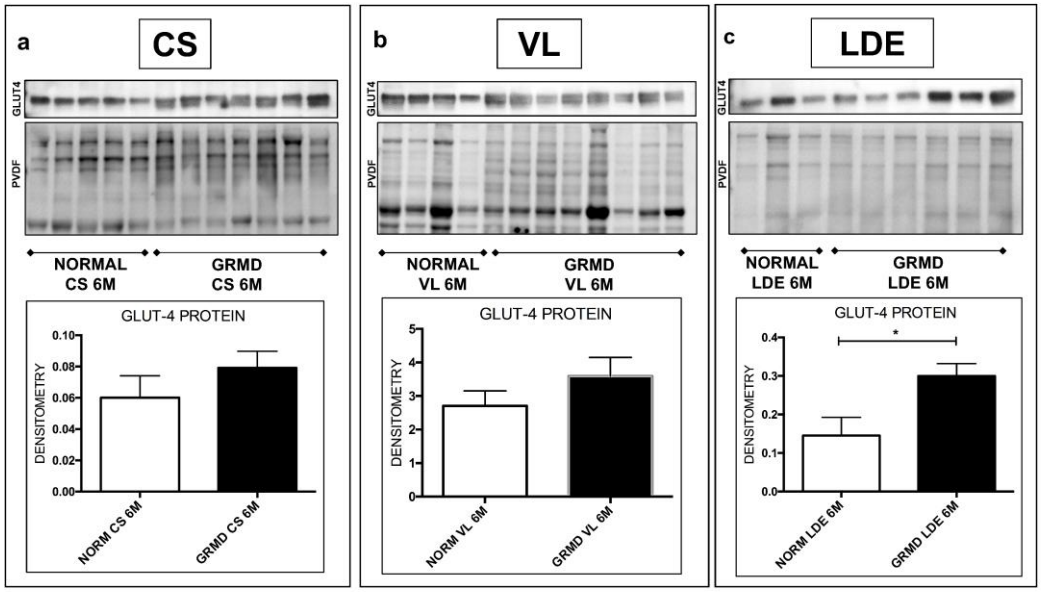

Confocal microscopy

Confocal microscopy showed diffuse GLUT4 localization at the myofiber membrane in all GRMD skeletal muscles evaluated (CS, LDE, VL, cranial tibial, and diaphragm; $p = .047$; Figures 13B, D, G), whereas normal muscle showed minimal membrane localization (Figure 13A, B). Cytoplasmic GLUT4 aggregates were present in both GRMD and normal muscle (Figure 13A, B). On the other hand, in the left ventricle of the heart, there was no difference in membrane expression between normal and GRMD (Figures 13E, F).

Intravenous glucose tolerance test (IV-GTT)

Based on the increased skeletal muscle membrane localization of GLUT4 demonstrated on confocal microscopy, we hypothesized that GRMD dogs would have more rapid clearance of plasma glucose and performed an IV-GTT. For BG values, both genotype ($p=.002$), and the interaction of time and genotype ($p=.003$) had a significant effect. Specifically, GRMD dogs had higher basal BG levels compared to normal and carrier dogs (time 0; Figure 14A). At 5-min post dextrose injection, there was rapid tissue uptake of glucose from the blood in GRMD (mean 507 mg/dl) compared to carriers (mean 644 mg/dl; $p < .05$) and normal dogs (mean 597 mg/dl; $p < .05$) (Figure 14A). Normal and carrier BG values were not significantly different.

Figure 13. Peri-membranous localization of GLUT4 in GRMD skeletal muscle. Confocal microscopy showed increased localization of GLUT4 (green) at the myofiber membrane (white asterisk and arrows) in GRMD skeletal muscle (CS, LDE, VL, cranial tibial, diaphragm; b, d) compared to normal (a, c). Mainly cytoplasmic GLUT4 localization was observed in normal muscle (asterisk; a, c). Note that GRMD also demonstrated cytoplasmic GLUT4 aggregates. In cardiomyocytes, there was no statistical difference in GLUT-4 expression at the membrane between normal and GRMD (e, f). Quantification (g) showed a nearly 4 fold increase of GLUT4 at the membrane in GRMD skeletal muscle (p=.047). a and b = 20X objective (oil immersion); c-f = 100X objective (oil immersion). Nuclei = blue. Spectrin = red. N = 5-6 per group for skeletal muscle; N = 3 per group for cardiac muscle. Reprinted.[138]

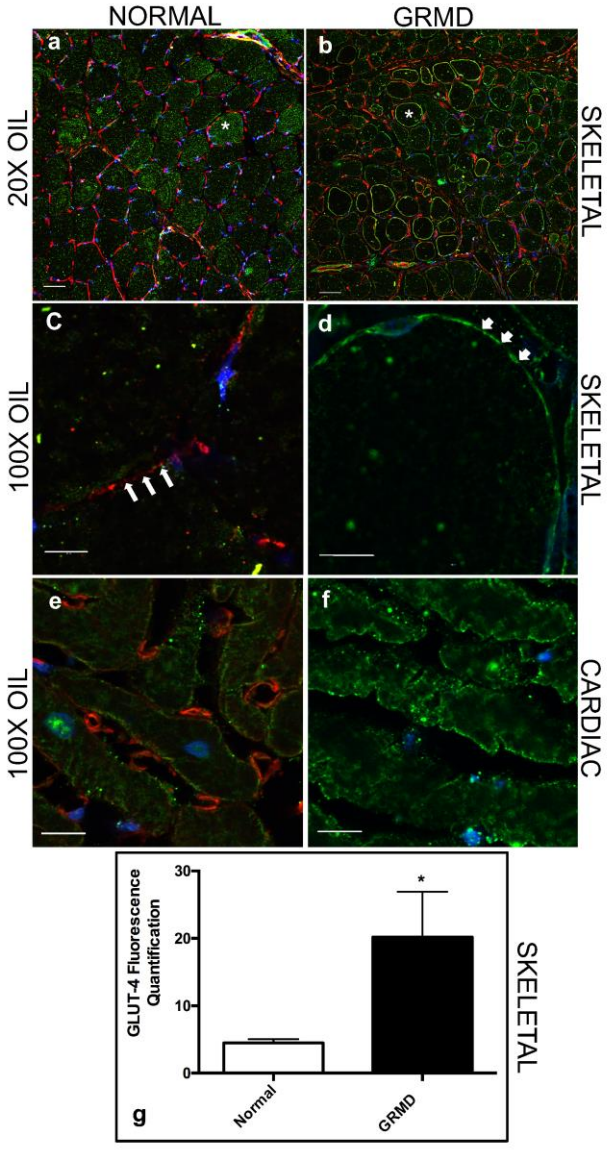

Figure 14. Rapid dextrose uptake in GRMD with an intravenous glucose tolerance test. At early time points, glucose (a) and insulin (b) curves were significantly different between GRMD and carrier/normal dogs. Resting (basal, time = 0) blood glucose was significantly higher in GRMD (104.5 mg/dl +/- 7.3) compared to normal/carrier dogs (92.0 mg/dl +/- 8.9). Dextrose uptake was rapid in GRMD dogs compared to normal 5 min post injection. Glucose levels were similar between genotypes at later time points. Resting (basal) insulin levels were significantly higher in GRMD dogs (31.26 uIU/ml +/- 6.1; 35% increase) vs. normal and carrier dogs (21.61 uIU/ml +/- 7.27) and GRMD insulin peaked at the 5-min time point compared to 15 min in carrier and normal dogs. Insulin levels were similar between genotypes at later time points. **=p<.01. Reprinted.[138]

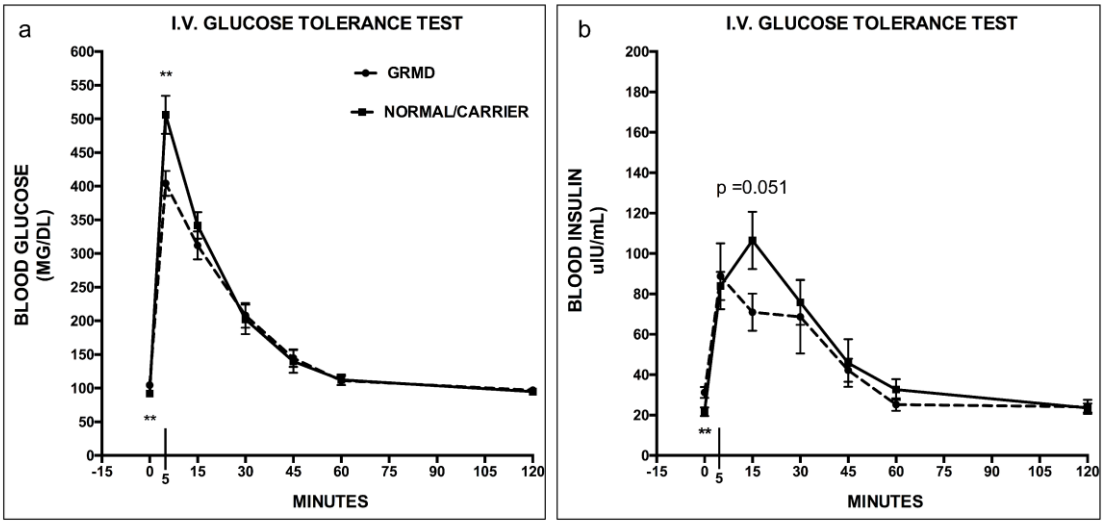

Insulin curve

With regards to the IV-GTT, insulin values were also significantly affected by genotype (p=.007), although the interaction with time was not significant. There was a 45% increase in basal (time 0; pre-dextrose injection) insulin levels in GRMD (mean 31.26 µIU/ml; $p < .05$) compared to combined normal/carrier groups (mean 21.61 µIU/ml; $p < .05$) (Figure 14B). The GRMD insulin levels peaked at the 5-min time point, while both carrier and normal dogs did not peak until the 15-min time point (Figure

14B). GRMD dogs had a lower insulin trend at 15 min post-dextrose injection compared to normal/carrier dogs (p = .051).

PET-CT: skeletal muscle

Based on the increased membrane localization of GLUT4 detected by confocal microscopy and the initial rapid uptake of BG demonstrated in the IV-GTT results, we hypothesized that *in vivo* imaging would be able to detect more rapid glucose uptake in GRMD skeletal muscle compared to normal/carrier dogs. On PET-CT with [^{18}F]DG (glucose analogue) and insulin co-administration, genotype significantly influenced mean skeletal muscle SUV at the initial 5 min postinjection scan (p=.03). Specifically, GRMD dogs had higher average [^{18}F]DG uptake compared to carrier and normal dogs at 5 min (Figure 15A-B); this difference was lost at the 1 hr time point. The mean SUV was significantly different among the CS, VL, and rectus femoris muscles at both time points (p< .01), regardless of genotype. Max SUV was not significantly different between muscles, genotype, or scan time.

In order to normalize the scans for blood flow to the limb, we assessed SUV in a nearby tissue (pelvic fat) that should not be influenced by disease status. Mean SUV in a 1cm ROI of pelvic fat showed no significant differences between the groups at either time point; however, max SUV was significantly higher in normal dog pelvic fat (p=.03). Additionally, we assessed systolic, diastolic, and mean blood pressure between groups at the time points before [^{18}F]DG administration, just after [^{18}F]DG administration, and 1 hour after [^{18}F]DG administration (Supplement 9). There were no

significant differences between groups for systolic, diastolic, or mean pressure at any time point.

We hypothesized that severely affected muscles, which have heterogeneous muscle composition due to segmental necrosis, including areas of fibrosis, inflammation, degeneration, and myofiber regeneration would have more heterogeneous [^{18}F]DG uptake. Using CoV (SD SUV/mean SUV) as a marker for heterogeneous uptake, values were significantly higher in GRMD VL muscle (CoV = .204; p = .02) versus normal dogs (CoV=.174) at the 1 hr scan (Figure 15C). Average CoV for carriers was midway between the GRMD and normal averages (CoV=.181; p=.29), although significance was not reached. The CoV of the hypertrophied CS muscle, which is relatively spared with minimal pathology (inflammation, degeneration),[152] did not differ between GRMD and normal/carrier dogs.

PET-CT: cardiac muscle

Based on preferential involvement of the posterobasal heart region in DMD histopathologically and in previous imaging studies,[36,175,176] we hypothesized that [^{18}F]DG uptake would differ between GRMD and normal hearts. At the 5 min post-[^{18}F]DG/insulin scan, both mean (2.7 vs 4.8; p=.007) and max (4.5 vs 7.1; p=.04) SUV were significantly *lower* in GRMD versus carrier and normal hearts (Figure 15 D-H). At one hr post [^{18}F]DG administration, mean SUV (2.8 vs 4.7; p=.02) was still significantly lower in GRMD, though the difference in max SUV (4.9 vs 7.8; p=.06) was no longer significant. Mean and max SUV did not differ among the standard 16 LV segments

(p>.5). Similarly, using CoV to detect heterogeneous glucose uptake in the heart, there was no significant difference among the groups (p>.3).

Figure 15. Differential [^{18}F]DG uptake with PET-CT in GRMD versus normal/carrier dogs in skeletal and cardiac muscle. (a) GRMD VL, rectus femoris, and CS (top, white oval) had higher SUV than a normal littermates (bottom; white oval). (b)The skeletal muscle had significantly increased mean SUV at 5 min post [^{18}F]DG/insulin in GRMD compared to normal. (c)GRMD skeletal muscle had significantly higher CoV at 1 hour. In cardiac muscle, max (d) and mean (g) SUV were lower in the GRMD left ventricle (f, top) compared to normal (f, bottom) and carrier at 5 minutes post ^{18}FDG/insulin (white circle outlining the heart). At 1 hour, max SUV (e) trended and mean SUV (h) were significantly lower compared to normal left ventricle. *=p<.05. Reprinted.[138]

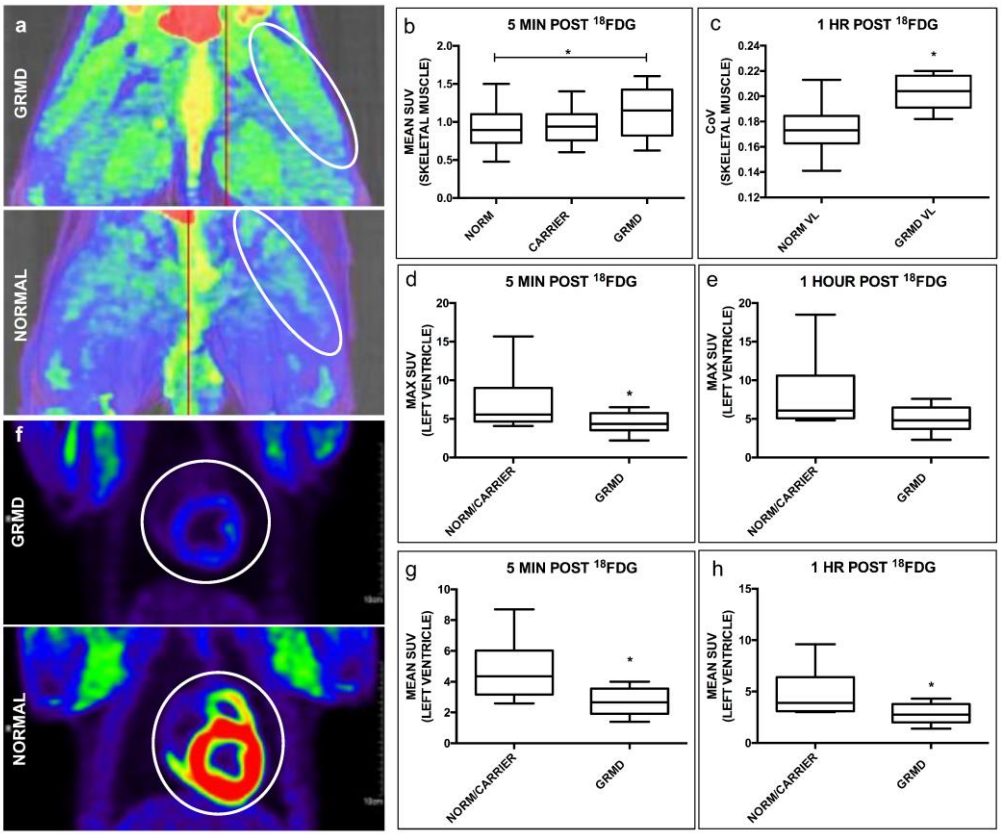

Discussion

Lesions and associated clinical disease occur much earlier in skeletal versus cardiac muscle in DMD and GRMD, raising questions of factors that could either accelerate skeletal muscle or delay cardiac involvement. Our results were consistent with this differential pattern of involvement between skeletal and cardiac muscle. GTT and PET-CT imaging demonstrated that GLUT4 is dysregulated in GRMD skeletal muscle, resulting in rapid glucose and analogue uptake. Cardiac PET imaging showed decreased uptake in GRMD hearts compared to normal. This difference in skeletal versus cardiac muscle metabolism could help explain some of the differences in disease progression between the two tissues.

In addition to the mechanical fragility of the sarcolemma, dystrophin deficiency is characterized by metabolic dysregulation, manifesting as reduced glycolytic enzymes, mitochondrial structural and functional abnormalities, and altered glucose uptake and response to insulin.[103,108,114,167,177–179] Reduced muscle mass and increased fat could contribute to altered insulin sensitivity and are risk factors for insulin insensitivity, independent of dystrophin. However, the presence of hyperglycemia and hypoglycemia in boys with normal or low body mass index[114] suggests that the dystrophy state, and not just body composition, alters insulin sensitivity in DMD. Dystrophin deficient cells have a decreased capacity for glycolysis and glycogenolysis and concurrently depressed intracellular ATP and mitochondrial dysfunction.[103,167,178,180] These changes lead to a ‘metabolic crisis’ in dystrophin deficient myofibers, which could result in greater susceptibility to ischemia, metabolic stress, and reduced regenerative capacity.

Glucose transport into muscle cells in response to insulin or contraction[181] occurs primarily through translocation of GLUT4 from the cytoplasm to the sarcolemma/T-tubules.[109] As such, alterations in GLUT4 levels or trafficking within the cell significantly impact overall glucose metabolism. Changes in GLUT4 localization has been noted in both DMD and mdx muscles, but it is unclear if this altered trafficking is a direct result of dystrophin loss or a secondary response to metabolic stress. We hypothesized that GLUT4 alterations in GRMD would be similar to DMD muscle,[114] contributing to the metabolic dysregulation in dystrophic muscle.

To pursue this hypothesis, GLUT4 mRNA and protein expression levels were first compared between GRMD and normal skeletal muscle. We queried previously performed microarray profiles and found reduced GLUT4 mRNA in dystrophin-deficient muscles. However, our follow-up studies showed varying protein levels, being similar to normal dogs in GRMD CS and VL muscles, but increased in GRMD LDE. The protein results in the CS and VL are in keeping with unchanged levels of GLUT4 protein expression in type II diabetes, though mRNA is also unchanged in that disease.[182,183] On the other hand, increased levels in GRMD LDE were consistent with elevated values in hind limb muscles of the mdx mouse, regardless of age.[115] Interestingly, GRMD LDE had the most profound changes in GLUT4 mRNA and protein, suggesting a negative feedback loop may be involved between mRNA and protein. Moreover, these molecular changes in GRMD LDE may be due to the severe dystrophic phenotype and significant degeneration/regeneration observed in this muscle (LDE is atrophied/wasted to half the size of normal).[184] With regards to the left ventricle

of the heart, there was a trend for increased GLUT-4 in GRMD ($p = 0.06$). Perhaps with the availability of more samples, statistical significance could be achieved.

While overall GLUT4 protein levels in the tissues were not increased in most GRMD muscles evaluated, immunofluorescence microscopy surprisingly revealed increased GLUT4 localization at the myofiber cell membrane in all GRMD skeletal muscle evaluated. This membrane localization could represent a dysregulation in cellular trafficking or a physiological response to increased metabolic demand for glucose (due to the metabolic crisis). On that note, GLUT4 translocation to the muscle membrane in this model may represent a sort of 'priming' to allow for rapid extracellular glucose uptake. Interestingly, normal and GRMD muscles had similar amounts of cytoplasmic GLUT4 aggregates, representing a potential therapeutic reservoir for the latter. With regards to cardiomyocytes, we did not detect a statistical difference in GLUT4 membrane expression between normal and GRMD left ventricle samples. Taken together, the differences in skeletal vs. cardiac muscle GLUT4 translocation may represent the differences in severity between the two tissues.

Although we did not co-stain for GLUT-4 and fiber type, it should be noted that most dystrophin-deficient myofibers undergo fiber type switching from fast to slow twitch.[103] We can then infer that GRMD myofibers with GLUT-4 membranous expression were of the slow twitch phenotype. A previous study in human muscle showed small, but significant differences in GLUT-4 expression and fiber type; however, the authors concluded that GLUT-4 protein content was related more closely to activity level than fiber type.[185]

We recently revealed that the morphologically spared and hypertrophied GRMD CS muscle had a reduction in expression in several glycolytic enzymes, including phosphoglucomutase-1, 6-phosphofructokinase, and glucose-6-phosphate isomerase.[103] In the current study, we evaluated at the mRNA level, HK-1, the first enzyme of the glycolytic pathway, and observed an increased expression in GRMD LDE muscle. These differences in glycolytic enzyme expression may be due to muscle specific changes that occur between hypertrophied (CS) and atrophied (LDE) muscle in GRMD and should be further explored. Nevertheless, the increased HK1 is in keeping with our hypothesized compensatory mechanism within dystrophic muscle to rapidly metabolize glucose.

We used an IV-GTT in another GRMD cohort to test the hypothesis that increased sarcolemmal GLUT4 permits rapid and immediate glucose uptake into skeletal muscle. Indeed, GRMD dogs had rapid BG uptake 5 min after the dextrose challenge, as indicated by the differences in glucose peaks at this time point between GRMD and normal/carrier dogs. Also, the insulin peak occurred at 5 min post injection in GRMD compared to 15 minutes for normal/carrier dogs. This truncated insulin response shows that the apparently quicker glucose uptake was not due to a larger overall insulin level. In conjunction with rapid glucose uptake, GRMD dogs had higher basal (pre-dextrose injection) BG and insulin levels, suggesting dystrophic muscle is under higher metabolic demand and requires a slightly higher level of BG and insulin levels to compensate. Area under the BG curves did not differ between GRMD and normal/carrier dogs, perhaps because of our failure to sample frequently over the first 15 min and continue sampling for 3 hr.[186] Had we employed more frequent early sampling, the slope of GRMD curves

might have been increased. In addition, because glucose metabolism varies with age, GRMD and normal/carrier dogs should be matched more closely in future studies. Here, we tested the response to insulin-mediated GLUT4 uptake of glucose. Ideally, contraction-mediated GLUT4 uptake should be tested, but performing a treadmill exhaustion protocol in GRMD dogs, as seen in mice, would not be feasible.[187]

We employed PET imaging to further study the role of GLUT4 in glucose metabolism. We hypothesized that GLUT-4 localization at the dystrophic myofiber membrane would produce a measurable increase in the immediate uptake of [^{18}F]DG. In order to force rapid and specific uptake into skeletal muscle, we co-administered insulin and [^{18}F]DG tracer at the initiation of scanning. Similar to our IV-GTT results, [^{18}F]DG uptake was higher in GRMD versus normal/carrier dogs at 5 min post [^{18}F]DG/insulin administration but not at 1hr, consistent with an early, transient response.[187] Most likely, this early transient response to glucose (and a glucose analogue) partially compensates for metabolic dysregulation in dystrophic muscle. Other methods such as dynamic PET after [^{18}F]DG administration might demonstrate differences in uptake over time.[188] With regards to exercise, all dogs are provided daily enrichment, including exercise (walking and running outside for a period of time). Normal animals are inherently more active than GRMD dogs, but regular conditioning would be expected to create increased insulin sensitivity in normal muscle (i.e. increasing glucose and glucose analogue uptake). For these imaging studies, exercise was minimized in all groups the morning prior to the PET-CT studies to reduce any exercise-related short-term effects on [^{18}F]DG uptake. Nevertheless, our findings that [^{18}F]DG and dextrose uptake at 5 min post administration

provides a potential biomarker 'window' to assess treatments intended to improve muscle metabolism in GRMD dogs.

Blood flow and inflammation can be contributors to differences in [^{18}F]DG uptake, particularly in early PET scans. Due to prolonged washout times and concerns about prolonged anesthesia in the dogs, as well as not wanting to administer an additional tracer to confound results, we did not assess blood flow or inflammation directly in this study. However, blood pressure, which is measured in the pelvic limb, was not significantly different between groups before, during, or after [^{18}F]DG and insulin administration. Additionally, SUV measurements of pelvic fat, which should not be affected by the GLUT4 differences observed in the skeletal muscle, did not show significant differences in mean SUV. However, pelvic fat max SUV was higher in normal dogs compared to other groups. Overall, these results suggest that altered blood flow was not a major contributor to increased skeletal muscle SUV in GRMD dogs.

Likewise, we assessed multiple GRMD muscles in the thigh which naturally show differences in degree of pathology, including inflammation. These include the CS, which is hypertrophied but has minimal inflammation, and the VL and rectus femoris that show classic dystrophic changes of inflammation/degeneration.[152,184] Our statistical analysis revealed that GRMD skeletal muscle had a significant increase in mean SUV at 5 min post [^{18}F]DG/insulin, but the GRMD genotype did not influence uptake between the individual muscles (CS, VL, rectus femoris). Elevated blood glucose from feeding has been shown to interfere with [^{18}F]DG uptake, while co-administration of insulin results in a rapid uptake of 85-90% of glucose within the first 5 minutes.[189] Additionally,

although inflammatory cells have insulin responsive GLUT4 translocation,[190] the inflammatory infiltrate present in GRMD muscle would be expected to interfere with insulin sensitivity, rather than increasing uptake.[191] Therefore, we hypothesize that the primary driver of increased SUV in GRMD skeletal muscle was due to insulin-stimulated GLUT-4 uptake of [^{18}F]DG. We acknowledge that further studies should be performed to co-administer [^{18}F]DG, a blood flow tracer, and an inflammatory marker in GRMD dogs to further clarify this issue.

Like skeletal muscle, GLUT4 is the major transporter of glucose into cardiomyocytes.[111,192] Surprisingly, mean and max SUVs were lower on PET studies of the left ventricle in GRMD versus normal/carrier dogs. Since this reduction persisted beyond the 5-min time point, this likely did not occur simply because of selective skeletal muscle uptake. Instead, this presumably reflects a primary cardiac insulin resistance associated with dystrophic cardiomyopathy.[164] While we further hypothesized that [^{18}F]DG distribution would correspond to the regional nature of lesions within the dystrophic heart, mean or max SUV did not vary among the 16 LV segments analyzed. Similarly, GLUT4 protein expression and translocation differences could not be confirmed in the heart, though there was a trend toward increased GLUT4 protein expression in GRMD, which appeared to be affected by higher levels in older dogs. Indeed, further studies in GRMD are needed to confirm GLUT-4 trafficking abnormalities due to potential aberrant insulin and/or contraction stimulation.

Taken together, these findings reiterate that glucose dynamics vary between cardiac and skeletal muscle. We hypothesized that the two muscle cell types have

different GLUT4 vesicle populations with varying responses to insulin and contraction.[111,192] This metabolic dissimilarity could also help explain the difference in disease progression between these two tissues, as suggested by recent gene microarray studies in GRMD dogs.[16] Most affected dogs from the PET-CT study are thriving in the colony, which has precluded assessment of GLUT4 expression in their hearts to better clarify these differences.

One potential confounding factor is the age differences between the molecular and PET studies. For our initial molecular assessment of mRNA, protein expression, and qPCR, we used a cohort of frozen samples banked from previous biopsies and muscle sampling at disease-specific time points. When we moved to in vivo imaging, we utilized breeder dogs with a wider age range that were currently available and attempted to best match between the examined groups. It is possible that the gene expression and GLUT4 localization profiles in older, affected dogs are different than those seen in younger animals. However, disease differences are manifested and stratified by 6 months of age, and would be expected to be similar or worse in older affected dogs. Likewise, gender is a potential confounding factor. In people, there are differences in GLUT4 expression and insulin resistance between males and females.[111] Such sex differences could affect our results, as carrier animals were all female, while GRMD and normal animals were of mixed gender. Female dogs in diestrus or pregnancy can have increased insulin resistance and higher insulin, but we did not include females which had recently been in heat in this study. Analysis of glucose or insulin levels stratified by gender did not show a significant difference between genders in our cohort. Similarly, previous

studies of glucose transporters in monocytes in the circulating blood of dogs did not show a difference between gender.[190] We have not detected any functional differences between genders in GRMD dogs, either.[193] As such we believe sex differences were likely not a major contributor in this study.

This study evaluated multiple muscles with various fiber types and actions (both extensors and flexors). While two-way ANOVA showed muscle had a significant effect on [^{18}F]DG SUV, there was no interaction between muscle and disease status, and disease status had an independent, significant effect on [^{18}F]DG SUV. Future imaging studies to evaluate tracers of inflammation, blood flow and fatty acid metabolism in the heart/skeletal muscle would further resolve some of the remaining questions regarding confounding factors of [^{18}F]DG uptake in GRMD.

CONCLUSION

The three studies presented here offer insight into the phenotypic, genetic and metabolic derangements that may influence progression of cardiomyopathy in the golden retriever muscular dystrophy (GRMD) model of Duchenne muscular dystrophy. Although the general features of the DMD and GRMD cardiomyopathies have been established, pathogenetic features to account for the delayed onset of cardiac disease and preferential involvement of certain anatomical areas are poorly understood.

More aggressive respiratory care in DMD has greatly improved longevity in recent years, such that cardiomyopathy is now the major cause of death. While clinical cardiac dysfunction does not develop until later in life, there is increasing recognition that early detection and intervention are important for maintaining cardiac function over the long term. Additionally, as newer genetic therapies enter the market, specific evaluation of cardiac end points will be essential for comprehensive treatment. In this context, there is a need for biomarkers to define disease risk and both allow longitudinal monitoring and earlier treatment of susceptible DMD patients.

Given the outbred nature of dogs, in keeping with humans as opposed to inbred mouse lines, and the relative comparable size of humans and dogs, GRMD is an important preclinical model for DMD. As opposed to the relatively mild cardiomyopathy in mdx mice, GRMD dogs develop a progressive form of disease similar to that of DMD. Thus, it is important to more fully understand disease pathogenesis and the use of both genetic and imaging biomarkers that can be used to predict and track disease progression.

Chapters 2-4 of this dissertation detail three separate studies that define pathologic, genetic, and imaging features of GRMD cardiomyopathy. The study outlined in chapter 2 provides the largest comprehensive gross pathologic and histopathologic review of GRMD cardiomyopathy to date. Our findings highlight differences in disease severity and suggest that, at least in our hands, semi-quantitative scoring is preferable to fibrosis quantification for assessing overall lesion severity. The severity of the semi-quantitative histopathologic changes correlated positively with the degree of vascular hypertrophy on pathology and late gadolinium enhancement (LGE) on cardiac magnetic resonance imaging (CMR). Fatty infiltration was particularly pronounced in older dogs. Finally, the nature of some lesions suggested functional hypoxia or non-thrombotic ischemia may contribute to disease progression.

In chapter 3, we evaluated gene and protein expression in GRMD, carrier, and normal hearts. Our findings support earlier microarray work suggesting that brain-derived neurotropic factor (BDNF) is involved in modulating lesion progression in the dystrophic heart and may be useful as a cardiac disease marker in GRMD dogs. We also showed for the first time that BDNF is differentially expressed in the left (LV) and right (RV) ventricles, perhaps accounting at least in part for preferential LV involvement. Although low numbers precluded significance, BDNF values were also higher in carriers versus normal dogs, suggesting its potential involvement in their intermediate phenotype. For the first time, we also showed a differential pattern of SPP1 expression that appeared to track with GRMD cardiomyopathy progression. Supporting the relative specificity of BDNF and SPP1 as DMD/GRMD cardiac biomarkers, three other genes,

utrophin, matrix-metalloproteinase-9, and a-disintegrin-and-metallopeptidase-domain-12 were not differentially expressed in GRMD versus normal hearts.

These findings illustrate how studies in dogs are necessary to validate findings in mice, and substantiate that cardiac specific biomarkers may be available. Because BDNF has been linked with prognosis and disease severity in other human cardiac diseases, we and others have been intrigued by its role in DMD and GRMD disease pathogenesis. While previous work had shown BNDF to be a potential important biomarker in these conditions, our ability to replicate and extend these findings further validate its role as a pathogenetic factor and biomarker. Importantly, the ability to track BDNF in serum would greatly facilitate its role as a disease biomarker. Future studies should include longitudinal testing of serum BDNF levels in conjunction with cardiac function tests and other cardiac biomarkers in GRMD and normal dogs.

Finally, chapter 4 assessed metabolic derangements in GRMD skeletal and cardiac muscle. Measurable alterations in glucose metabolism further demonstrated the complexity of dystrophin-deficient disease, with structural, functional, and metabolic components interacting to produce lesions. Overall, our results suggested that glucose handling and metabolism differ between GRMD and normal/carrier dogs. In particular, GRMD dogs had higher levels of both resting insulin and glucose and more rapid glucose uptake, which peaked at different levels. We theorized that an increase of the primary glucose transporter, GLUT4, at the cell membrane primes GRMD muscle to induce rapid glucose uptake. With positron emission tomography-computed tomography (PET-CT), these changes correlated with increased mean standard uptake (SUV) values

immediately after [18F]DG/insulin administration. These data suggest that glucose metabolism, specifically GTT and PET-CT testing, may be utilized as surrogate biomarkers to assess disease progression and normalization of muscle metabolism in GRMD dogs following various treatments. In the future, assessment of cardiac muscle oxygenation and fatty acid metabolism, using similar techniques, may provide better guidance and understanding of pressures that are placed on the dystrophic heart. Further studies are needed to determine if GRMD cardiac cells are more or less insulin responsive than normal. I am particularly interested in demonstrating oxygenation and blood flow levels in the cardiac muscle of GRMD dogs.

The studies presented here add to the foundation of understanding of both cardiomyopathy and the GRMD model. The natural history histological studies highlight some intriguing histologic features, including evidence supporting recently recognized syndromes of acute progression of cardiomyopathy in DMD boys and dogs and possible involvement of the vasculature in disease expression. The gene expression and metabolism studies further demonstrate the utility of the GRMD model in developing potential biomarkers for DMD progression and should also broaden our understanding of treatments for this devastating disease.

REFERENCES

1. Mendell, J. R. *et al.* Evidence-based path to newborn screening for Duchenne muscular dystrophy. *Ann Neurol* **71**, 304–313 (2012).
2. Hoffman, E. P., Brown, R. H. & Kunkel, L. M. Dystrophin: The protein product of the Duchenne muscular dystrophy locus. *Cell* **51**, 919–928 (1987).
3. Spurney, C. F. Cardiomyopathy of Duchenne muscular dystrophy: Current understanding and future directions. *Muscle Nerve* **44**, 8–19 (2011).
4. Bushby, K. *et al.* Diagnosis and management of Duchenne muscular dystrophy, part 1: diagnosis, and pharmacological and psychosocial management. *Lancet* **9**, 177–89 (2010).
5. Mendell, J. R. *et al.* Eteplirsen for the treatment of Duchenne muscular dystrophy: Eteplirsen for DMD. *Ann Neurol* **74**, 637–647 (2013).
6. Juan-Mateu, J. *et al.* Prognostic value of X-chromosome inactivation in symptomatic female carriers of dystrophinopathy. *Orphanet J Rare Dis* **7**, 82–93 (2012).
7. Birnkrant, D. J., Ararat, E. & Mhanna, M. J. Cardiac phenotype determines survival in Duchenne muscular dystrophy. *Pediatric pulmonology* **51**, 70–6 (2016).
8. Nigro, G., Comi, L. I., Politano, L. & Bain, R. J. I. The incidence and evolution of cardiomyopathy in Duchenne muscular dystrophy. *Int J Cardiol* **26**, 271–277 (1990).
9. Finsterer, J. & Stöllberger, C. The heart in human dystrophinopathies. *Cardiol* **99**, 1–19 (2003).

10. McNally, E. M. *et al.* Contemporary cardiac issues in Duchenne muscular dystrophy. *Circulation* **131**, 1590–1598 (2015).
11. D'Amario, D. *et al.* A current approach to heart failure in Duchenne muscular dystrophy. *Heart* **103**, 1770–1779 (2017).
12. Heymsfield, S. B., McNish, T., Perkins, J. V. & Felner, J. M. Sequence of cardiac changes in Duchenne muscular dystrophy. *Am Heart J* **95**, 283–294 (1978).
13. Prosser, B. L., Ward, C. W. & Lederer, W. J. X-ROS signaling: Rapid mechano-chemo transduction in heart. *Science* **333**, 1440–1445 (2011).
14. Viola, H. M. *et al.* Impaired functional communication between the L-type calcium channel and mitochondria contributes to metabolic inhibition in the mdx heart. *Proc Natl Acad Sci* **111**, E2905–E2914 (2014).
15. Fanchaouy, M. *et al.* Pathways of abnormal stress-induced Ca2+ influx into dystrophic mdx cardiomyocytes. *Cell Calcium* **46**, 114–121 (2009).
16. Markham, L. W. *et al.* GRMD cardiac and skeletal muscle metabolism gene profiles are distinct. *BMC Med Genom* **10**, 21 (2017).
17. Klietsch, R., Ervasti, J. M., Arnold, W., Campbell, K. P. & Jorgensen, A. O. Dystrophin-glycoprotein complex and laminin colocalize to the sarcolemma and transverse tubules of cardiac muscle. *Circ Res* **72**, 349–360 (1993).
18. Holland, A. & Ohlendieck, K. Proteomic profiling of the dystrophin-deficient mdx phenocopy of dystrophinopathy-associated cardiomyopathy. *BioMed Res Int* **2014**, 1–15 (2014).

19. Iwata, Y., Pan, Y., Hanada, H., Yoshida, T. & Shigekawa, M. Dystrophin–glycoprotein complex purified from hamster cardiac muscle. Comparison of the complexes from cardiac and skeletal muscles of hamster and rabbit. *J Mol Cell Cardiol* **28**, 2501–2509 (1996).
20. Fayssoil, A., Nardi, O., Orlikowski, D. & Annane, D. Cardiomyopathy in Duchenne muscular dystrophy: pathogenesis and therapeutics. *Heart Fail Rev* **15**, 103–107 (2010).
21. Bostick, B. *et al.* Cardiac expression of a mini-dystrophin that normalizes skeletal muscle force only partially restores heart function in aged mdx mice. *Mol Ther* **17**, 253–261 (2009).
22. Willmann, R., Possekel, S., Dubach-Powell, J., Meier, T. & Ruegg, M. A. Mammalian animal models for Duchenne muscular dystrophy. *Neuromuscul Disord* **19**, 241–249 (2009).
23. Kornegay, J. N. *et al.* Canine models of Duchenne muscular dystrophy and their use in therapeutic strategies. *Mamm Genome* **23**, 85–108 (2012).
24. Valentine, B. A. *et al.* Canine X-linked muscular dystrophy as an animal model of Duchenne muscular dystrophy: A review. *Am J Mol Genet* **42**, 352–356 (1992).
25. McGreevy, J. W., Hakim, C. H., McIntosh, M. A. & Duan, D. Animal models of Duchenne muscular dystrophy: from basic mechanisms to gene therapy. *Dis Model Mech* **8**, 195–213 (2015).

26. Valentine, B. A., Cummings, J. F. & Cooper, B. J. Development of Duchenne-type cardiomyopathy: Morphologic studies in a canine model. *Am J Pathol* **135**, 671–678 (1989).

27. Quinlan, J. G. *et al.* Evolution of the mdx mouse cardiomyopathy: physiological and morphological findings. *Neuromuscul Disord* **14**, 491–496 (2004).

28. Cooper, B. J. Animal models of Duchenne and Becker muscular dystrophy. *Br. Med. Bull.* **45**, 703–718 (1989).

29. Coulton, G. R., Morgan, J. E., Partridge, T. A. & Sloper, J. C. The mdx mouse skeletal muscle myopathy: I. A histological, morphometric and biochemical investigation. *Neuropathol Appl Neurobiol* **14**, 53–70 (1988).

30. Casal, M. & Haskins, M. Large animal models and gene therapy. *Eur J Hum Genet* **14**, 266–272 (2006).

31. Frankel, K. & Rosser, R. The pathology of the heart in progressive muscular dystrophy: epimyocardial fibrosis. *Hum Pathol* **7**, 375–86 (1976).

32. Yugeta, N. *et al.* Cardiac involvement in Beagle-based canine X-linked muscular dystrophy in Japan (CXMDJ): electrocardiographic, echocardiographic, and morphologic studies. *BMC Cardiovascul Disord* **6**, 1–13 (2006).

33. Moise, S. N. *et al.* Duchenne's cardiomyopathy in a canine model: Electrocardiographic and echocardiographic studies. *J Am Coll Cardiol* **17**, 812–820 (1991).

34. James, J. *et al.* Electrocardiographic abnormalities in very young Duchenne muscular dystrophy patients precede the onset of cardiac dysfunction. *Neuromuscul Disord* **21**, 462–467 (2011).

35. Perloff, J. K., Roberts, W. C., de Leon, A. C. & O'Doherty, D. The distinctive electrocardiogram of Duchenne's progressive muscular dystrophy. *Am J Med* **42**, 179–188 (1967).

36. Perloff, J., Henze, E. & Schelbert, H. Alterations in regional myocardial metabolism, perfusion, and wall motion in Duchenne muscular dystrophy studied by radionuclide imaging. *Circulation* **69**, 33–42 (1984).

37. Quinlivan, R. *et al.* Cardiac function, metabolism and perfusion in Duchenne and Becker muscular dystrophy. *Neuromuscul Disord* **6**, 237–246 (1996).

38. Khairallah, M. *et al.* Metabolic and signaling alterations in dystrophin-deficient hearts precede overt cardiomyopathy. *J Mol Cell Cardiol* **43**, 119–129 (2007).

39. Devaux, J.-Y., Cabane, L., Esler, M., Flaouters, H. & Duboc, D. Non-invasive evaluation of the cardiac function in Golden Retriever dogs by radionuclide angiography. *Neuromuscul Disord* **3**, 429–432 (1993).

40. Nigro, G. *et al.* Structural basis of cardiomyopathy in Duchenne/Becker carriers. *Ann NY Acad Sci* **752**, 108–110 (1995).

41. Politano, L., Nigro, V., Nigro, G. & Jama, P. V. Development of cardiomyopathy in female carriers of Duchenne and Becker muscular dystrophies. *JAMA* **275**, 1335–1338 (1996).

42. Hoogerwaard, E. M. *et al.* Cardiac involvement in carriers of Duchenne and Becker muscular dystrophy. *Neuromusc Disord* **9**, 347–351 (1999).

43. Kane, A. M. *et al.* Cardiac structure and function in female carriers of a canine model of Duchenne muscular dystrophy. *Res Vet Sci* **94**, 610–617 (2013).

44. van Westrum, S., Hoogerwaard, E. & Neurology, D. L. Cardiac abnormalities in a follow-up study on carriers of Duchenne and Becker muscular dystrophy. *Neurol* **77**, 62–66 (2011).

45. Holloway, S. *et al.* Life expectancy and death from cardiomyopathy amongst carriers of Duchenne and Becker muscular dystrophy in Scotland. *Heart* **94**, 633–636 (2008).

46. Hoogerwaard, E. M. *et al.* Signs and symptoms of Duchenne muscular dystrophy and Becker muscular dystrophy among carriers in The Netherlands: a cohort study. *Lancet* **353**, 2116–2119 (1999).

47. Urasawa, N. *et al.* Selective vacuolar degeneration in dystrophin-deficient canine Purkinje fibers despite preservation of dystrophin-associated proteins with overexpression of Dp71. *Circulation* **117**, 2437–2448 (2008).

48. Miyazato, L. G., Beretta, D. C., Engracia Filho, J. R., Moraes, F. R. & Moraes, J. R. Involvement of organic systems in golden retriever X-linked muscular dystrophy. *Braz J Vet Pathol* **4**, 87-94. 52 ref (2011).

49. Malvestio, L., Martins, I., Moares, F. & Moares, J. R. E. Histopathologic evolution of cardiomyopathy in a canine model of Duchenne muscular dystrophy. *J Adv Vet Res* **5**, 121–126 (2015).

50. Galindo, C. *et al.* Translating golden retriever muscular dystrophy microarray findings to novel biomarkers for cardiac/skeletal muscle function in Duchenne muscular dystrophy. *Pediatr Res* **79**, 629–636 (2015).

51. Fine, D. M. *et al.* Age-matched comparison reveals early electrocardiography and echocardiography changes in dystrophin-deficient dogs. *Neuromuscul Disord* **21**, 453–461 (2011).

52. Zatz, M. *et al.* A normal life without muscle dystrophin. *Neuromuscul Disord* **25**, 371–374 (2015).

53. Koh, G. Y. *et al.* Stable fetal cardiomyocyte grafts in the hearts of dystrophic mice and dogs. *J.Clin.Invest.* **96**, 2034–2042 (1995).

54. Cheng, C.-P. *et al.* Cardiomyopathy in a canine model of Duchenne Muscular Dystrophy: Effects of left ventricle and myocyte systolic and diastolic functional performance, L-type calcium current response and beta-adrenergic modulation. *Circulation* **120**, S667–S667 (2009).

55. Cheng, C. P., Cheng, H.-J., Zhou, P. & Shao, Q. Intrinsic cardiomyocyte defects and dystrophic cardiomyocyte in a canine model of Duchenne Muscular Dystrophy. *Circulation* **128**, (2013).

56. Kellman, P. *et al.* Myocardial fibro-fatty infiltration in Duchenne Muscular Dystrophy canine model detected using multi-echo Dixon method of water and fat separation imaging. 1

57. Townsend, D. *et al.* Chronic administration of membrane sealant prevents severe cardiac injury and ventricular dilatation in dystrophic dogs. *J Clin Investig* **120**, 1140–1150 (2010).

58. Yue, Y., Binalsheikh, I. M., Leach, S. B., Domeier, T. L. & Duan, D. Prospect of gene therapy for cardiomyopathy in hereditary muscular dystrophy. *Expert Opin Orphan Drugs* **4**, 169–183 (2015).

59. Hammers, D. W. *et al.* Tadalafil treatment delays the onset of cardiomyopathy in dystrophin-deficient hearts. *J Am Heart Assc* **5**, e003911 (2016).

60. Habeler, W. *et al.* Direct myocardial implantation of human embryonic stem cells in a dog model of Duchenne cardiomyopathy reveals poor cell survival in dystrophic tissue. *J Stem Cell Regen Med* **7**, 80–86 (2011).

61. Yokota, T. *et al.* Efficacy of systemic morpholino exon-skipping in duchenne dystrophy dogs. *Ann Neurol* **65**, 667–676 (2009).

62. Bish, L. T. *et al.* Long-term restoration of cardiac dystrophin expression in golden retriever muscular dystrophy following rAAV6-mediated exon skipping. *Mol Ther* **20**, 580–589 (2012).

63. Barbash, I. M. *et al.* MRI roadmap-guided transendocardial delivery of exon-skipping recombinant adeno-associated virus restores dystrophin expression in a canine model of Duchenne muscular dystrophy. *Gene Ther.* **20**, 274–282 (2013).

64. Hayashita-Kinoh, H. *et al.* Intra-amniotic rAAV-mediated microdystrophin gene transfer improves canine X-linked muscular dystrophy and may induce immune tolerance. *Mol Ther* **23**, 627–637 (2015).

65. Pan, X. *et al.* AAV-8 is more efficient than AAV-9 in transducing neonatal dog heart. *Hum Gene Ther Method* **26**, 54–61 (2015).

66. Muntoni, F., Torelli, S. & Ferlini, A. Dystrophin and mutations: one gene, several proteins, multiple phenotypes. *Lancet Neurol* **2**, 731–740 (2003).

67. Nakamura, A. *et al.* Initial pulmonary respiration causes massive diaphragm damage and hyper-CKemia in Duchenne muscular dystrophy dog. *Sci Rep* **3**, (2013).

68. Birnkrant, D. J. *et al.* Cardiac and pulmonary function variability in Duchenne/Becker muscular dystrophy: An initial report. *J Child Neurol* **25**, 1110–1115 (2010).

69. Sharp, N. J. H. *et al.* An error in dystrophin mRNA processing in golden retriever muscular dystrophy, an animal homologue of Duchenne muscular dystrophy. *Genomics* **13**, 115–121 (1992).

70. Ambrósio, C. E. *et al.* Ringo, a golden retriever muscular dystrophy (GRMD) dog with absent dystrophin but normal strength. *Neuromusc Disord* **18**, 892–893 (2008).

71. Wasala, N. B., Bostick, B., Yue, Y. & Duan, D. Exclusive skeletal muscle correction does not modulate dystrophic heart disease in the aged mdx model of Duchenne cardiomyopathy. *Hum Mol Genet* **22**, 2634–2641 (2013).

72. Zhu, X., Wheeler, M. T., Hadhazy, M., Lam, M.-Y. J. & McNally, E. M. Cardiomyopathy is independent of skeletal muscle disease in muscular dystrophy. *FASEB J* (2002). doi:10.1096/fj.01-0954fje

73. Barp, A. *et al.* Genetic modifiers of Duchenne muscular dystrophy and dilated cardiomyopathy. *PLoS One* **10**, e0141240 (2015).

74. Dahiya, S. *et al.* Osteopontin-stimulated expression of matrix metalloproteinase-9 causes cardiomyopathy in the mdx model of Duchenne muscular dystrophy. *J Immunol* **187**, 2723–2731 (2011).

75. Spurney, C. F. *et al.* Dystrophin-deficient cardiomyopathy in mouse: Expression of Nox4 and Lox are associated with fibrosis and altered functional parameters in the heart. *Neuromuscul Disord* **18**, 371–381 (2008).

76. Vo, A. H. & McNally, E. M. Modifier genes and their effect on Duchenne muscular dystrophy: *Curr Opin Neurol* **28**, 528–534 (2015).

77. Pons, F. *et al.* Utrophin localization in normal and dystrophin-deficient heart. *Circulation* **90**, 369–374 (1994).

78. Taylor, J., Muntoni, F., Dubowitz, V. & Sewry, C. The abnormal expression of utrophin in Duchenne and Becker muscular dystrophy is age related. *Neuropathol Appl Neurobiol* **23**, 399–405 (1997).

79. Kleopa, K. A., Drousiotou, A., Mavrikiou, E., Ormiston, A. & Kyriakides, T. Naturally occurring utrophin correlates with disease severity in Duchenne muscular dystrophy. *Hum Mol Genet* **15**, 1623–1628 (2006).

80. Karpati, G. *et al.* Localization and quantitation of the chromosome 6-encoded dystrophin-related protein in normal and pathological human muscle. *J Neuropathol Exp Neurol* **52**, 119–128 (1993).

81. Zucconi, E. *et al.* Ringo: Discordance between the molecular and clinical manifestation in a golden retriever muscular dystrophy dog. *Neuromuscul Disord* **20**, 64–70 (2010).

82. Rivier, F., Robert, A., Hugon, G. & Histochemical …, B.-K. A. Dystrophin and utrophin complexed with different associated proteins in cardiac Purkinje fibres. *Histochem J* **31**, 425–432 (1999).

83. Zanotti, S. *et al.* Osteopontin is highly expressed in severely dystrophic muscle and seems to play a role in muscle regeneration and fibrosis. *Histopathol* **59**, 1215–1228 (2011).

84. Pegoraro, E. *et al.* SPP1 genotype is a determinant of disease severity in Duchenne muscular dystrophy. *Neurol* **76**, 219–226 (2011).

85. Haslett, J. N. *et al.* Gene expression comparison of biopsies from Duchenne muscular dystrophy (DMD) and normal skeletal muscle. *Proc Natl Acad Sci* **99**, 15000–15005 (2002).

86. Vetrone, S. A. *et al.* Osteopontin promotes fibrosis in dystrophic mouse muscle by modulating immune cell subsets and intramuscular TGF-β. *J Clin Investig* **119**, 1583–1594 (2009).

87. Hindi, S. M., Shin, J., Ogura, Y., Li, H. & Kumar, A. Matrix metalloproteinase-9 inhibition improves proliferation and engraftment of myogenic cells in dystrophic muscle of mdx mice. *PLoS One* **8**, e72121 (2013).

88. Kumar, A., Bhatnagar, S. & Kumar, A. Matrix metalloproteinase inhibitor batimastat alleviates pathology and improves skeletal muscle function in dystrophin-deficient mdx mice. *Am J Pathol* **177**, 248–260 (2010).

89. Delfín, D. A. *et al.* Cardiomyopathy in the dystrophin/utrophin-deficient mouse model of severe muscular dystrophy is characterized by dysregulation of matrix metalloproteinases. *Neuromuscul Disord* **22**, 1006–1014 (2012).

90. Fukushima, K. *et al.* Activation and localization of matrix metalloproteinase-2 and -9 in the skeletal muscle of the muscular dystrophy dog (CXMDJ). *BMC Musculoskelet Disord* **8**, (2007).

91. Moghadaszadeh, B. Compensation for dystrophin-deficiency: ADAM12 overexpression in skeletal muscle results in increased 7 integrin, utrophin and associated glycoproteins. *Hum Mol Genet* **12**, 2467–2479 (2003).

92. Kronqvist, P. *et al.* ADAM12 alleviates the skeletal muscle pathology in mdx dystrophic mice. *Am J Pathol* **161**, 1535–1540 (2002).

93. Fedak, P. W. M. Altered expression of disintegrin metalloproteinases and their inhibitor in human dilated cardiomyopathy. *Circulation* **113**, 238–245 (2006).

94. Jørgensen, L. H., Jensen, C. H., Wewer, U. M. & Schrøder, H. D. Transgenic overexpression of ADAM12 suppresses muscle regeneration and aggravates dystrophy in aged mdx mice. *Am J Pathol* **171**, 1599–1607 (2007).

95. COMIM, C. M. *et al.* Neurotrophins, cytokines, oxidative parameters and funcionality in Progressive Muscular Dystrophies. *Anais da Academia Brasileira de Ciências* **87**, 1809–1818 (2015).

96. Matthews, V. B. *et al.* Brain-derived neurotrophic factor is produced by skeletal muscle cells in response to contraction and enhances fat oxidation via activation of AMP-activated protein kinase. *Diabetologia* **52**, 1409–1418 (2009).

97. Fukushima, A. *et al.* Serum brain-derived neurotropic factor level predicts adverse clinical outcomes in patients with heart failure. *J Card Fail* **21**, 300–306 (2015).

98. Fukushima, A. *et al.* Decreased serum brain-derived neurotrophic factor levels are correlated with exercise intolerance in patients with heart failure. *International Journal of Cardiology* **168**, e142–e144 (2013).

99. Takashio, S. *et al.* Significance of low plasma levels of brain-derived neurotrophic factor in patients with heart failure. *Am J Cardiol* **116**, 243–249 (2015).

100. Cai, D. *et al.* BDNF-mediated enhancement of inflammation and injury in the aging heart. *Physiol Genom* **24**, 191–197 (2006).

101. Kermani, P. & Hempstead, B. Brain-derived neurotrophic factor: A newly described mediator of angiogenesis. *Trends Cardiovasc Med* **17**, 140–143 (2007).

102. Katare, R. G., Kakinuma, Y., Arikawa, M., Yamasaki, F. & Sato, T. Chronic intermittent fasting improves the survival following large myocardial ischemia by activation of BDNF/VEGF/PI3K signaling pathway. *J Mol Cell Cardiol* **46**, 405–412 (2009).

103. Nghiem, P. P. *et al.* Changes in muscle metabolism are associated with phenotypic variation in golden retriever muscular dystrophy. *Yale J Biol Med*

104. Timpani, C. A., Hayes, A. & Rybalka, E. Revisiting the dystrophin-ATP connection: How half a century of research still implicates mitochondrial

dysfunction in Duchenne Muscular Dystrophy aetiology. *Medicine Hypotheses* **85**, 1021–1033 (2015).

105. Sharma, U., Atri, S., Sharma, M. C., Sarkar, C. & Jagannathan, N. R. Skeletal muscle metabolism in Duchenne muscular dystrophy (DMD): an in-vitro proton NMR spectroscopy study. *Magn Reson Imaging* **21**, 145–153 (2003).
106. Onopiuk, M. *et al.* Mutation in dystrophin-encoding gene affects energy metabolism in mouse myoblasts. *Biochem Biophys Res Comm* **386**, 463–466 (2009).
107. Rando, T. A. Oxidative stress and the pathogenesis of muscular dystrophies. *Am J Phys Med Rehab* **81**, S175 (2002).
108. Chi, M. M.-Y. *et al.* Effect of Duchenne muscular dystrophy on enzymes of energy metabolism in individual muscle fibers. *Metab Clin Exp* **36**, 761–767 (1987).
109. Birnbaum, M. J. Identification of a novel gene encoding an insulin-responsive glucose transporter protein. *Cell* **57**, 305–315 (1989).
110. Klip, A., Sun, Y., Chiu, T. T. & Foley, K. P. Signal transduction meets vesicle traffic: the software and hardware of GLUT4 translocation. *Am J Physiol - Cell Physiol* **306**, C879–C886 (2014).
111. Zorzano, A. *et al.* GLUT4 trafficking in cardiac and skeletal muscle: isolation and characterization of distinct intracellular GLUT4-containing vesicle populations. *Biochem Soc Trans* **25**, 968–974 (1997).

112. Kraegen, E. W. *et al.* Glucose transporters and in vivo glucose uptake in skeletal and cardiac muscle: fasting, insulin stimulation and immunoisolation studies of GLUT1 and GLUT4. *Biochemical Journal* **295**, 287–293 (1993).

113. Szablewski, L. Glucose transporters in healthy heart and in cardiac disease. *Int J Cardiol* **230**, 70–75 (2017).

114. Rodríguez-Cruz, M. *et al.* Evidence of insulin resistance and other metabolic alterations in boys with Duchenne or Becker muscular dystrophy. *Int J Endocrinol* **2015**, 1–8 (2015).

115. Olichon-Berthe, C., Gautier, N., van Obberghen, E. & Le Marchand-Brustel, Y. Expression of the glucose transporter GLUT4 in the muscular dystrophic mdx mouse. *Biochem J* **291**, 257–261 (1993).

116. Jin, J. B., Carter, J. C., Sheehan, D. W. & Birnkrant, D. J. Cardiopulmonary phenotypic discordance is common in Duchenne muscular dystrophy. *Pediatr. Pulmonol.* **54**, 186–193 (2019).

117. Posner, A. D. *et al.* The correlation of skeletal and cardiac muscle dysfunction in Duchenne muscular dystrophy. *J Neuromusc Dis* **3**, 91–99 (2016).

118. Hor, K. N., Mah, M. L., Johnston, P., Cripe, T. P. & Cripe, L. H. Advances in the diagnosis and management of cardiomyopathy in Duchenne muscular dystrophy. *Neuromusc Disord* **28**, 711–716 (2018).

119. Birnkrant, D. J. *et al.* Diagnosis and management of Duchenne muscular dystrophy, part 2: respiratory, cardiac, bone health, and orthopaedic management. *Lancet Neurol* **17**, 347–361 (2018).

120. Cooper, B. J., Gallagher, E. A., Smith, C. A., Valentine, B. A. & Winand, N. J. Mosaic expression of dystrophin in carriers of canine X-linked muscular dystrophy. *Lab Investig* **62**, 171–178 (1990).

121. Cerqueira, M. D. *et al.* Standardized myocardial segmentation and nomenclature for tomographic imaging of the heart. *J Cardiovasc Magn Reson* **4**, 203–210 (2002).

122. Palate, B. M., Denoël, S. R. & Roba, J. L. A simple method for performing routine histopathological examination of the cardiac conduction tissue in the dog. *Toxicol Pathol* **23**, 56–62 (1995).

123. Northup, D. W., Liere, E. J. van & Stickney, J. C. The effect of age, sex, and body size on the heart weight-body weight ratio in the dog. *Anat Rec* **128**, 411–417 (1957).

124. Dewald, O. *et al.* Of Mice and dogs: Species-specific differences in the inflammatory response following myocardial infarction. *Am J Pathol* **164**, 665–677 (2004).

125. Nomura, H. & Hizawa, K. Histopathological study of the conduction system of the heart in Duchene progressive muscular dystrophy. *Pathol Int* **32**, 1027–1033 (1982).

126. Bilchick, K. C. *et al.* Prevalence and distribution of regional scar in dysfunctional myocardial segments in Duchenne muscular dystrophy. *J Cardiovasc Magn Reson* **13**, 1–8 (2011).

127. Bienvenu, J. G. & Drolet, R. A quantitative study of cardiac ventricular mass in dogs. *Can J Vet Res* **55**, 305–309 (1991).

128. Tidholm, A. & Jönsson, L. Histologic characterization of canine dilated cardiomyopathy. *Vet Pathol* **42**, 1–8 (2005).

129. Meurs, K. M. Boxer dog cardiomyopathy: an update. *Vet Clin N Am Small Anim Pract* **34**, 1235–1244 (2004).

130. Lobo, L. *et al.* Histologic characterization of dilated cardiomyopathy in Estrela mountain dogs. *Vet Pathol* **47**, 637–642 (2010).

131. Agudelo, C., Svoboda, M., Husnik, R. & Dvir, S. Heart lipomatosis in domestic animals: a review. *Vet Med* **58**, 252–259 (2013).

132. Everett, R. M., McGann, J., Wimberly, H. C. & Althoff, J. Dilated cardiomyopathy of Doberman Pinschers: Retrospective histomorphologic evaluation of heart from 32 cases. *Vet Pathol* **36**, 221–227 (1999).

133. Nucifora, G. *et al.* Lipomatous metaplasia in ischemic cardiomyopathy: Current knowledge and clinical perspective. *Int J Cardiol* **146**, 120–122 (2011).

134. Baroldi, G., Silver, M. D., De, R. M., Parodi, O. & Pellegrini, A. Lipomatous metaplasia in left ventricular scar. *Can J Cardiol* **13**, 65–71 (1997).

135. Samanta, R., Pouliopoulos, J., Thiagalingam, A. & Kovoor, P. Role of adipose tissue in the pathogenesis of cardiac arrhythmias. *Heart Rhythm* **13**, 311–320 (2016).

136. Schneider, S. *et al.* Suspected acute myocardial infarction in a dystrophin-deficient dog. *Neuromusc Disord* **26**, 361–366 (2016).

137. Sander, M. *et al.* Functional muscle ischemia in neuronal nitric oxide synthase-deficient skeletal muscle of children with Duchenne muscular dystrophy. *Proc Natl Acad Sci* **97**, 13818–13823 (2000).

138. Schneider, S. M. *et al.* Glucose metabolism as a pre-clinical biomarker for the golden retriever model of Duchenne muscular dystrophy. *Mol Imaging Biol* **20**, 780–788 (2018).

139. M. Grant Maxie & Robinson, W. F. Cardiovascular System. in *Jubb, Kennedy & Palmer's Pathology of Domestic Animals* **3**, 1–105

140. Rauch, U. *et al.* Increased neointimal thickening in dystrophin-deficient mdx mice. *PLoS ONE* **7**, e29904 (2012).

141. Tomanek, R. J., Aydelotte, M. R. & Torry, R. J. Remodeling of coronary vessels during aging in purebred beagles. *Circ Res* **69**, 1068–1074 (1991).

142. Kodippili, K. *et al.* Nitric oxide-dependent attenuation of noradrenaline-induced vasoconstriction is impaired in the canine model of Duchenne muscular dystrophy. *J Physiol* **596**, 5199–5216 (2018).

143. Harricane, M.-C. *et al.* Dystrophin does not influence regular cytoskeletal architecture but is required for contractile performance in smooth muscle aortic cells. *Cell Biol Interntl* **18**, 947–958 (1994).

144. Dye, W. W., Gleason, R. L., Wilson, E. & Humphrey, J. D. Altered biomechanical properties of carotid arteries in two mouse models of muscular dystrophy. *J Appl Physiol* **103**, 664–672 (2007).

145. Ito, K. *et al.* Smooth muscle-specific dystrophin expression improves aberrant vasoregulation in mdx mice. *Hum Mol Genet* **15**, 2266–2275 (2006).

146. Rando, T. A. Role of nitric oxide in the pathogenesis of muscular dystrophies: A 'two hit' hypothesis of the cause of muscle necrosis. *Microsc Res Tech* **55**, 223–235 (2001).

147. Ergul, Y. *et al.* Evaluation of the North Star Ambulatory Assessment scale and cardiac abnormalities in ambulant boys with Duchenne muscular dystrophy. *J Paediatr Child Health* **48**, 610–616 (2012).

148. Wilson, L. A., Cooper, B. J., Dux, L., Dubowitz, V. & Sewry, C. A. Expression of utrophin (dystrophin–related protein) during regeneration and maturation of skeletal muscle in canine X–linked muscular dystrophy. *Neuropathol Appl Neurobiol* **20**, 359–367 (1994).

149. Soslow, J. *et al.* Osteopontin and brain derived neurotrophic factor: Biomarkers of cardiovascular disease in Duchenne muscular dystrophy. *J Am Coll Cardiol* **67**, 1510 (2016).

150. Comim, C. M. *et al.* Striatum brain-derived neurotrophic factor levels are decreased in dystrophin-deficient mice. *Neurosci Lett* **459**, 66–68 (2009).

151. Arikawa, E. *et al.* Cross-platform comparison of SYBR Green real-time PCR with TaqMan PCR, microarrays and other gene expression measurement technologies evaluated in the MicroArray Quality Control (MAQC) study. *BMC Genomics* **9**, 328 (2008).

152. Nghiem, P. P. *et al.* Sparing of the dystrophin-deficient cranial sartorius muscle is associated with classical and novel hypertrophy pathways in GRMD dogs. *Am J Pathol* **183**, 1411–1424 (2013).

153. Jennifer E. Gilda. Western Blotting using in-gel protein labeling as a normalization control: Stain-free technology. in *Proteomic Profiling. Methods in Molecular Biology* (ed. Aldrin V. Gomes) **1295**, (Humana Press, 2015).

154. Schmittgen, T. D. & Livak, K. J. Analyzing real-time PCR data by the comparative CT method. *Nat Protoc* **3**, 1101–1108 (2008).

155. Halade, G. V. *et al.* Reduced BDNF attenuates inflammation and angiogenesis to improve survival and cardiac function following myocardial infarction in mice. *Am J Physiol - Heart Circ Physiol* **305**, H1830–H1842 (2013).

156. Bonilla, E., Schmidt, B., Samitt, C. E., Miranda, A. F. & Hays, A. P. Normal and dystrophin-deficient muscle fibers in carriers of the gene for Duchenne muscular dystrophy. *Am J Pathol* **133**, 6 (1988).

157. Walcher, T. *et al.* Cardiac involvement in a female carrier of Duchenne muscular dystrophy. *Int J Cardiol* **138**, 302–305 (2010).

158. Nghiem, P. P. *et al.* Osteopontin is linked with AKT, FoxO1, and myostatin in skeletal muscle cells: Osteopontin inhibits myostatin. *Muscle Nerve* **56**, 1119–1127 (2017).

159. Uaesoontrachoon, K. *et al.* Osteopontin and skeletal muscle myoblasts: Association with muscle regeneration and regulation of myoblast function in vitro. *Int J Biochem Cell Biol* **40**, 2303–2314 (2008).

160. Mizuno, Y. *et al.* Improvement of cardiac function after implanting the osteopontin-derived peptide SVVYGLR in a hamster model of dilated cardiomyopathy. *Interact Cardiovasc Thorac Surg* **21**, 506–514 (2015).

161. Lanfossi, M. *et al.* Development of muscle pathology in canine X-linked muscular dystrophy. I. Delayed postnatal maturation of affected and normal muscle as revealed by myosin isoform analysis and utrophin expression. *Acta Neuropathol* **97**, 127–138 (1999).

162. McDonald, C. M. *et al.* Profiles of neuromuscular diseases: Duchenne muscular dystrophy. *Am J Phys Med Rehab* **995**, S70–S92 (1995).

163. Lund, S., Holman, G. D., Schmitz, O. & Pedersen, O. Contraction stimulates translocation of glucose transporter GLUT4 in skeletal muscle through a mechanism distinct from that of insulin. *Proc Natl Acad Sci* **92**, 5817–5821 (1995).

164. Nikolaidis, L. A. *et al.* The development of myocardial insulin resistance in conscious dogs with advanced dilated cardiomyopathy. *Cardiovasc Res* **61**, 297–306 (2004).

165. Luiken, J. J. F. P., Glatz, J. F. C. & Neumann, D. Cardiac contraction-induced GLUT4 translocation requires dual signaling input. *Trend Endocrinol Metab* **26**, 404–410 (2015).

166. Kornegay, J. N., Tuler, S. M., Miller, D. M. & Levesque, D. C. Muscular dystrophy in a litter of golden retriever dogs. *Muscle & Nerve* **11**, 1056–1064 (1988).

167. Terrill, J. R. *et al.* Levels of inflammation and oxidative stress, and a role for taurine in dystropathology of the Golden Retriever Muscular Dystrophy dog model for Duchenne Muscular Dystrophy. *Redox Biology* **9**, 276–286 (2016).

168. Kornegay, J. N. *et al.* Pharmacologic management of Duchenne muscular dystrophy: Target identification and preclinical trials. *ILAR Journal* **55**, 119–149 (2014).

169. Gassmann, M., Grenacher, B., Rohde, B. & Vogel, J. Quantifying Western blots: Pitfalls of densitometry. *Electrophoresis* **30**, 1845–1855 (2009).

170. Ghosh, R., Gilda, J. E. & Gomes, A. V. The necessity of and strategies for improving confidence in the accuracy of western blots. *Expert Rev Proteom* **11**, 549–560 (2014).

171. Tai, M. M. A Mathematical Model for the Determination of Total Area Under Glucose Tolerance and Other Metabolic Curves. *Diabetes Care* **17**, 152–154 (1994).

172. Bengel, F. M., Higuchi, T., Javadi, M. S. & Lautamäki, R. Cardiac positron emission tomography. *J Am Coll Cardiol* **54**, 1–15 (2009).

173. Fan, Z. *et al.* Characteristics of magnetic resonance imaging biomarkers in a natural history study of golden retriever muscular dystrophy. *Neuromusc Disord* **24**, 178–191 (2014).

174. Tahara, N. *et al.* Heterogeneous myocardial FDG uptake and the disease activity in cardiac sarcoidosis. *JACC: Cardiovasc Imaging* **3**, 1219–1228 (2010).

175. Momose, M. *et al.* Depressed myocardial fatty acid metabolism in patients with muscular dystrophy. *Neuromusc Disord* **11**, 464–469 (2001).

176. Nishimura, T. *et al.* Thallium-201 single photon emission computed tomography (SPECT) in patients with Duchenne's progressive muscular dystrophy. *Jpn Circ j* **65**, 99–105 (2001).

177. Santacatterina, F. *et al.* Quantitative analysis of proteins of metabolism by reverse phase protein microarrays identifies potential biomarkers of rare neuromuscular diseases. *J Trans Med* **13**, 1–11 (2015).

178. Rayavarapu, S. *et al.* Identification of disease specific pathways using in vivo SILAC proteomics in dystrophin deficient mdx mouse. *Mol Cellul Proteom* **12**, 1061–1073 (2013).

179. Kemp, G. J., Taylor, D. J., Dunn, J. F., Frostick, S. P. & Radda, G. K. Cellular energetics of dystrophic muscle. *J Neuol Sci* **116**, 201–206 (1993).

180. Chen, Y.-W., Zhao, P., Borup, R. & Hoffman, E. P. Expression profiling in the muscular dystrophies: Identification of novel aspects of molecular pathophysiology. *J Cell Biol* **151**, 1321–1336 (2000).

181. Richter, E. A. & Hargreaves, M. Exercise, GLUT4, and skeletal muscle glucose uptake. *Physiol Rev* **93**, 993–1017 (2013).

182. Garvey, W. T. *et al.* Evidence for defects in the trafficking and translocation of GLUT4 glucose transporters in skeletal muscle as a cause of human insulin resistance. *J Clin Invest* **101**, 2377–2386 (1998).

183. Garvey, W. T., Maianu, L., Hancock, J. A., Golichowski, A. M. & Baron, A. Gene expression of GLUT4 in skeletal muscle from insulin-resistant patients with obesity, IGT, GDM, and NIDDM. *Diabetes* **41**, 465–475 (1992).

184. Kornegay, J. N., Cundiff, D. D., Bogan, D. J., Bogan, J. R. & Okamura, C. S. The cranial sartorius muscle undergoes true hypertrophy in dogs with golden retriever muscular dystrophy. *Neuromusc Disord* **13**, 493–500 (2003).

185. Daugaard, J. R. *et al.* Fiber type-specific expression of GLUT4 in human skeletal muscle: influence of exercise training. *Diabetes* **49**, 1092–1095 (2000).

186. Pacini, G. & Bergman, R. N. MINMOD: a computer program to calculate insulin sensitivity and pancreatic responsivity from the frequently sampled intravenous glucose tolerance test. *Comp Method Prog Biomed* **23**, 113–122 (1986).

187. Ahmad, N. *et al.* Use of imaging biomarkers to assess perfusion and glucose metabolism in the skeletal muscle of dystrophic mice. *BMC Musculoskeletal Disorders* **12**, 1–12 (2011).

188. Reinhardt, M. J. *et al.* Metastatic lymph nodes in patients with cervical cancer: Detection with MR Imaging and FDG PET. *Radiology* **218**, 776–782 (2001).

189. DeFronzo, R. A., Gunnarsson, R., Björkman, O., Olsson, M. & Wahren, J. Effects of insulin on peripheral and splanchnic glucose metabolism in noninsulin-dependent (type II) diabetes mellitus. *J Clin Invest* **76**, 149–155 (1985).

190. Schnurr, T. M., Reynolds, A. J., Komac, A. M., Duffy, L. K. & Dunlap, K. L. The effect of acute exercise on GLUT4 levels in peripheral blood mononuclear cells of sled dogs. *Biochem Biophys Rep* **2**, 45–49 (2015).

191. Varma, V. *et al.* Muscle inflammatory response and insulin resistance: synergistic interaction between macrophages and fatty acids leads to impaired insulin action. *Am J Physiol - Endocrinol Metab* **296**, E1300–E1310 (2009).

192. Horie, T. *et al.* Oxidative stress induces GLUT4 translocation by activation of PI3-K/Akt and dual AMPK kinase in cardiac myocytes. *J Cell Physiol* **215**, 733–742 (2008).

193. Kornegay, J. N., Bogan, J. R., Bogan, D. J., Childers, M. K. & Grange, R. W. Golden retriever muscular dystrophy (GRMD): Developing and maintaining a colony and physiological functional measurements. *Muscle Gene Therapy* **709**, 105–123 (2011).

APPENDIX

Supplement 1.

1.1 Background area Macro
Input select file
Output select File or make new file
Select Output Format:TIFF
Add Macro Code:choose [Select from list]

```
run("Colour Deconvolution", "vectors=[Masson Trichrome]");
close();
close();
setAutoThreshold("Default");
//run("Threshold...");
setThreshold(0, 200);
run("Measure");
close();
selectWindow("Colour Deconvolution");
close();
```

1.2 Fibrosis macro
Input select file
Output select File or make new file
Select Output Format:TIFF or JPEG
Add Macro Code:choose [Select from list]

```
run("Colour Deconvolution", "vectors=[Masson Trichrome]");
close();
close();
setAutoThreshold("Default");
//run("Threshold...");
setThreshold(0, 120);
run("Measure");
close();
selectWindow("Colour Deconvolution");
close();
```

Supplement 2. Signalment, gross measurements, and HW/BW ratios for all dogs.

Age (m) and sex	Fixed HW (g)	BW (kg)	LV (cm)	RV (cm)	Septum (cm)	HW/BW (g/kg)	LV/RV	LV/Sept	LV/HW (mm/g)
GRMD									
3 F	50	7	0.6	0.3	0.7	7.14	0.50	0.86	0.12
3 F	42	5.7	1	0.3	0.8	7.37	0.30	1.25	0.24
3 F	41	6.6	0.7	0.3	0.7	6.21	0.43	1.00	0.17
3 M	49	8	0.9	0.3	1.1	6.13	0.33	0.82	0.18
3 M	49	8.5	0.8	0.3	0.6	5.76	0.38	1.33	0.16
10 M	116	27	1	0.6	1.1	4.30	0.60	0.91	0.09
11 F	90	9.7	1.1	0.4	1.3	9.28	0.36	0.85	0.12
11 M	130	15.6	1.5	0.7	1.5	8.33	0.47	1.00	0.12
12 F	126	30	1.4	0.7	1.4	4.20	0.50	1.00	0.11
12 F	118	15.1	1.3	0.6	1.1	7.81	0.46	1.18	0.11
12 F	109	13.3	1.1	0.6	1	8.20	0.55	1.10	0.10
12 M	80	13	0.9	0.4	0.8	6.15	0.44	1.13	0.11
15 M	81	9.3	0.8	0.4	0.9	8.71	0.50	0.89	0.10
17 M	98	12.5	1.2	0.4	1	7.84	0.33	1.20	0.12
21 F	98	24.3	0.7	0.3	1	4.03	0.43	0.70	0.07
21 F	102	21	1.1	0.45	1	4.86	0.41	1.10	0.11
28 F	132	13.8	1.8	0.4	1.3	9.57	0.22	1.38	0.14
36 M	132	7.9	1.1	0.4	0.9	16.71	0.36	1.22	0.08
38 M	188	21.9	1.3	0.5	1.1	8.58	0.38	1.18	0.07
40 F	160	5.1	1.3	0.5	1	31.37	0.60	1.00	0.08
40 F	164	13.8	1	0.6	1	11.88	0.38	1.30	0.06
40 M	158	27	1.2	0.4	0.9	5.85	0.33	1.33	0.08
45 F	238	17.3	1	0.4	0.8	13.76	0.40	1.25	0.04
51 M	132	17.6	1	0.8	0.4	7.50	0.80	2.50	0.08
76 M	192	28.3	1.1	0.5	0.8	6.78	0.45	1.38	0.06
76 M	194	21.9	1.5	0.5	1.3	8.86	0.33	1.15	0.08
Carrier									
3 F	62	14.9	1.2	0.6	1	4.16	0.50	1.20	0.19
12 F	160	21.3	1.5	0.6	1.5	7.51	0.40	1.00	0.09
46 F	202	15.1	1.6	0.7	1.3	13.38	0.44	1.23	0.08
56 F	272	11.8	1.4	0.7	1.1	23.05	0.50	1.27	0.05
65 F	182	13.5	1.2	0.7	1.2	13.48	0.58	1.00	0.07
Normal									
22 F	210	25.8	2	1	1.9	8.14	0.50	1.05	0.10
36 F	186	23.8	1.7	0.8	1.7	7.82	0.47	1.00	0.09
46 F	201	24.3	1.5	0.7	1.8	8.27	0.47	0.83	0.07
61 M	236	26.9	2	1.1	2	8.77	0.53	0.95	0.08
75 F	208	21	1.9	0.8	1.7	9.90	0.55	1.00	0.09
102 F	224	28	1.9	1	2	8.00	0.42	1.12	0.08
124 M	--	25.8	2	0.9	2.3	--	0.45	0.87	--

Supplement 3. Semi-quantitative cross-sectional area score for LV and RV sections with means.

age (mo)	Basal anterior	Basal anteroseptal	basal inferoseptal	basal inferior	basal inferolateral	basal anterolateral	mid anterior	mid anteroseptal	mid inferoseptal	mid inferior	mid inferolateral	mid anterolateral	apical anterior	apical septal	apical inferior	apical lateral	Apex	RV basal anterior	RV basal inferior	RV mid anterior	RV mid inferior
GRMD																					
3	0	0	0	0		0	0	0	0	0	1	1	1	0	0	0	1	0	0	0	0
3	0	0	0	0	0		0	0	0	1	0	0	1	1	0	0	1	1	1	1	1
3	1	1	1	1	0	0	0	0	0	1	0		0	1	1	0	1	1	1		1
3	0	0	0	1	1		0	0	0	0		0	0	0	0	0	1	0	0	0	0
3	0	0	0	0	0	0	1	0	0	0	0		1	0	0			1	1	0	0
10	0	0	0	0	0	0	0	1	0	0	0	1	0	0	0	0	0	0	0	1	1
11	1	1	1	3		1	2	1	1	1	1	1	2	1	0	0	1	1	1	1	0
10	1	0	1	0	0		0	0	0	0	0	0	0	1	0	1	1	0	1	0	0
12	1	2	1	1	1	3	1	2	1	1	1	2	2	2	1	2	1	1	2		
12	1	1	0	1	1	1	1	1	0	1	1	0	2	1	0	0	0	1	1	1	1
12	1		1	2	1	4	1	1	1	1	1	2	1	1	0	0	0		4		3
12	0	1	1	0	0	1	1	0	1	1	0	1	1	2	1	1	1	1	1	1	1
15	0	1	1	1	1	1	0	0	0	1	0	1	0	0	1	1	1	1	1	1	1
17	0	0	0	0	0	0	0	0	0	0	0	0	0	0	0	0	0	0	0	0	0
21	1	2	1	1	1	1	1	2	1	1	3	1	2	1	1	3	1	1	1	1	0
21	0	1	1	1	1	0	1	2	2	1		1	1	1	1	0	1	1	1	1	1
28	1	1	2	2	1	2				4		3	1	0	1	2	2	4	3		
36	1	1	1	1	1	1	1	1	1	1	1	1	1	1	1	1	0	1	1	1	1
38	1	1	2	1	2	2	1	1	1	1	2	1	1	1	1	1	1	1	1	1	1
40	1	2	1	1	1	3	2	1	1	2	2			1	1	2	1	3	3	2	3
40	2	2	1	1	3		2	1	1	1	3	2	2	2	2	2	2	4	2	2	2
40	1	1	1	1	2	3	3	1	1	1	2	1	3	1	1	3	2	4	2	1	4
45	1	1	2	3	2	3	3	2	1	2	2		3	2		3	3	3	4	1	2
51	2	3	4	1	2	2	2	2	3	3	2	2	3	3	1	3	2	2	4	2	2
76							1	1	1	1	1	1	1	1	2	1	1	1	1	1	1
76	1	1	1	1	0	1	1	1	1	1	1	1	2	1	1	1	1	1	1	1	1
Mean	0.7	1.0	1.0	1.0	0.9	1.4	1.0	0.8	0.7	1.0	1.0	1.0	1.2	1.0	0.7	1.1	1.0	1.4	1.5	0.9	1.1
Carrier																					
3							0	0	0	0			0		0					0	1
12	0	0	0	0	0	1	0	0	0	0	0		0	0	0		0	0	0	0	0
46	2	1	1	1	1		1	1	2	1	2	2	2	1	2	1	1	1	1	1	3
56			0	0	0	0	0	0	0	0	1	1	0	0	1	0	0	1	1	1	1
65	1	1	1	1	1	0	1	1	0	1		0	1	1	1	1	1	1	1	0	1
Mean	1	0.7	0.5	0.5	0.5	0.3	0.4	0.4	0.4	0.4	1	1	0.6	0.5	0.8	0.7	0.5	0.8	0.8	0.4	1.2
Normal																					
22	0	0	0	1	1	0	1	0	0	0	0	0	0	1	1	0	1	1	0	1	0
36	0	0	0	0	0	0	0	0	0	0	0	0	0	0	0	0	0	0	0	0	0
46	1	1	1	1		1	0	1	1	1		0	0	0	1	1	0	0	1	1	1
61	0	0	1	0	0	1	0	0	0	0	0	0	0	0	0	0	1	0	0	0	0
75	0	0	0	1	0	0	1	0	0	0	1	1	0	0	0	0	1	0	1	1	
102	0	0	0	1	0	0	0	0	0	0	0	0	0	0	1	0	0	0	0	0	0
124	1	1	0	1	1	0	0	0	0	0		0	1	1	1	0	1	0	0	1	0
Mean	0.3	0.3	0.3	0.7	0.3	0.3	0.3	0.1	0.1	0.1	0.2	0.1	0.1	0.3	0.6	0.1	0.6	0.1	0.3	0.6	0.2

Numbers are a semi-quantitative grade for approximate percent of cross-sectional area affected by histopathologic lesions, generally following the system described by Kane et al. 2013 [43] 0 = none, 1 = 1 to 10%, 2 = 11-20%, 3 = 21 to 30%, and 4 > 30%. Color intensity from white (0) to red (4) visually highlight the different values. Gray squares lack a value.

Supplement 4.
Population characteristics of normal dogs

Characteristics	N (%)
Age (months)	
Mean (SD)	42.5 (38.00)
Age in months	
0-10	6 (19.35)
11-24	9 (29.03)
Over 24	16 (51.61)

Supplement 5. Primers used in qRT-PCR

Gene	Acc. No.	Primer Oligonucleotide Sequence	Tm	bp
UTRO	NM_001012395.1	F 5'-CAGACAGTACTTGAAGGTGACA-3' R 5'-CATAGTGCTCCGGCCACA-3'	57 59	70
SPP1	XM_003434023.3	F 5'-GGGAGCTCTGAGGAAAAGCA-3' R 5'-GCTTCTGAGATGGGTCAGGC-3'	60 60	82
BDNF	NM_001002975.1	F 5'-GGACATATCCATGACCAGAAGGG-3' R 5'-TCGAGGAATGTAATGCAGACTT-3'	60 57	73
ADAM12	XM_536508.6	F 5'-CCTTGCTTTGAAGGTGGCAA-3' R 5'-AGTCACAGCCGACCATCTTAC-3'	59 60	70
MMP9	NM_001003219.2	F 5'-TTTCGACGTGAAGACGCAGA-3' R 5' TTCCGAGAATTCACACGCCA-3'	60 60	156
HPRT	XM_014111318.1	F 5'-AGCTTGCTGGTGAAAAGGAC-3' R 5'-TTATAGTCAAGGGCATATCC-3'	59 51	104
GAPDH	NM_001003142.2	F 5'-CCAGGTGGTCTCCTGTGACT-3' R 5'-GGCCATGTAGACCATGAGGTC-3'	60 60	160

Supplement 6. Western blot analysis. (A) SPP1 expression in the LV and RV of normal (WT) controls at 6 and 12 m. (B) BDNF expression in the LV and RV of normal controls at 6 and 12m.

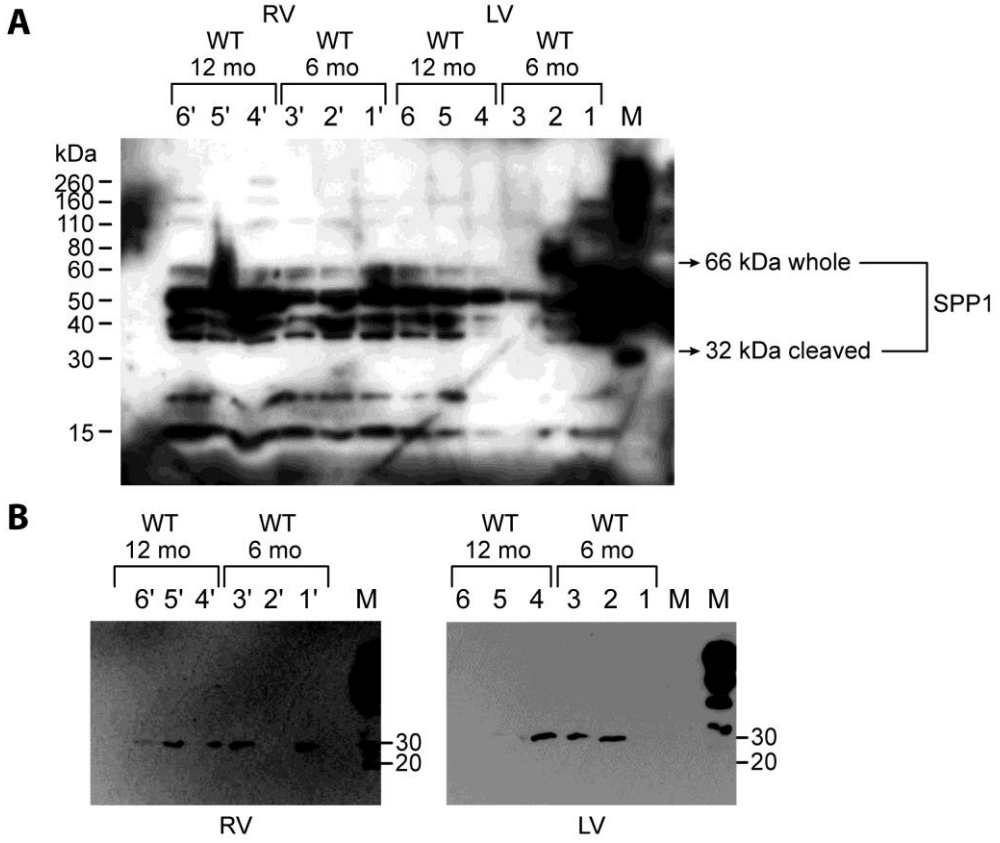

Supplement 7. Western blot analysis. SPP1 expression in the LV and RV of GRMD dogs at 6 m and 12 m and >40 m.

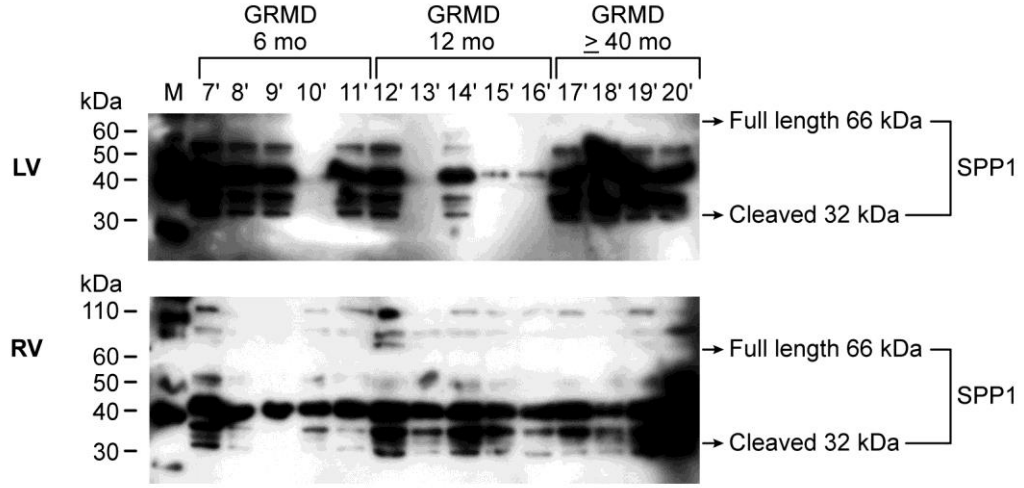

Supplement 8. Western blot analysis. BDNF expression in the LV and RV of GRMD dogs at 6 m and 12 m and >40 m.

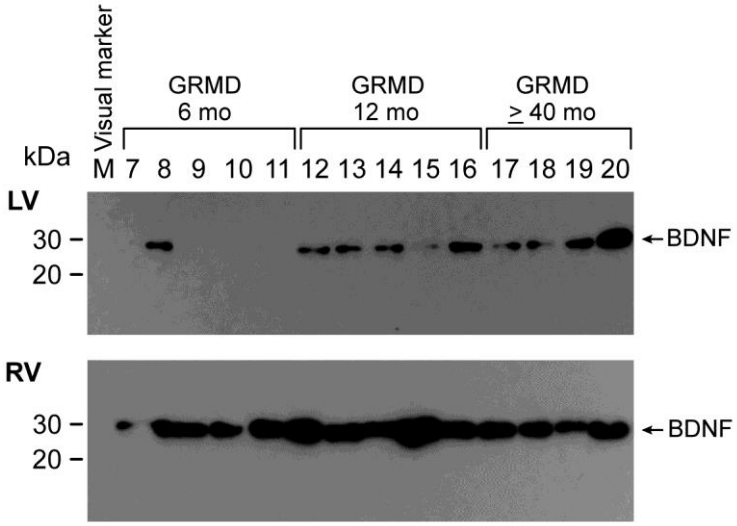

Supplement 9. Systolic, Diastolic, and Mean Blood Pressures for dogs before, 5-min post and 1-hr Post [^{18}F]DG/insulin administration. Reprinted.[138]

Dogs	10min Prior to [^{18}F]DG			5 min post [^{18}F]DG administration			1 hour post [^{18}F]DG		
	Syst	Diast	Mean	Syst	Diast	Mean	Syst	Diast	Mean
GRMD									
F (8m)	119	45	94	120	54	79	131	62	109
M(2y)	129	48	74	105	43	69	152	70	96
M(6y)	93	31	61	99	35	63	118	45	77
M(4y)	113	85	95	102	36	60	103	42	68
F(4y)	NR	NR	NR	NR	NR	NR	NR	NR	NR
M(6y)	NR	NR	NR	91	36	60	128	56	83
Carrier									
F(2y)	93	33	57	92	34	55	116	52	80
F(6y)	115	44	90	164	82	111	146	77	94
F(2y)	NR	NR	NR	108	41	70	113	53	75
F(8m)	92	36	70	79	34	60	101	43	73
F(4y)	93	47	66	91	48	67	123	67	94
F(6y)	79	33	62	80	32	62	101	55	70
Normal									
M(8m)	134	69	103	133	64	97	110	47	81
F(3y)	121	51	78	115	46	79	153	72	103
M(8m)	101	33	63	103	32	40	92	29	55
F(2y)	92	33	58	92	32	62	105	54	75
M(8m)	93	34	65	88	33	64	95	35	54
M(8m)	76	32	55	93	29	55	76	24	54

NR=Not recorded.